9-22-2015 12:00 AM

Shear and Peel Stresses at the Interface between Hollowcore Slabs and the Topping Concrete

Aiham Adawi
The University of Western Ontario

Supervisor
Dr. Maged A. Youssef
The University of Western Ontario

Graduate Program in Civil and Environmental Engineering
A thesis submitted in partial fulfillment of the requirements for the degree in Doctor of Philosophy

SHEAR AND PEEL STRESSES AT THE INTERFACE BETWEEN HOLLOWCORE SLABS AND THE TOPPING CONCRETE

(Thesis format: Integrated Article)

by

Aiham Adawi

Graduate Program in Engineering Science
Department of Civil and Environmental Engineering

A thesis submitted in partial fulfillment
of the requirements for the degree of
Doctor of Philosophy

The School of Graduate and Postdoctoral Studies
The University of Western Ontario
London, Ontario, Canada

Abstract

Hollowcore slabs are used in floors and roofs of residential, commercial, industrial and institutional buildings. They are precast/prestressed concrete elements produced using the extrusion process. Their surface finish can be “machine-cast” or “intentionally roughened”.

A typical floor consists of a number of hollowcore slabs that are connected together. Prestressing causes hollowcore slabs to camber, which results in an uneven floor surface. A 50 mm topping concrete is commonly cast to level the floor surface. To avoid delamination, engineers require bonding agents to be applied on the hollowcore slab surface before pouring the topping concrete. The concrete topping can be used compositely with the hollowcore slabs to increase the floor’s load carrying capacity. However, North American design standards require intentional roughening of the hollowcore slab surface to consider such composite action. This requirement results in added cost that manufacturers are keen to avoid.

This thesis presents a comprehensive experimental program to assess the performance of composite hollowcore slabs with machine-cast and lightly-roughened surface finishes. Three types of tests were performed: pull-off, push-off and full-scale. They provided an overall understanding of the interfacial shear and peel behaviors at the interface between hollowcore slabs and the topping concrete. The tested slabs were found to sustain higher interfacial shear stresses than the limits set by the design standards and to provide adequate composite behavior up to failure. Linear analytical modeling in which closed-form solutions for differential equations governing the interfacial shear and peel stresses during the push-off tests was conducted. Two analytical methods were developed to estimate the shear and peel stresses during the full-scale tests utilizing the interface stiffness determined from the push-off tests. Linear finite element analysis was performed to validate and compare the proposed methods.

To better understand the experimental results and to provide engineers with more accurate tools for estimating the interfacial stresses, nonlinear finite element analysis of the push-off and the full-scale tests were conducted. Interfacial shear and peel stiffness values associated

with the tested slabs were also determined to assist design engineers in predicting failure modes of composite hollowcore slab.

Keywords

Hollowcore slabs, Composite behavior, Concrete topping, Interfacial shear stress, Interfacial peel stress, Finite Element Modeling, Analytical modeling, Pull-off tests, Push-off tests, Full-scale tests, Machine-cast, Lightly-roughened.

Co-Authorship Statement

All the work presented in this thesis including experimental testing, analyzing of the collected data, development and validation of the analytical and FE models and drafting of publications manuscripts was conducted by the candidate under the supervision of Dr. Maged Youssef. Dr. Mohamed Meshaly (Assistant Professor, Structural Engineering Department, Alexandria University, Egypt) has assisted in the initial development of the analytical models presented in Chapter 4 and contributed to the finite element analysis of the push-off tests using ANSYS R15 presented in Chapter 5.

Modified versions of Chapters 2 and 3 have been published as follows:

- **Aiham Adawi**, Maged A. Youssef, Mohamed Meshaly, "Experimental investigation of the composite action between hollowcore slabs with machine-cast finish and concrete topping," *Engineering Structures*, 91 (2015), p.p. 1-15.
- **Aiham Adawi**, Maged A. Youssef, Mohamed Meshaly, "Analytical Modeling of the Interface between Lightly Roughened Hollowcore Slabs and Cast-In-Place Concrete Topping," *Journal of Structural Engineering* (ASCE), April 2015, Volume 141, Issue 4, p.p. 1-9.

Parts of Chapters 2 and 3 were presented by the candidate at the 2013 PCI convention and National Bridge Conference in Grapevine, Texas as shown below:

- Maged Youssef and **Aiham Adawi**, "COMPOSITE BEHAVIOR OF HOLLOWCORE SLABS AND CAST-IN-SITU CONCRETE TOPPING," *Proceedings of PCI Convention and National Bridge Conference*, 21-24 Sept., 2013, p. 20.

Revised versions of Chapters 4 and 5 will be submitted to the following peer-reviewed technical journals or presented at international conferences:

- **Aiham Adawi**, Maged A. Youssef, Mohamed Meshaly, "Analytical Modeling of Composite Hollowcore Slabs," *Journal of structural Engineering* (ASCE).

- **Aiham Adawi**, Maged A. Youssef, Mohamed Meshaly, "Investigating the Interfacial Shear and Peel Stresses in Composite Hollowcore Slabs using Finite Element Modeling," *Engineering Structures*.

“Recite in the name of your Lord who created,

Created man from a clinging substance,

Recite, and your Lord is the most Generous,

Who taught by the pen,

Taught man that which he knew not.”

Holy Quran, Chapter 96, Verses 1 to 5

To my outstanding parents:

Mousa Odeh Adawi and Nawal Youssef Al Ayasah

To my wonderful parents-in-law:

Nabeel Almadhoon and Khawla Abu Samrah

To my beloved wife and children:

Reem Almadhoon, Sally, Sarah and Issa

To my dear siblings:

Shaden, Hazem, Shada, Ahmed and Rahaf

To all my family and family-in-law members

And,

To my homeland, Palestine, and to all people who sacrificed for it.

Acknowledgments

I would like to express my sincere gratitude to Dr. Maged Youssef for his outstanding supervision and mentorship during the period of my graduate studies including my M.Eng. degree. Not only that Dr. Maged shared with me his vast technical knowledge but also guided and advised me during many important events that greatly helped developing my academic skills.

A great thank you goes to my research colleague Dr. Mohamed Meshaly for his enthusiasm and support. His strong technical and learning skills helped me considerably in the analytical and finite element analyses.

I am thankful to the owners, administration and staff of "The Prestressed Group" in Windsor, Ontario, for their financial and technical support during my Ph.D. studies. I would like to greatly thank Mr. Anil Mehta in particular for his support, mentorship and guidance on both the professional and personal levels. He was generous in sharing his extraordinary expertise in the precast/prestressed concrete industry throughout this study. The appreciation is extended to Mr. Neb Mladenovic and Mr. Milenko Simic for their valuable technical input.

Thanks and appreciation go to the National Sciences and Engineering Research Council of Canada (NSERC) for funding my IPS scholarship, The Ontario Centers of Excellence (OCE), Canadian Precast/Prestressed Concrete Institute (CPCI) and The Prestressed Group for providing generous financial and technical support during my Ph.D. studies.

The experimental work would not have been perfected without the help of Mr. Wilbert Logan and his great experience in the structures lab. The staff at the Civil and Environmental Engineering Dept. and the Engineering Stores facilitated all logistics for my Ph.D. work so thank you very much.

Without the sincere prayers and care of my parents, I could not have reached this level of education and success. I am endlessly grateful to their love and guidance all my life and simply owe them all of my achievements. I hope this accomplishment brings joy to their hearts and ask God to always make me a source of happiness to them.

No words of acknowledgment can describe my gratefulness to my wife, Reem Almadhoon. Her outstanding compassion for me and our three children Sally, Sarah and Issa has been remarkable during my studies. Her patience and encouragement have been my backbone through the ups and downs of this period. I hope I will be able to pay her back even a little of all the support and effort she unconditionally gave to me. The appreciation is also extended to my parents-in-law, who have surrounded me with kindness and support ever since we have become a family.

My friends and colleagues are a major component of this success. I owe those people a huge thank you for their technical and personal support, for their kindness and for all the good times we have spent together during this journey. I wish all of them the best of luck in their future endeavors.

Table of Contents

List of Tables

List of Figures

List of Symbols

A	interface area in push-off tests,
A_{cv}	contract area between the hollowcore slab and the concrete topping
A_{hc}	cross sectional area of the hollowcore slab
A_t	cross sectional area of the concrete topping
b	width of the concrete topping in the push-off tests, 508 mm
b_t	width of the concrete topping in the full-scale test
b_v	width of the interface between the concrete topping and the hollowcore slab
b_w	effective web width for the hollowcore slab cross section
d	location of the strands from the top of the top of the hollowcore slabs
d_v	effective strands location measured from the top of the hollowcore slab
E_c	modulus of elasticity of concrete
E_c	young's modulus of concrete
E_{hc}	concrete young's modulus for the hollowcore slab
E_p	young's modulus of strands
E_t	concrete young's modulus for the concrete topping
f'_c	concrete compressive strength
f'_{chc}	concrete compressive strength of the hollowcore slab

f'_{ct}	concrete compressive strength of the topping
f_c	concrete compressive stress
f_{cr}	flexural tensile strength of concrete
F_p	out-of-plane force on element T
f_p	tensile stress in strands
f_{pu}	ultimate tensile stress of strands
F_s	in-plane force on element T in the X direction
f_t	concrete tensile stress
I_{hc}	moment of inertia of the hollowcore slab
I_t	moment of inertia of the concrete topping
K	general stiffness of the interface between the hollowcore slab and the concrete topping
k	post peak ductility factor for high strength concrete
k_p	interfacial peel stiffness
k_s	interfacial shear stiffness
k_{sm}	slope of the measured load-displacement graph in the push-off tests
k_x	shear springs stiffness
k_z	peel springs stiffness

L	concrete topping length (push-off tests) and composite slab span (full-scale tests)
L_t	length of the concrete topping in the full-scale test
$m(x)$	external applied moment on the concrete topping (push-off tests)
M	internal moment in the concrete topping (push-off tests)
M_{hc}	internal bending moment of the hollowcore slab during the full-scale test
M_t	internal bending moment of the concrete topping during the full-scale test
M_T	total external bending moment applied on the hollowcore slab during the full-scale test
n	concrete stress-strain curve fit parameter
N	internal axial force in the composite hollowcore slab during the full-scale test
P_{hc}	load applied on the hollowcore slab using the hydraulic actuator during the push-off test
P_t	reaction on the concrete topping during the push-off tests
P_u	ultimate applied load.
P_{ux}	ultimate force in the shear springs
P_{uz}	ultimate force in the peel springs
P_y	yielding load during the full-scale test

P_{yx}	yielding force in the shear springs
P_{yz}	yielding force in the peel springs
s	slip between the strand and the surrounding concrete
t	concrete topping thickness in the push-off tests
$u(L)$	in-plane displacement corresponding to the yielding load in the push-off tests
$u(x)$	in-plane displacement profile along the axis X in the push-off test
u_{hc}	displacement of the top of the hollowcore slab during the full-scale test
u_t	displacement of the bottom of the concrete topping during the full-scale test
V	internal shear force in the concrete topping
V_{hc}	internal vertical shear force in the hollowcore slab during the full-scale test
V_t	internal vertical shear force of the topping during the full-scale tests
$w(x)$	calculated out-of-plane displacement profile of the concrete topping
$w(x)_{hc}$	vertical displacement profile of top of the hollowcore slab during the full-scale test
$w(x)_m$	measured out-of-plane displacement profile of the concrete topping
$W(x)_t$	vertical displacement profile of the concrete topping bottom during the full-scale test
Y_{hc}	distance from the hollowcore slab centroid to the interface layer

Y_t	distance from the concrete topping centroid to the interface layer
$\sigma(x)$	interfacial peel stress distribution during the full-scale test
$\tau(x)$	interfacial shear stress distribution during the full-scale tests
ε'_c	peak concrete compressive strain
α_1 and β_1	concrete stress block parameters
τ_b	bond stress between the strand and the hollowcore slab
ε_c	concrete compressive strain
$\upsilon_{h\ avg.}$	average interfacial shear stress in the push-off tests
$v_{h\ max}$	maximum shear tress calculated using the analytical model in the push-off tests
v_h	shear stress in the push-off tests
ε_{hc}	strain of the top of the hollowcore slab during the full-scale test
ε_o	peak concrete strain in concrete stress-strain curve
ε_p	tensile strain in strands
ε_{pr}	strands rupture strain
ε_t	concrete strain in the sectional strain distribution
ε_t	strain of the bottom of the concrete topping during the full-scale test

$\tau_{test\ avg.}$ average interfacial shear stress in the full-scale tests

CHAPTER ONE

1 Introduction

Hollowcore slabs, Fig. 1.1, are precast/prestressed structural concrete elements that are used in many structures including large occupancy residential, institutional, office and commercial buildings as well as warehouses and detention centers. They are also utilized in bridge decks. The voids within the hollowcore slabs run along their length reducing their own weight. They can be solid filled with concrete near the supports to enhance the vertical shear resistance. The voids can also be used as part of the ventilation system and to conceal electrical and mechanical ducts.

Hollowcore slabs can cover significantly larger spans than solid slabs because of their reduced weight and prestressing advantage. Longer spans mean larger usable spaces with no intermediate supports. Other advantages of hollowcore slabs include: fire resistance with up to 4 hours of endurance, sound insulation and energy savings.

Fig. 1.1: Hollowcore slab.

Thickness of hollowcore slabs range between 150 mm and 500 mm and their typical width is 1220 mm. Their spans can reach up to 24 m. The joints between adjacent hollowcore slabs are filled with non-shrink grout. Reinforcement can be provided in the joints if required by design.

1.1 Manufacturing of Hollowcore Slabs

The two basic manufacturing procedures currently used in the production of hollowcore slabs are: (1) dry-cast and (2) wet-cast. In the dry-cast procedure, the prestressing strands are first laid over the casting beds, 100 to 200 meters long, and then tensioned to the desired prestressing force. The extrusion machine is placed over the casting bed and concrete with a typical water to cement ratio of 0.3 is poured. The extrusion machine has a number of augers that form the voids and vibrate at high frequency to properly compact the low-slump concrete. The hollowcore slab is then cured over the casting bed using accelerated heated systems to reduce production time.

After curing, strands are released and the long slab is cut into several segments. The resulting hollowcore slab surface finish using this procedure is called “machine-cast finish”. Light roughening of the slab surface can be achieved by using a steel broom, Fig. 1.2. The surface finish in this case is referred to as “lightly-roughened”. When a higher surface roughness is required, a concrete screed is poured on top of the slab surface.

The wet-cast procedure uses higher slump concrete with a water to cement ratio of 0.4 to 0.45. The cores in this procedure are commonly formed using: (1) light-weight aggregate fed through tubes that are attached to the casting machine, (2) anchored pneumatic tubes, or (3) tubes fixed to the slip form casting machine.

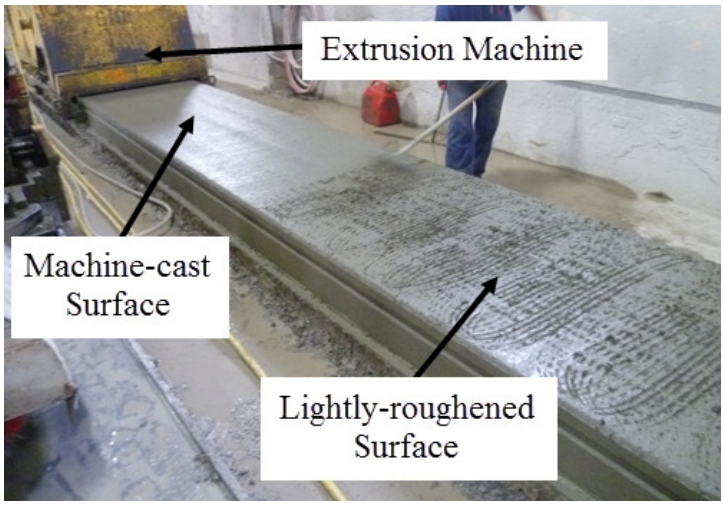

Fig. 1.2: Machine-cast versus lightly-roughened surface finish.

1.2 Problem Description and Motivation

Hollowcore slabs camber due to prestressing. Difference in camber between slabs in a given floor causes floor surface irregularities. Thus, a 50 mm concrete topping is commonly cast on top of the hollowcore slabs to achieve a flat surface finish. Design engineers might require bonding the concrete topping to the slab surface using cement/sand gout, latex modified grout or epoxy bonding materials. This requirement is meant to prevent delamination between the two surfaces, which can cause cracks in the concrete topping. A field test that follows procedure A of the standard test method A23.2-6B (CSA A23.2, 2009) is usually requested. If the composite action between the concrete topping and the slab is considered, the load carrying capacity of the floor increases. This requires roughening of the surface of the hollowcore slab to an amplitude of 6.35 mm or 5.00 mm according to ACI 318-08 (2008) and CSA A23.3-04 (2004), respectively. Design engineers may also require the use of bonding agents in addition to the roughening mentioned in the design standards.

The implementation of the requirements of the design engineers and the design standards induce additional material and manpower costs that hollowcore slab manufacturers are keen to avoid. There is also a general consensus among manufacturers that the bond

between hollowcore slabs with machine-cast surface and topping concrete is sufficient to develop adequate composite action.

The argument, whether hollowcore slabs with machine-cast or lightly-roughened surface are capable of providing the necessary design strength, was the main motivation for this research.

1.3 Literature Review

This section sheds light on the mechanism of shear stresses along the interface between concrete overlays and reviews previous research that pertains to composite behaviour in precast concrete elements.

1.3.1 Shear Transfer at the Interface between Two Concrete Layers

The shear force along the interface between two monolithic or composite concrete layers is transferred by "shear-friction". Birkeland and Birkeland (1966) and Mast (1968) proposed models to predict the shear strength at the interface based on its roughness and the yield strength of the interface steel bars. The models considered that the shear strength of an unreinforced interface to be equal to zero. Several research work had been published afterwards that further discussed this subject (Hofbeck et al., 1969; Mattock and Hawkins, 1972; Houde and Mirza, 1974). Shaikh (1978) modified the models and included the effect of the concrete type. The models were then added to the shear-friction provisions of the ACI 318-83 (1983) design standard.

A typical concrete surface has a general roughness and a local roughness (Walraven, 1987), Fig. 1.3. Mattock (1974) introduced the cohesion component in the shear-friction equation. The cohesion component is provided by the local roughness of the interface.

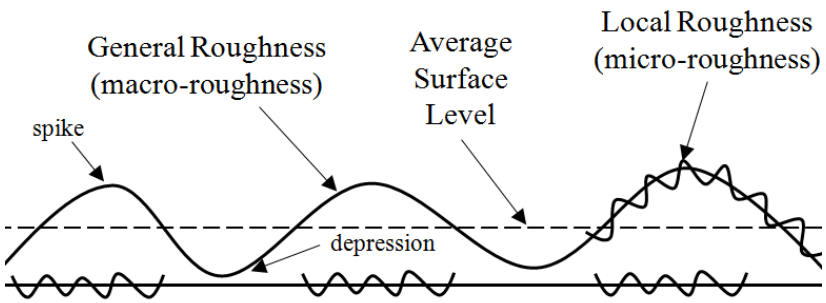

Fig. 1.3: Roughness illustration.

Using interfacial shear reinforcement in hollowcore slab construction is extremely inconvenient. Thus, the composite action in such construction mainly relies on friction and cohesion of the interface.

1.3.2 Composite Precast Concrete Elements

The horizontal shear strength at the interface between precast elements and topping concrete was examined by many researchers. Ozell and Cochran (1956) tested nine prestressed composite lintel beams. The beams did not contain any horizontal shear reinforcement and their surface was very smooth. None of the beams failed due to horizontal shear. The authors concluded that reliable horizontal shear strength can be developed without roughening the surface of precast beams.

Hanson (1960) conducted tests on smooth specimens and concluded that the horizontal shear strength can reach 2.1 MPa without roughening the surface. He also tested a composite beam that had an intentionally roughened surface. The roughness amplitude was 9.5 mm measured from the spikes and depressions to the average surface level as shown in Fig. 1.3. The beam suffered a significant loss of composite action before failure. The maximum horizontal shear stress was estimated at 2.76 MPa.

CTA Technical Bulletins TB74-B6 (1974) and TB76-B4 (1976) presented the results for 16 tests on prestressed composite solid slabs with different surface finishes and concluded that horizontal shear levels given in ACI Code are highly conservative.

Scott (1973) performed a full-scale test on a hollowcore slab with machine-cast finish that was topped with 50 mm of concrete. The slab was 200 mm deep, 610 mm wide and simply supported over a span of 9600 mm. The slab failed at a slightly higher load than that calculated using ACI 318 (1971) and composite action was maintained up to failure.

Girhammar and Pajari (2008) investigated the shear capacity of composite hollowcore slabs with machine-cast finish and concluded that the composite action increased the shear capacity by 35%. The surface of the tested hollowcore slabs was not treated or roughened by any means.

Ibrahim et al. (2006) studied the horizontal shear transfer along the interface of hollowcore slabs and concrete topping using 14 specimens that vary in surface roughness. Concrete topping area was 300 mm by 300 mm with thickness of 100 mm. It was concluded that slip was not significant for shear forces up to 50 kN.

Ibrahim et al. (2008) conducted full-scale tests on hollowcore slabs with concrete topping. Two main variables were investigated: (1) surface roughness of the hollowcore slabs (smooth and roughened) and (2) moisture condition of the hollowcore slab surface before casting the concrete topping. Their study found that the ponded condition can reduce the bending moment capacity by 5% compared with the optimum wet condition. It also stated that the slip in the bonded smooth specimens can be eliminated by roughening the surface of the hollowcore slabs.

Mones (2012) studied the properties of the interface between hollowcore slabs with various surface finishes and concrete topping. Push-off tests were used to evaluate the shear stiffness of the composite hollowcore slabs with various surface finishes including machine-cast, wet-cast and sandblasted wet-cast. All specimens showed higher interfacial shear strength than required by the North American standards and averaged at 1.57 MPa. The wet-cast slabs showed the least strength because of the laitance layer covering their

surface. Sand blasting of such slabs showed an increase of 51% in their interfacial shear strength. Mones (2012) implemented the push-off test results into a 2-D finite element analysis to study the interface behaviour in full-scale conditions. While multilinear shear stiffness was used to model the interfacial shear strength, linear behaviour of the hollowcore slab was assumed. The results were not validated and the interfacial peel strength was not considered in the analysis.

Previous work generally agrees with hollowcore slab manufacturers about the adequacy of machine-cast surface finish to achieve composite action. However, it is not comprehensive. The interfacial shear and peel behaviours at the interface between hollowcore slabs and the topping concrete are not well studied. Most of the efforts were experimental and lack analytical modeling techniques. The work presented in this thesis sheds light on the properties of the interface between hollowcore slabs and the topping concrete and provides design engineers with analytical tools to investigate interfacial shear failures that can be compared against design standards to obtain a more realistic solution.

1.4 Research Objectives

The general objective for this thesis is to evaluate the interface behaviour between hollowcore slabs with machine-cast or lightly-roughened surfaces and cast-in-situ concrete topping. Specific objectives are given below:

1- Experimentally estimate the surface roughness of hollowcore slabs with machine-cast finish.
2- Experimentally examine the bond strength between hollowcore slabs with machine-cast or lightly-roughened surface and the topping concrete.
3- Experimentally evaluate the shear and peel behaviours between hollowcore slabs and the topping concrete.
4- Analytically determine the interfacial shear and peel stiffness between hollowcore slabs and the topping concrete.

5- Investigate the performance of composite hollowcore slabs with concrete topping through full-scale tests.
6- Develop closed-form solutions that can be used by design engineers to evaluate the levels of shear and peel stresses for composite hollowcore slabs.
7- Investigate the nonlinear behaviour of the interfacial shear and peel stiffness between hollowcore slabs and the topping concrete using finite element analyses.

1.5 Original Contribution

Most of the prior research work conducted on composite hollowcore slabs was aimed towards determining their capacity without studying the behaviour at the interface layer. The research conducted in this thesis provides design engineers and hollowcore slab manufacturers with a comprehensive evaluation of the interface behaviour for composite hollowcore slabs. The thesis proposes a surface roughness threshold that can be used as a quality control measure. The linear and nonlinear analyses of the composite hollowcore slabs provide credible estimates for the actual interfacial stresses and analytical techniques for engineers to accurately analyze composite slabs. The analytical solutions presented in this thesis account for the deformations of the interface layer, which are not considered in design provisions of North American building codes.

1.6 Thesis Outline

The thesis is structured using the “Integrated-Article” format following the guidelines of the Graduate and Postdoctoral Studies at Western University. It consists of six chapters. Chapter 1 introduces the dissertation subject by providing a general review and background about hollowcore slabs. Literature review is also included. The chapter concludes by stating the objectives of the conducted research and its original contribution. Abstracts of the following chapters are given below:

Chapter 2

Following installation of hollowcore slab floors, a layer of concrete topping is usually cast to connect the slabs and to have a level surface. According to current North American design standards, the topping should not be considered to act compositely with the slabs except if their surface satisfies a strict roughness requirement. This chapter evaluates if such a restriction is justified for hollowcore slabs with machine-cast and lightly-roughened surface finishes through an experimental program that involves pull-off, push-off and full-scale tests. The surface roughness was first evaluated. The peel (bond) and shear strengths of the interface between the slabs and the topping were then assessed using pull-off and push-off tests. Full-scale tests examined the overall behaviour of the composite slabs. The tested composite slabs exhibited higher tensile and shear stresses than the minimum limits set by North American design standards. The surface roughness threshold for machine-cast hollowcore slabs is estimated. The chapter presents the initial evidence that hollowcore slabs with machine-cast or lightly-roughened surfaces can be considered to act compositely with the concrete topping.

Chapter 3

Structural engineers can use the typical 50 mm topping concrete, usually cast on top of hollowcore slab floors, to increase the load-carrying capacity. North American design standards relate the horizontal shear strength at the interface between hollowcore slabs and the concrete topping to the slab surface roughness. Utilizing results of the push-off tests, an analytical model was applied to evaluate the shear and peel stiffness, (k_s) and (k_p), of the interface between the hollowcore slabs and the topping concrete. Structural engineers can utilize (k_s) and (k_p) values to model the composite action between hollowcore slabs and concrete topping. The analytical model was also used to evaluate the actual distribution of shear and peel stresses.

Chapter 4

Two analytical methods are presented in this chapter to evaluate the interfacial shear and peel stresses between hollowcore slabs and the topping concrete. The two methods consider linear behaviour of the composite section and utilize the shear and peel stiffness (k_s and k_p) obtained from the push-off tests in Chapter 3. Predictions of the two methods are then compared with the methods mentioned in the related provisions in the North American design standards. The two proposed methods take into account the deformations along the interface and utilize the interfacial stiffness to calculate the resulting stresses.

Chapter 5

Post-cracking behaviour of hollowcore slabs greatly affects their ultimate strength. Composite action adds another level of nonlinearity. This chapter presents a comprehensive nonlinear 3-D finite element analysis to study the behaviour of composite hollowcore slabs. The push-off and the full-scale tests were modeled using the finite element analysis software, ANSYS R15 (2013). The linear shear and peel interfacial stiffness were utilized to initiate the analysis. Iterations were conducted to obtain the final nonlinear stiffness that resembles the behaviour of the interface during those tests. The interface layer was modeled using nonlinear spring elements and the nonlinear material behaviour of the concrete and the prestressing strands were accounted for. The chapter demonstrates the innovative analysis techniques that were used to simulate the staged construction nature of the concrete topping. The results highlight the contribution of the applied load in increasing the interfacial shear stiffness through the confinement effect. They have also demonstrated a reduction in the shear stiffness due to the combined effect of shear and peel stresses along the interface.

Chapter 6

A conclusive summary of the work performed in this thesis is presented in this chapter along with recommendations for future research.

1.7 References

ACI 318, 1971, "Building Code Requirements for Structural Concrete (ACI 318-71) and Commentary," American Concrete Institute, Michigan, United States.

ACI 318, 1983, "Building Code Requirements for Structural Concrete (ACI 318-83) and Commentary," American Concrete Institute, Michigan, United States.

ACI 318, 2008, "Building Code Requirements for Structural Concrete (ACI 318-08) and Commentary," American Concrete Institute, Michigan, United States.

ANSYS® Academic Research, Release 15.0, 2013, ANSYS, Inc.

Birkeland, P.W., & Birkeland H.W., 1966. Connections in precast concrete construction. ACI Journal, 63(15), 345-368.

CSA A23.2, 2009, "Test methods and standard practices for concrete," Canadian Standard Association (CSA), Mississauga, Canada.

CSA A23.3, 2004, "Design of concrete structures (CSA A23.3-04)," Canadian Standard Association (CSA), Mississauga, ON, Canada.

Girhammar, U.A. and Pajari, M., 2008, "Tests and analysis on shear strength of composite slabs of hollow core units and concrete topping," *Construction and Building Materials*, 22, 1708-1722.

Hanson, N.W., 1960, “Horizontal Shear connections,” *Journal of the Research and Development Laboratories*, Portland Cement Association, V. 2, No. 2, pp. 38-58.

Hofbeck, J. A., Ibrahim, 1.0., and Mattock, A. H., 1969, "Shear Transfer in Reinforced Concrete", *ACI Journal*, V. 66, No, 2, February 1969, pp. 119-128.

Houde, J., and Mirza, M. S., 1974, "A Finite Element Analysis of Reinforced Concrete Beams," *ACI Special Publication 42, Shear in Reinforced Concrete*, V. 1, American Concrete Institute, Detroit, Michigan, 1974, pp. 103-128.

Izni S. Ibrahim, Kim S. Elliott and Simon Copeland, 2008. "Bending Capacity of Precast Prestressed Hollow Core Slabs with Concrete Toppings,” *Malaysian Journal of Civil Engineering*, 20(2): 260 – 283.

Izni Syahrizal Ibrahim & Kim S. Elliott., 2006, “Interface Shear Stress of Hollow Core with Concrete Toppings,” *6th International Conference on Concrete Engineering and Technology (CONCET)*. Kuala Lumpur: Institution of Engineers Malaysia.

Mast, R. F., 1968, "Auxiliary Reinforcement in Concrete Connections," *Journal of the Structural Division, ASCE*, V. 94, ST6, June 1968, pp. 1485-1504.

Mattock, A. H., 1974, Discussion of the paper "Modified Shear Friction Theory for Bracket Design," by B. R. Hermansen and J. Cowan, *ACI Journal,* V. 71, No. 8, August, 1974, pp. 421-423.

Mattock, A. H., and Hawkins, N. M., 1972, "Research on Shear Transfer in Reinforced Concrete," *PCI Journal*, V. 17, No. 2, March-April, pp. 55-75.

Mones, R.M., 2012, “Interfacial Strength Between Prestressed Hollow Core Slabs and Cast-in-Place Concrete Toppings,” *Masters of Science in Civil Engineering Thesis*, University of Massachusetts, Amherst, Massachusetts, United States.

Ozell, A.M., and J.W. Cochran, 1956, "Behaviour of Composite Lintel Beams in Bending," *PCI Journal*, V. 1, No. 1, pp. 38-48.

Scott, N.L., 1973, "Performance of precast prestressed hollow core slab with composite concrete topping," *PCI Journal*, 18(2), 64-77.

Technical Bulletin 74-B6, 1974, "Composite Systems Without roughness," *Concrete Technology Association (CTA)*, CTA 35, pp 271-316.

Technical Bulletin 76-B4, 1976, "Composite Systems without Ties," *Concrete Technology Association (CTA)*, CTA 36, pp 317-360.

Walraven Joost, Frenay Jerome and Pruijssers Arjan, 1987, "Influence of Concrete Strength and Load History on the Shear Friction Capacity of Concrete Members," *PCI Journal*, January-February, pp. 66-84.

CHAPTER TWO

2 Experimental Investigation of the Composite Action between Hollowcore Slabs and Concrete Topping

Hollowcore slabs are used in floors and roofs of residential, industrial, and commercial buildings as well as detention centers. They are characterized by an initial camber that is formed during the prestressing process. To account for surface irregularities resulting from this camber and to connect the slabs, a layer of concrete topping is usually cast. If the interface between the topping and the slabs has adequate shear resistance, the composite action developed between the two concrete layers increases the rated capacity of the slabs. Values of 0.70 MPa and 0.55 MPa are specified by CSA A23.3-04 (2004) and ACI 318-08 (2008), respectively, for the interface shear resistance. Intentional roughening of the slabs surface is accepted as a method to guarantee achieving such shear strength. The minimum acceptable amplitudes for such roughness are 6.35 mm (clauses 11.6.9 and 17.5.3.3 of ACI 318-08 (2008)) and 5.00 mm (explanatory note N17.4.3.2 of CSA A23.3-04 (2004)). These amplitudes induce additional costs to hollowcore slab manufacturers. In a typical precast operation, the default surface finish for hollowcore slabs is generally referred to as ‘‘machine-cast finish.’’ This finish, although different from manufacturer to manufacturer, has a surface roughness that does not satisfy the aforementioned requirement. The literature review mentioned in Chapter 1 provided some evidence about the composite action for hollowcore slabs. However, details about slip and peel deformations, acceptable levels of peel and shear stresses and full-scale composite behavior are scarce in the literature.

This chapter presents a comprehensive experimental program to assess the composite action between hollowcore slabs and the concrete topping by using: (1) pull-off tests, (2) push-off tests and (3) full-scale tests. The tested hollowcore slabs were supplied by two Ontario manufacturers, A and B, and had two surface finish designations: “machine-cast finish” and “lightly-roughened finish.” The tested slabs were overlaid with a 50 mm concrete topping similar to common practice.

Before conducting the experimental tests, the surface roughness of the tested slabs was evaluated using the ASTM E965 (2006) standard method. The method was only carried out for the slabs with machine-cast surface. A total of sixty nine pull-off tests and twelve push-off tests were attempted. Six full-scale tests were performed to examine the overall behaviour.

2.1 Test Specimens

The tested hollowcore slabs were received from two manufactures (A and B) in Ontario, Canada in four shipments. Their surface finish was either machine-cast or lightly-roughened using a conventional steel broom. Table 2.1 summarizes information about the tested slabs and the conducted tests. The table also shows the approximate dates of delivery for each shipment. The nominal concrete compressive strength was 41 MPa as per manufacturer's specifications. Typical surface finishes are shown in

Fig. 2.. The depth and width of the surface grooves for the lightly-roughened slabs were about 1 mm and they were spaced at about 25 mm. The corresponding uniform roughness for these grooves is about 0.04 mm.

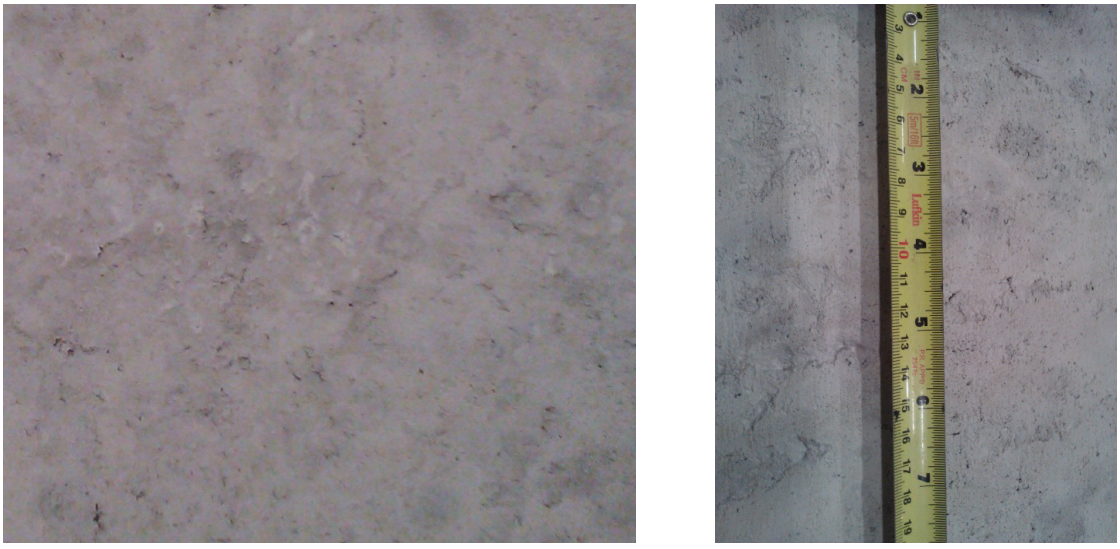

(a) Machine-cast finish.

(b) Lightly-roughened slab (A).

(c) Lightly-roughened slab (B).

Fig. 2.1: Typical surface finishes.

Table 2.1: Hollowcore slab specimens.

Shipment	**Manufacturer**	**Qty.**	**Slab Label**	**Surface Finish***	**Tests**	**Size, mm (L,W,T)***
Sept. 2011 **Shipment #1**	A	2	PMA1-1, PMA1-2	M	6 Pull-off	1220, 1220, 203
		3	PRA1-1, PRA1-2, PRA1-3	R	9 Pull-off	1220, 1220, 203
		3	SMA1-1, SMA1-2	M	2 Push-off	1220, 1220, 203
		3	SRA1-1, SRA1-3	R	2 Push-off	1220, 1220, 203
	B	3	PRB1-1, PRB1-2, PRB1-3	R	9 Pull-off	1220, 1220, 203
		3	SRB1-1, SRB1-2	R	2 Push-off	1220, 1220, 203
Dec. 2012 **Shipment #2**	A	2	FMA2-1, FMA2-2C	M	6 Pull-off, 2 Full-scale	3658, 1220, 203
		1	FRA2-3	R	3 Pull-off, 1 Full-scale	3658, 1220, 254
	B	2	FMB2-1C, FMB2-2	M	6 Pull-off, 2 Full-scale	3658, 1220, 203
		1	FMB2-3	M	3 Pull-off, 1 Full-scale	3658, 1220, 254
May 2013 **Shipment #3**	A	1	FMA3-1	M	3 pull-off	3658, 1220, 254
July 2013 **Shipment #4**	A	3	PSMA4-1, PSMA4-2, PSMA4-3	M	12 Pull-off, 3 Push-off	1220, 1220, 203
	B	3	PSMB4-1, PSMB4-2, PSMB4-3	M	12 Pull-off, 3 Push-off	1220, 1220, 203

* M: machine-cast, R: lightly-roughened, L: length of slab, W: width of slab, T: thickness of slab

The concrete compressive strength for the full-scale test specimens was evaluated using ASTM C349 (2008) "*standard procedure for evaluating the compressive strength of concrete for a lab tested specimen.*" After completing the full-scale tests, three 50 mm cubes were sampled from the edges of each slab as shown in Fig. 2.. The equivalent cylinder concrete compressive strengths are given in Table 2.2. The Number of prestressing strands for each slab is also given in the table. Fig. 2. illustrates a typical cross section of the slabs.

Fig. 2.2: 50 mm cubes for compressive strength test.

Table 2.2: Information for the full-scale slabs.

Slab Label	**Average Concrete Compressive Strength f'_c (MPa)**		**Strand Pattern**
	Average Value	**Standard Deviation**	
FMA2-1	53	2.9	4- ½" strands
FMA2-2C	50	3.1	4- ½" strands
FRA2-3	51	1.2	6- ½" strands
FMB2-1C	62	4.1	7- ½" strands
FMB2-2	58	3.8	7- ½" strands
FMB2-3	60	1.4	7- ½" strands

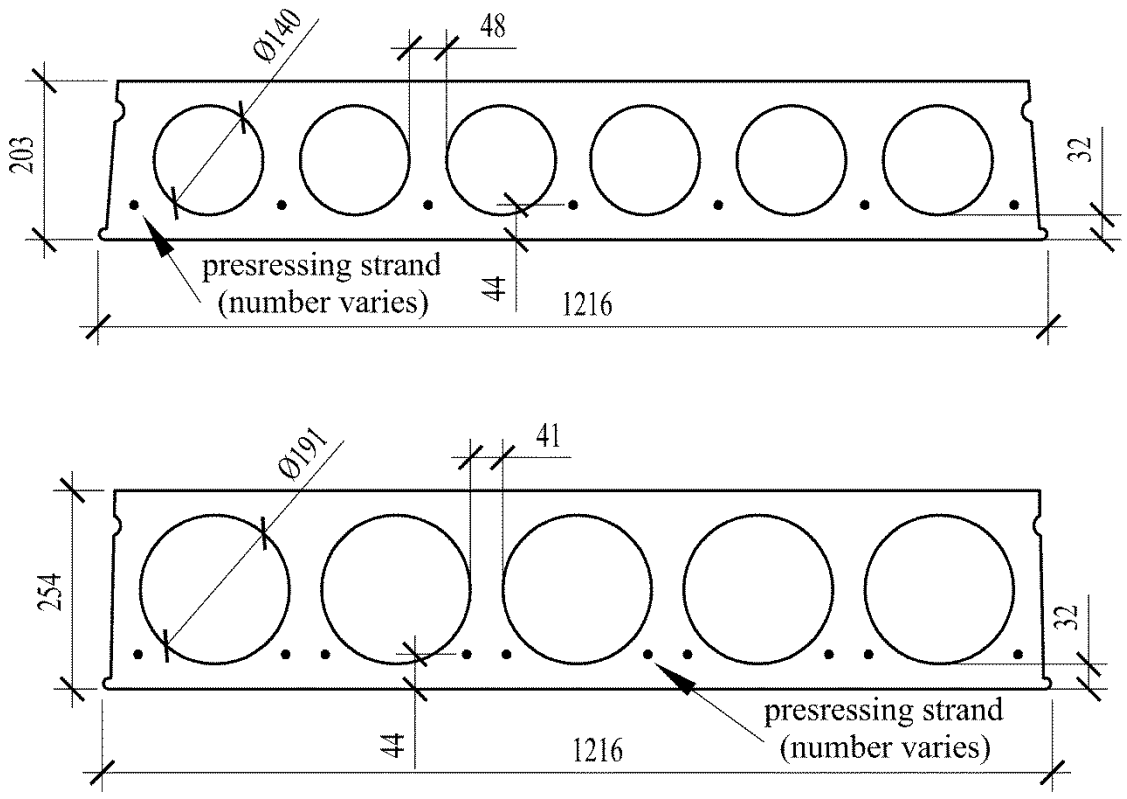

Fig. 2.3: Typical cross-section of the tested hollowcore slabs.

2.2 Concrete Topping

Properties of the concrete topping were chosen in accordance with the industry standards. A thickness of 50 mm was used. The concrete mix contained 10 mm pea stone aggregates and had an average slump of 120 mm. Before casting the topping, the surface of the hollowcore slabs was submerged with water and then dried to obtain a Saturated Surface Dry (SSD) condition, which prevents the surface from absorbing water from the concrete topping. The area of the concrete topping varied as shown in Table 2.3.

Table 2.3: Concrete topping.

Slab Label	Tests	Topping Size mm (L, W, T)*	Avg. Concrete Compressive Strength and (STD)* MPa
PMA1-1, PMA1-2	Pull-off	1220, 1220, 50	32 (1.6)
PRA1-1, PRA1-2, PRA1-3	Pull-off	1220, 1220, 50	32 (1.6)
SMA1-1, SMA1-2	Push-off	508, 508, 50	32 (1.6)
SRA1-1, SRA1-3	Push-off	508, 508, 50	32 (1.6)
PRB1-1, PRB1-2, PRB1-3	Pull-off	1220, 1220, 50	32 (1.6)
SRB1-1, SRB1-2	Push-off	508, 508, 50	32 (1.6)
FMA2-1, FMA2-2C	Pull-off, Full-scale	3658, 1220, 50	30 (1.2)
FRA2-3	Pull-off, Full-scale	3658, 1220, 50	30 (1.2)
FMB2-1C, FMB2-2	Pull-off, Full-scale	3658, 1220, 50	30 (1.2)
FMB2-3	Pull-off, Full-scale	3658, 1220, 50	30 (1.2)
FMA3-1	Pull-off	1000, 500, 50	33 (0.8)
PSMA4-1, PSMA4-2, PSMA4-3	Pull-off Push-off	1000, 500, 50 508, 508, 50	33 (0.8)
PSMB4-1, PSMB4-2, PSMB4-3	Pull-off Push-off	1000, 500, 50 508, 508, 50	33 (0.8)

*L: length, W: width, T: thickness, STD: standard deviation

For the 4th shipment, two concrete areas were cast on each slab to conduct both pull-off and push-off tests. The two areas were separated by utilizing wood forms. Table 2.3 also presents the average compressive strength of the concrete topping as was determined using the standard method ASTM C39 (2005). Wet curing was applied for three days according to clause 7.4.2 of CSA A23.1-09 (2009). The slabs were also covered with moisture retaining plastic sheets for at least seven days after casting. Temperature of the laboratory was kept constant at 23° C. Formwork and casting of the concrete topping are illustrated in Fig. 2. .

(a) Before casting the topping

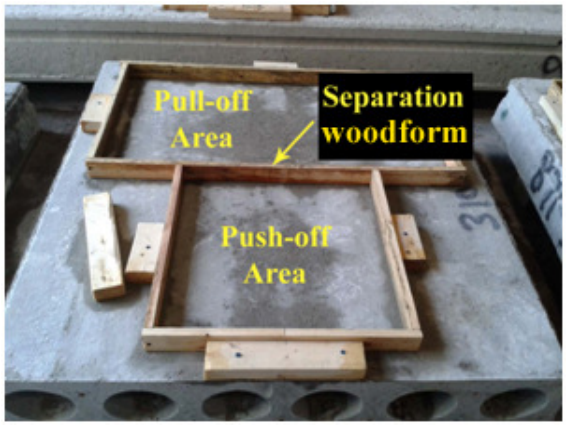

(b) Before casting (4th shipment)

(c) After casting the topping (1st shipment)

(d) After casting the topping (2nd shipment)

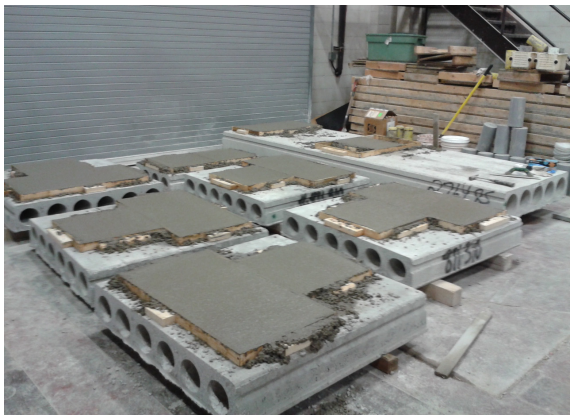

(e) After casting the topping (4th shipment)

(f) Curing of the concrete topping

Fig. 2.4: Formwork and casting of the concrete topping.

2.3 Pull-off Tests

The concrete topping can be considered fully bonded to the hollowcore slab if the bond strength between the two concrete layers is not less than 0.9 MPa (clause 7.6.4.3.2 of CSA A23.1-09 (2009)). This strength can be evaluated in the field using test method A23.2-6B (2009) *"Determination of bond strength of bonded toppings and overlays and of direct tensile strength of concrete, mortar, and grout"* of CSA A23.2-09 (2009). This method involves core drilling of an annular ring into the composite slab and applying a tensile force to the concrete topping. Similar procedure is used in Europe (FIP, 1982). This section provides details about the pull-off tests conducted in this research.

2.3.1 Surface Roughness Evaluation

The degree of surface roughness varies between hollowcore slabs because of differences in the manufacturing process and/or equipment maintenance. The surface roughness for hollowcore slabs with a machine-cast surface was evaluated using ASTM E965 (2006) "*Standard Test Method for Measuring Pavement Macrotexture Depth Using a Volumetric Technique*". This procedure is generally used for pavements and is suitable for surfaces with voids smaller than 25.4 mm, which is the case for the considered surface. The proviso, however, is that the voids should be uniformly distributed over the surface. The procedure is not feasible for surfaces with random grooves and irregular texture, and, thus cannot be used for steel broom roughened surfaces.

Fig. 2. gives details about the procedure. The tested surface is first cleaned using compressed air and a steel brush. Glass beads that pass through sieve No. 60 and are retained on sieve No. 80 are then spread over the slab surface in a circular motion using a hard plastic disk. When the beads are flush with the surface, three measurements of the diameter of the resulting circle are taken. Mean Texture Depth (MTD) is then calculated by dividing the volume of the used beads by the average area of the circle.

(a) Tools (b) Typical circle

Fig. 2.5: Surface Roughness Test.

Table 2.4: Surface roughness evaluation results

Slab Label	**Surface Roughness (mm)**	**Average Roughness, mm**
PMA1-1	0.341	0.353
PMA1-2	0.360	
SMA1-1	0.351	
SMA1-2	0.361	
FMA2-1	0.325	0.320
FMA2-2C	0.314	
FMB2-1C	0.320	0.311
FMB2-2	0.297	
FMB2-3	0.315	
FMA3-1	0.314	0.314
PSMA4-1	0.140	0.165
PSMA4-2	0.202	
PSMA4-3	0.152	
PSMB4-1	0.105	0.106
PSMB4-2	0.121	
PSMB4-3	0.093	

Results of surface roughness are shown in Table 2.4. It is clear that roughness of the machine-cast finish is significantly less than the intentional roughness specified by North American design standards. The results show the high variability of roughness from manufacturer to another and within the same manufacturer. The roughness of slabs delivered in the 4th shipment is significantly less than slabs from previous shipments.

2.3.2 Pull-off Test Setup

Pull-off tests were performed according to procedure A of the standard test method A23.2-6B[15] "*Determination of bond strength of bonded toppings and overlays and of direct tensile strength of concrete, mortar, and grout*" that is outlined CSA A23.2-09 (2009). In this procedure, the tensile strength of the interface between two bonded concrete surfaces is evaluated using a mechanical pullout apparatus that consists of three main components: 1) a pull-off steel disk, which is attached to the concrete topping; 2) a rigid frame to support the hydraulic jack applying the pull-off force and 3) a load cell to record the failure load. This apparatus was manufactured at Western University. The diameter of the used disks was 95 mm, which is slightly smaller than the inner diameter of the bit used for core drilling.

Two disk thicknesses were utilized in this project: 1) 100 mm to allow the tensile force to be uniformly distributed over the interface area as illustrated in Fig. 2.(a) and 2) 10 mm to match the common industry practice. The first and second disks were used for the (1st and 2nd) and the (3rd and 4th) shipments, respectively. The disks are shown in Fig. 2.. A steel pipe with thickness of 10 mm was used to provide the needed rigid frame. It encompassed the load cell and supported the hydraulic jack. Fig. 2. shows the pull-off apparatus and the general test setup.

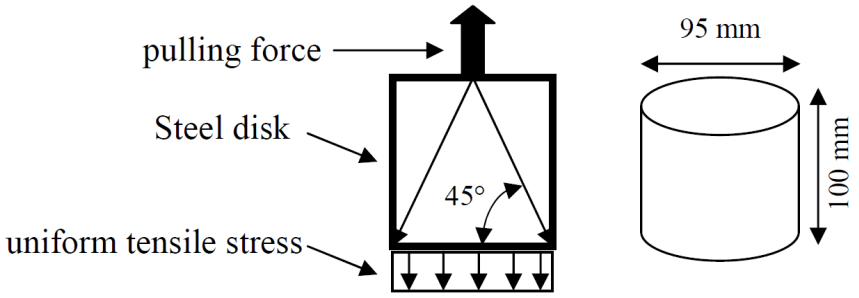

(a) Expected uniform stress distribution under disk No.1

(b) Disk No. 1 (thickness = 100 mm)

(c) Disk No. 2 (thickness = 10 mm)

Fig. 2.6: Steel disks for the pull-off tests.

2.3.3 Pull-off Test Procedure

The pull-off test was initiated by drilling a core through concrete topping that penetrates a minimum of 30 mm into the hollowcore slab surface as illustrated in Fig. 2.. The diameter of the core was 100 mm, matching the current industry practice. Fig. 2. shows the core drilling. The steel pull-off disks were bonded to the cores using epoxy compound after roughening the top surface of the core and the bottom surface of the disk as shown in Fig. 2.. The disks were installed on the core using a conventional 5 minute epoxy compound. Fig. 2. shows the core locations for the tested slabs.

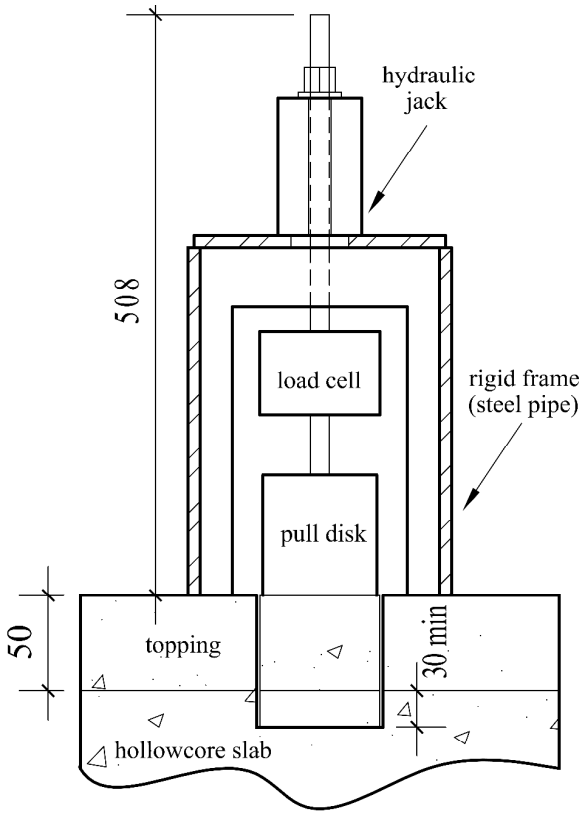

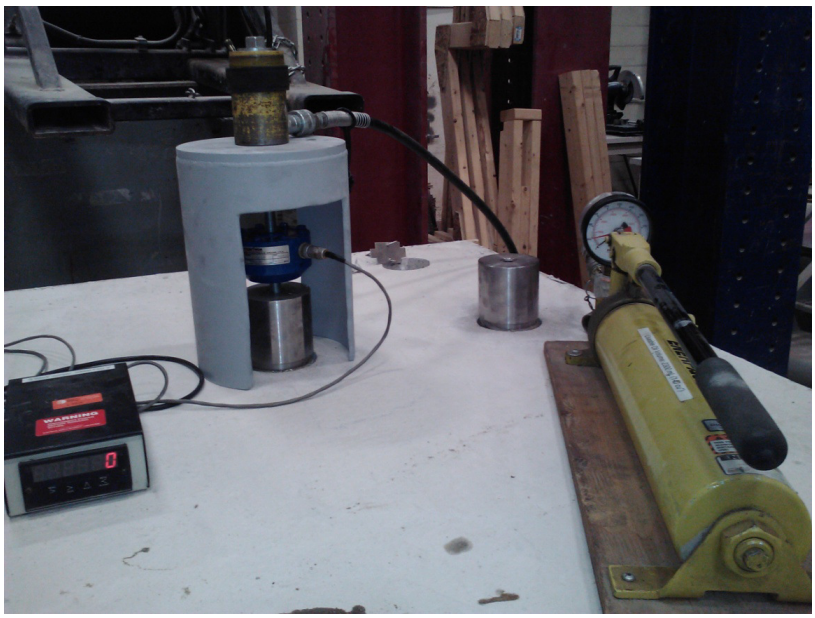

Fig. 2.7: Pull-off apparatus (dimensions in mm).

(a) Core drilling

(b) Core cleaning

(c) Roughening of core surface

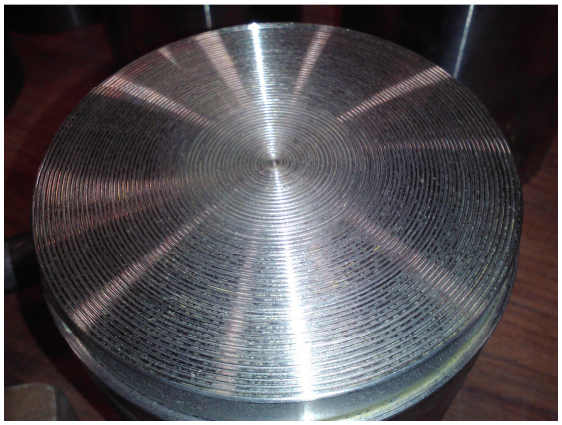

(d) Roughening of disk bottom surface

Fig. 2.8: Core drilling and roughening process.

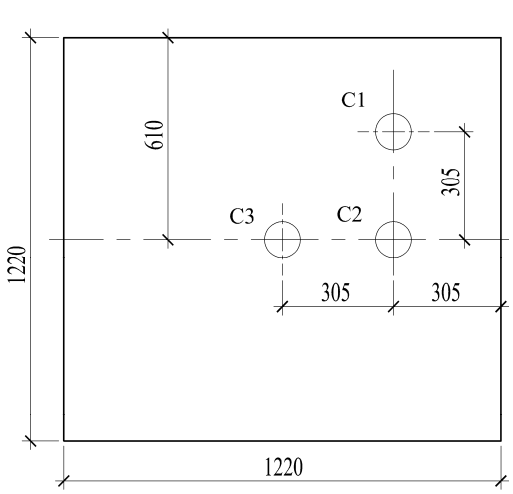

(a) 1st shipment

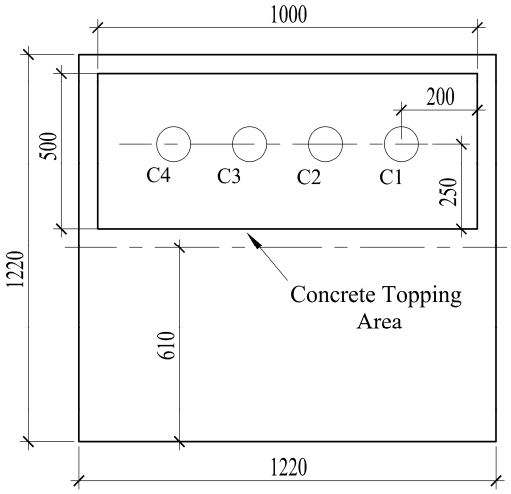

(b) 4th shipment

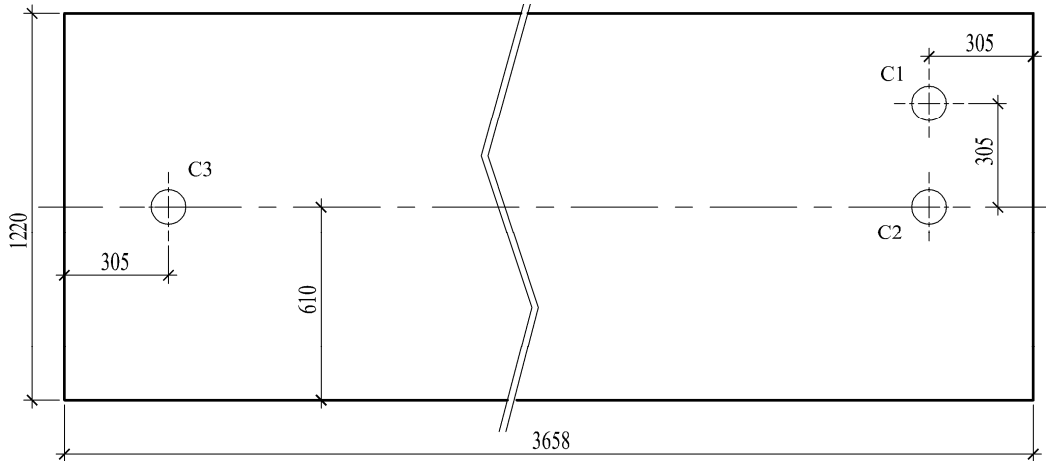

(c) 2nd shipment

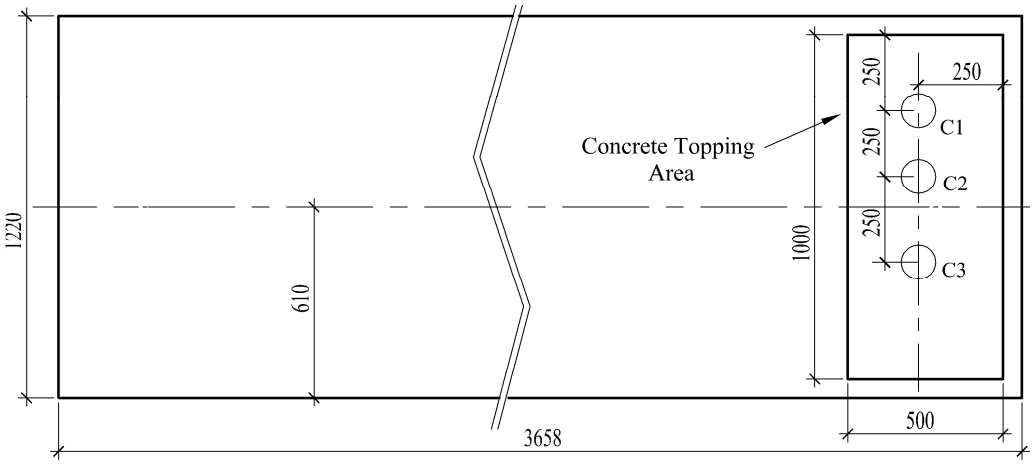

(d) 3rd shipment

Fig. 2.9: Core Locations (dimensions in mm).

Fig. 2. shows the process of leveling the pull-off disk and attaching the pull-off apparatus. Tests were conducted after 24 hours of the epoxy application. The load cell was first attached to the pull-off disk using a threaded rod. The rate of loading was approximately 80 N/s, which is within the (50 to 100 N/s) range specified in clause 5.1.4 of A23.2-6B (2009). It was controlled by monitoring the digital load meter while increasing the tensile load using a manual hydraulic pump.

(a) Bonding of the steel disk using epoxy.

(b) Disk attachment to pull-off apparatus.

Fig. 2.10: Pull-off test preparation.

2.3.4 Results and Discussion

The maximum load prior to failure was retrieved from the digital load meter and recorded for each test. The weights of the steel disk, load cell and threaded rods were deducted from the maximum load. The load was then divided by the cross sectional area of the core to obtain the bond strength at failure. Fig. 2. shows the observed types of failure during the pull-off tests. The bond strength and the type of failure associated with each core are summarized in Table 2.5. Test results are also presented in Fig. 2.. The 0.9 MPa limit required by A23.2-6B (2009) is highlighted. Results of 17 tests from manufacturer A and 17 tests from manufacturer B were below the 0.9 MPa limit. The thickness of the

steel disk did not seem to affect the results as specimen FMA3-1 that was tested using the 10 mm disk achieved comparable results to specimens of the 1st and 2nd shipments that had similar roughness and were tested using the 100 mm disk.

(a) Interface failure (I)

(b) Epoxy failure (X)

(c) Hollowcore slab failure (H)

Fig. 2.11: Failure types.

Table 2.5: Pull-off test results

Slab Label	**Core Bond Strength, MPa / Failure Type**				**Average Bond Strength, MPa**
	C1	**C2**	**C3**	**C4**	
Hollowcore slabs with machine-cast surface:					
PMA1-1	1.51/I	1.78/I	2.63/I	--	1.97
PMA1-2	3.91/H	3.06/H	2.81/H	--	3.26
FMA2-1	1.71/I	1.18/I	1.99/X	--	1.63
FMA2-2C	0.44/I	1.14/X	1.96/T	--	1.18
FMB2-1C	2.19/I	2.57/I	1.23/I	--	2.00
FMB2-2	0.00/D	0.77/I	1.70/I	--	0.80
FMB2-3	2.31/X	2.48/X	1.87/H	--	2.22
FMA3-1	1.52/X	1.34/X	1.44/I	--	1.43
PSMA4-1	0.00/I	0.00/I	0.00/I	0.00/I	0.00
PSMA4-2	0.58/X	0.78/I	0.60/X	0.76/I	0.68
PSMA4-3	0.00/I	0.00/I	0.00/I	0.00/I	0.00
PSMB4-1	0.00/I	0.00/I	0.00/I	0.00/I	0.00
PSMB4-2	0.00/I	0.00/I	0.51/I	0.61/X	0.56
PSMB4-3	0.00/I	0.00/I	0.00/I	0.00/I	0.00
Hollowcore slabs with lightly-roughened surface:					
PRA1-1	0.2/I	1.28/I	1.60/X	--	1.03
PRA1-2	0.66/I	0.30/I	1.23/I	--	0.73
PRA1-3	1.06/I	1.47/I	1.66/I	--	1.39
PRB1-1	1.84/X	1.65/X	2.09/I	--	1.86
PRB1-2	1.48/I	1.31/I	0.66/I	--	1.15
PRB1-3	1.36/I	0.02/I	0.81/I	--	0.73
FRA2-3	2.29/I	1.33/H	0.78/I	--	1.47

D: concrete topping debonded from hollowcore slabs during coring, H (hollowcore failure): failure occurred in the hollowcore slab, I (interface failure): failure occurred at the interface layer, T (topping failure): failure occurred in the concrete topping, X (epoxy failure): the pull-off disk separated from the concrete topping.

Note: underlined values indicate bond strength less than the 0.90 MPa required by A23.2-6B (2009).

Considering hollowcore slabs with machine-cast surface, Fig. 2. shows the pull-off test results in terms of surface roughness. It can be observed that slabs with surface roughnesses that exceed 0.30 mm achieved bond strength higher than 0.9 MPa with the exception of one test, slab FMA 2-2. Slabs of 4^{th} shipment showed poor performance (24 tests). Four of the specimens failed at the interface and did not provide any tensile resistance. Two slabs, PSMA4-2 and PSMB4-2, provided unacceptable bond strength. This poor performance can be attributed to the considerably low surface roughness for this shipment that is below 0.3 mm roughness. The bond between the concrete topping and the hollowcore slab surface is controlled by two mechanisms: chemical bond and mechanical bond. The latter is dependent on the surface roughness. The chemical bond is affected by the moisture content of the hollowcore slab surface, which was optimized utilizing the SSD moisture condition. The obtained results suggest that machine-cast surfaces with a minimum surface roughness of 0.3 mm will provide adequate mechanical bonding to achieve the 0.9 MPa bond strength specified by A23.2-6B (2009).

The light roughness produced by the steel broom was equivalent to a uniform roughness of about 0.04 mm. This additional roughness was very small and did not increase the pull-off strength. Six tests of the lightly-roughened slabs produced unsatisfactory strength. This low strength might be due to low roughness of the original machine-cast surface.

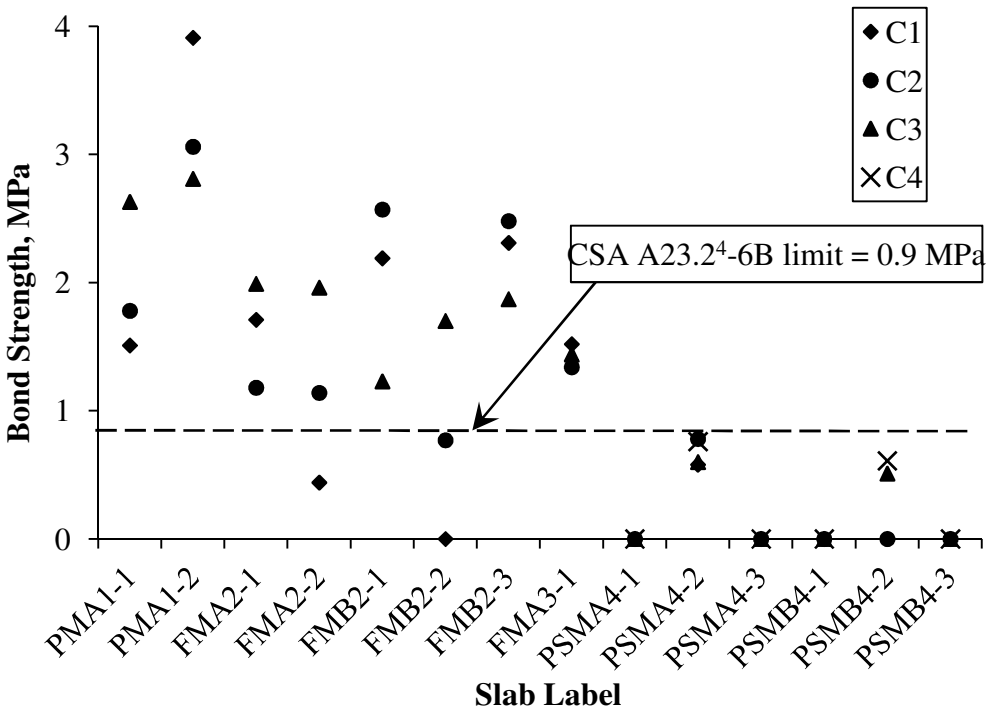

(a) Machine-cast slabs

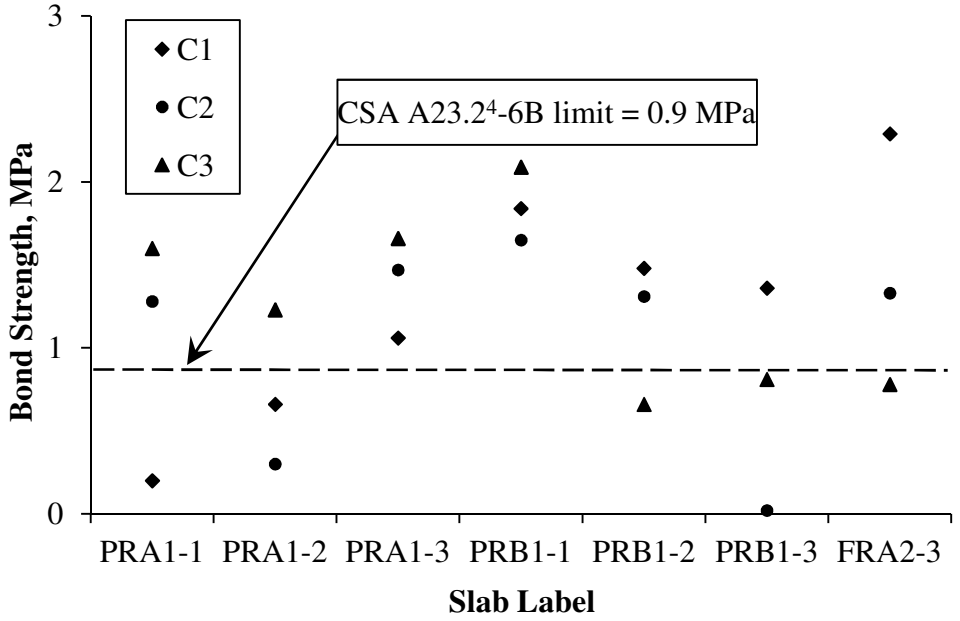

(b) Lightly-roughened slabs

Fig. 2.12: Pull-off test results

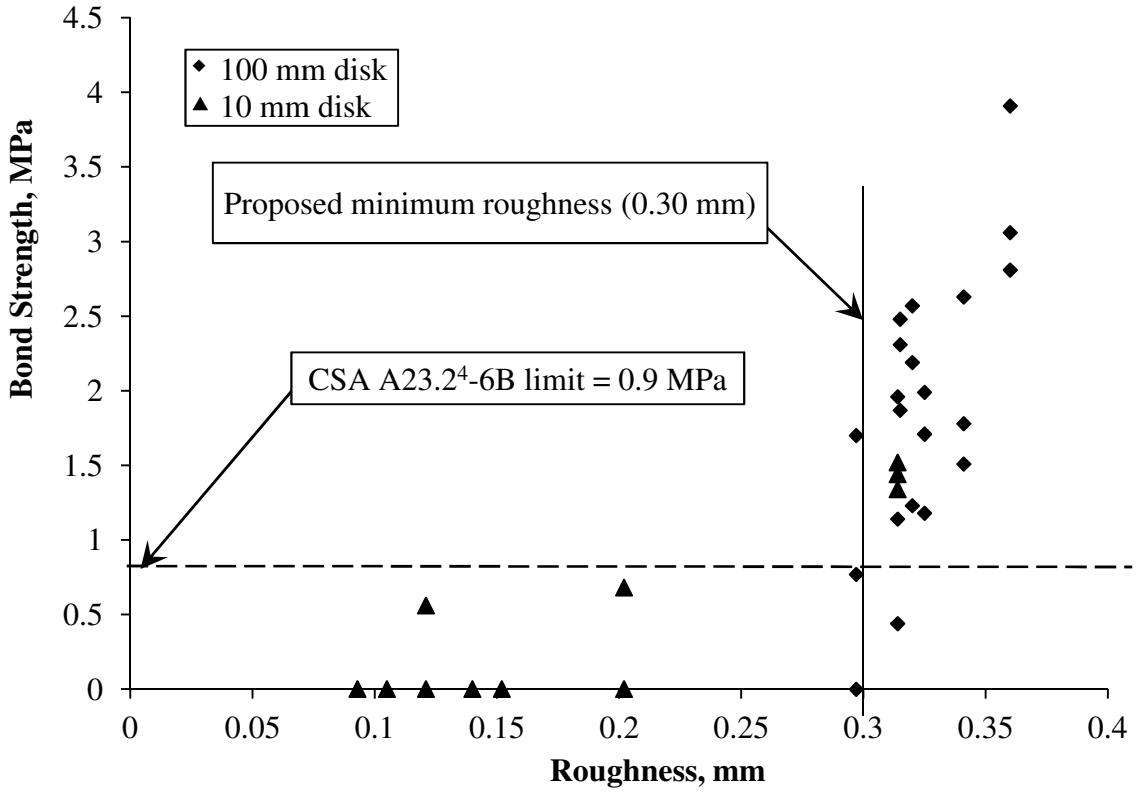

Fig. 2.13: Pull-off test results in terms of hollowcore slab surface roughness

2.4 Push-off Tests

The push-off tests were conducted in a vertical orientation to permit easier alignment of the MTS hydraulic actuator with the existing vertical support frame at the structures lab at Western. Fig. 2. shows a hollowcore slab installed in the vertical direction with its concrete topping resting on a 50 mm thick steel plate. When a vertical force is applied using the shown MTS hydraulic actuator, a spreader steel beam distributes the force on the hollowcore slab. The steel plate then reacts with a force on the concrete topping. This force generates shear stresses along the interface between the slab and the topping.

A steel frame, positioned behind the hollowcore slab, prevents the lateral movement. The soffit side of the hollowcore slab is sufficiently smooth, which allows free movement of the slab relative to the steel frame. 50 mm wide by 3 mm thick Korolath bearing pads are used under the steel spreader beam and between the steel plate and the concrete topping to guarantee a uniform stress distribution at those locations. The tests were conducted by applying the load using the MTS actuator at a rate of 10 kN per minute.

To capture the state of strains in the concrete topping, five strain gauges were attached to its top surface as illustrated in Fig. 2.. Strain gauges S1, S3, and S5 measured the strains in the direction of the applied load and strain gauges S2 and S4 measured the distribution of stresses across the topping width. The push-off test induced two types of stresses on the interface between the concrete topping and the hollowcore slab: (1) shear stresses (stresses parallel to the interface) and (2) peel stresses (stresses perpendicular to the interface).

Movement in the shear and peel directions were recorded using four Linear Variable Displacement Transducers (LVDTs), L1 to L4, as shown in Fig. 2.. LVDTs L1 and L2 measured the peel deformations and LVDTs L3 and L4 measured the shear deformations between the hollowcore slab and the concrete topping.

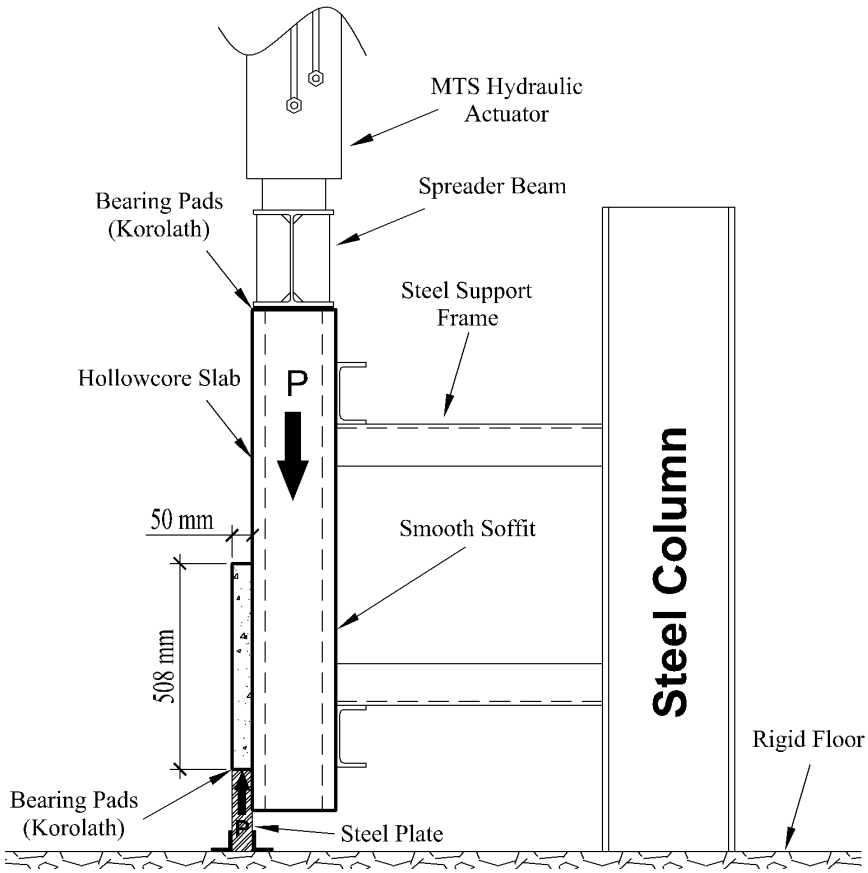

(a) Schematic

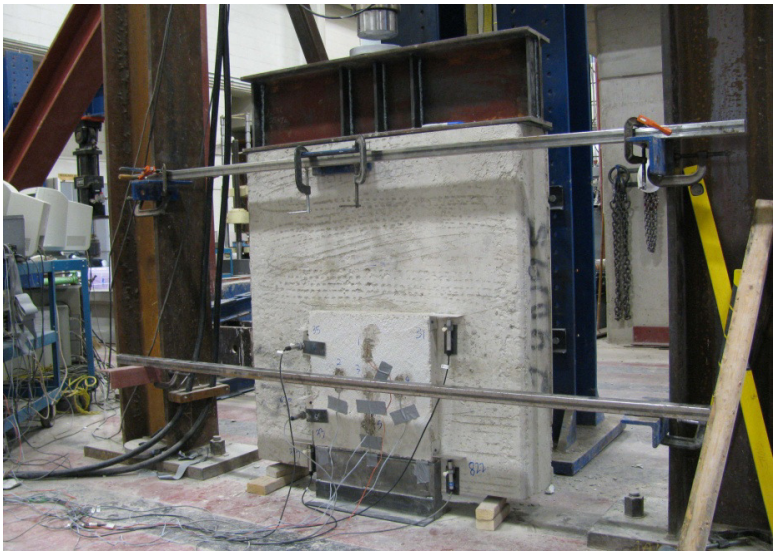

(b) Photo

Fig. 2.14: Push-off test setup.

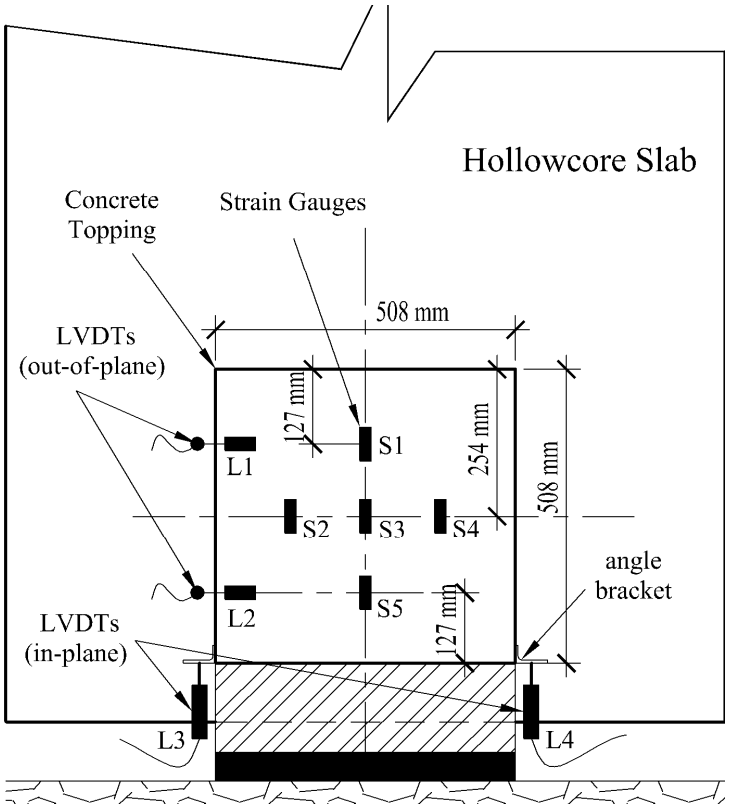

Fig. 2.15: Push-off test instrumentation.

2.4.1 Test Results and Discussion

The push-off tests were conducted on slabs of the 1st and the 4th shipments. Slabs PSMA4-1, PSMB4-1, PSMB4-2 and PSMB4-3 achieved zero shear strength, which is directly related to their low surface roughness. The average horizontal shear strength $v_{h\ \text{avg.}}$ can be obtained from the push-off tests using Eq. 2.1, where P_u is the ultimate applied load, at which the concrete topping is separated from the hollowcore slab, and A is the interface area. Values of P_u and the corresponding slip and peel deformations and $v_{h\ \text{avg.}}$ are shown in Table 2.6.

$$v_{h\ \text{avg.}} = \frac{P_u}{A} \qquad 2.1$$

Table 2.6: Push-off test results

Slab	P_u (kN)	Slip (mm)	Peel (mm)	$v_{h\ avg.}$ (MPa)
SMA1-1	510	__	__	1.98
SMA1-2	359	0.606	0.404	1.39
SRA1-1	504	0.956	0.913	1.95
SRA1-3	554	0.35	0.696	2.15
SRB1-1	223	0.311	0.582	0.860
SRB1-2	182	0.174	0.134	0.710
PSMA4-2	308	0.851	0.851	1.19
PSMA4-3	66.0	0.980	0.017	0.256

Interfacial shear between the concrete topping and the hollowcore slab was the dominant failure type observed in the tests, Fig. 16(a). However, failure of slab SRA1-1 was affected by the peel stresses as shown in Fig. 2.16(b).

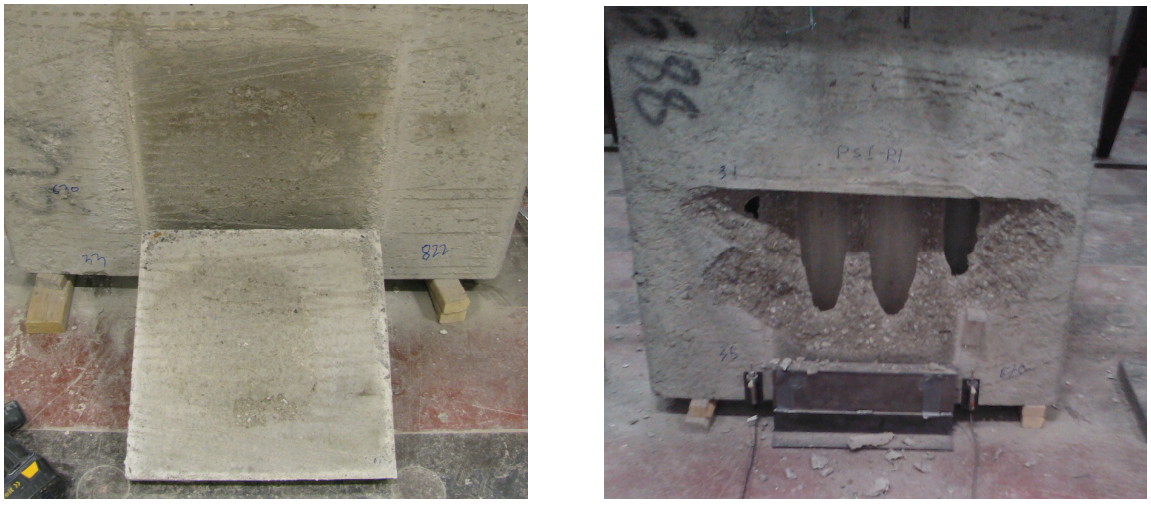

(a) Interface shear failure (b) Peel failure in hollowcore slab

Fig. 2.16: Failure types of push-off tests.

Three of the machine-cast finished slabs achieved average shear strength higher than 0.70 MPa and 0.55 MPa limits that are required by CSA A23.3-04 (2004) and ACI 318-08 (2008), respectively. However, one slab did not achieve the required limit, PSMA4-3 mainly because of its low surface roughness (0.152 mm). On the other hand, the lightly-roughened slabs, reported in Table 2.6, achieved the required limits. Considering manufacturer A, the lightly-roughened slabs demonstrated higher failure loads than the machine-cast slabs. Strains recorded by strain gauges S2, S3 and S4 exhibited close agreement in measured values and trends as illustrated in Fig. 2.. The slight variation in the readings may be due to misalignment of the direction of the strain gauges relative to the load direction.

These readings show that the load was almost uniformly distributed across the width of the topping. The concrete strain readings from strain gauges S1, S3 and S5 are shown in Fig. 2.. Strain gauge S5 initially recorded the highest readings. At failure, Strain gauges S3 and S1 recorded values higher than S5 in the majority of the samples indicating that the interface layer in the zone of S5 had fractured. Considering slab SMA1-2, strain gauge S5 initially recorded the highest readings.

At a load level of about 200 kN, strains measured by S3 started to increase at a high rate indicating a fracture in the zone of S5. At load level of about 320 kN, readings from strain gauge S1 started to rise. This mechanism illustrates a progressive type of failure, which is initiated by the fracture of the interface between the hollowcore slab and concrete topping at the loading end.

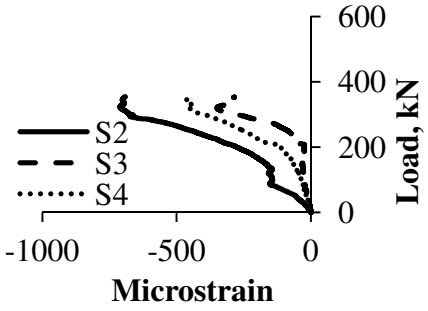

(a) Slab SMA1-2

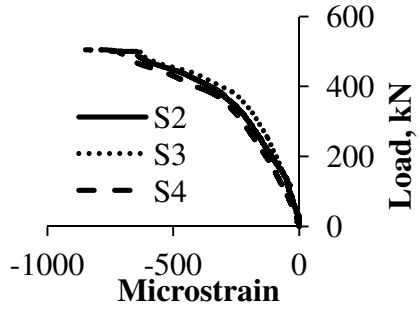

(b) Slab SRA1-1

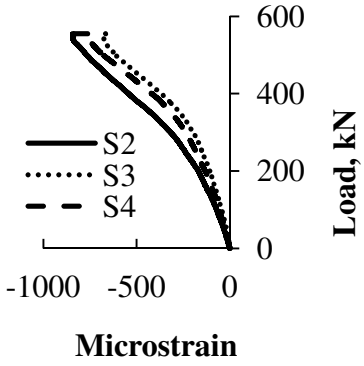

(c) Slab SRA1-3

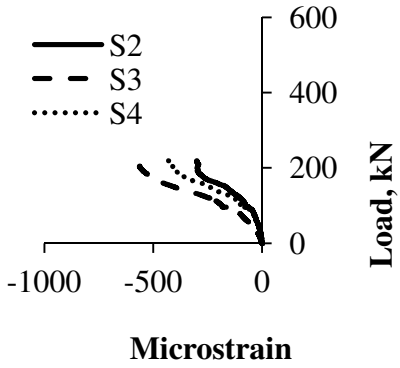

(d) Slab SRB1-1

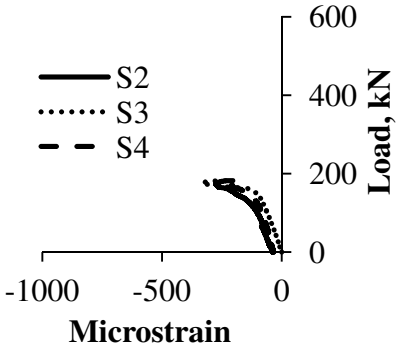

(e) Slab SRB1-2

Fig. 2.17: Readings of strain gauges S2, S3 and S4.

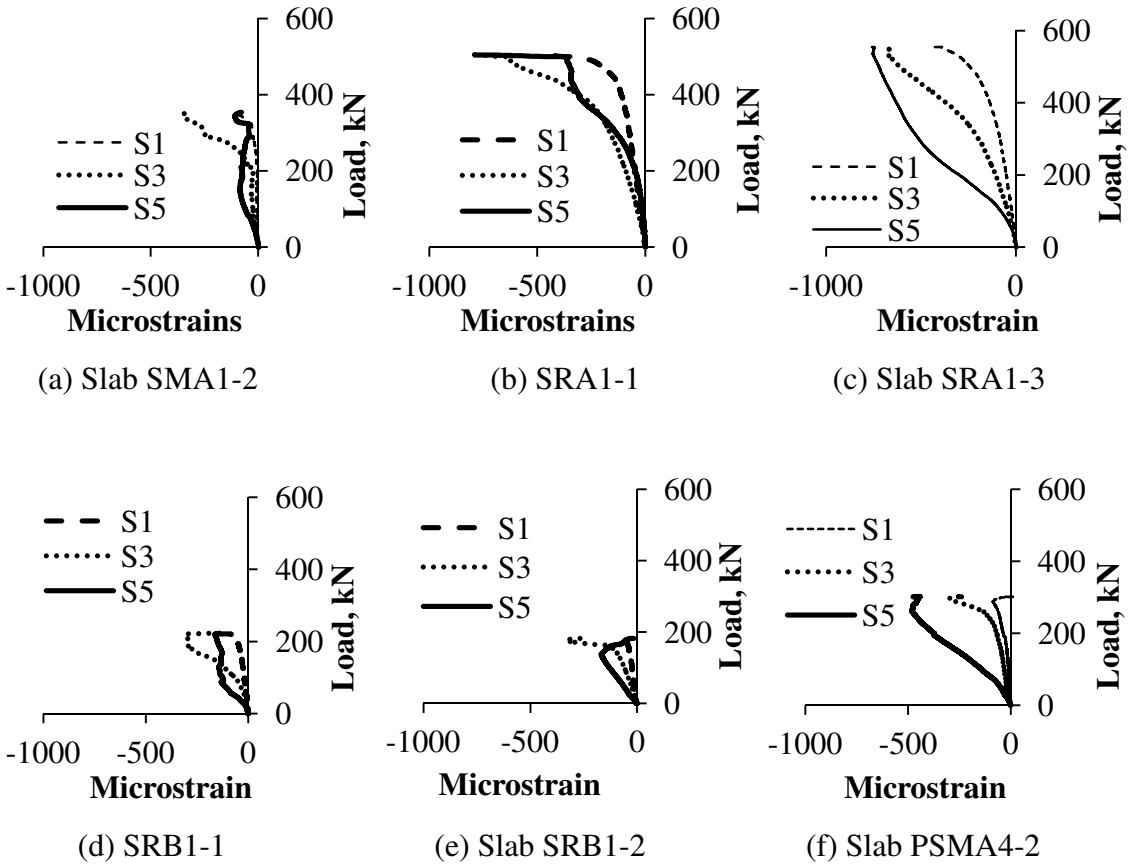

Fig. 2.18: Readings of strain gauges S1, S3 and S5.

Reading of the strain gauges gave evidence of load redistribution within the slab surface. However, extremely brittle and abrupt failure was observed because of the small recorded slips. The average slips at failure were calculated using readings of LVDTs L3 and L4 and are shown in Table 6. The load versus slip curves are also shown in Fig. 2.. The peel deformations recorded by LVDT L2 are shown in Fig. 2.. Readings from LVDT L1 were negligible.

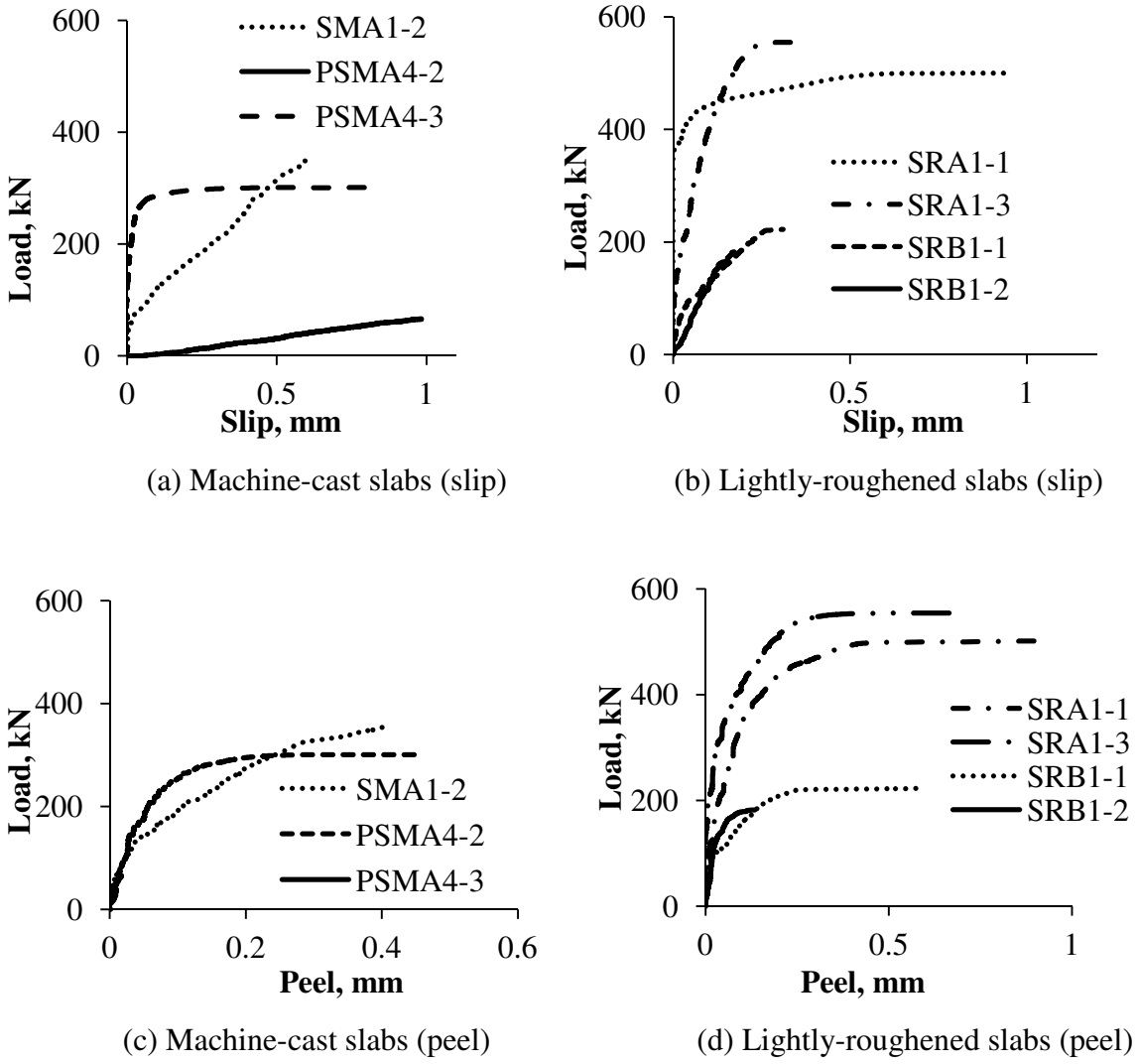

(a) Machine-cast slabs (slip)

(b) Lightly-roughened slabs (slip)

(c) Machine-cast slabs (peel)

(d) Lightly-roughened slabs (peel)

Fig. 2.19: Slip and peel results based on slabs' surface finish.

The shear force is resisted at the interface by two mechanisms, bond and friction. The shear and peel stiffness reduce when the bond between the hollowcore slab and the topping is lost. This is apparent in all the slip and peel graphs for all specimens, where for instance in slab SRA1-3, the slip and peel deformations did not initiate until load level of 100 kN at which the stiffness has decreased due to the loss of the interfacial bond. After that load level, resistance of the interface layer depends on the mechanical bond (shear-friction) to transfer shear stresses. By examining the slip and peel graphs, it can observed that slab PSMA4-3 achieved the lowest strength, which is directly attributed to the low

surface roughness for that slab. This specimen experienced low peel deformations and high slip values indicating low shear stiffness.

2.5 Full-scale Tests

The full-scale tests were conducted using three-point bending as shown in Fig. 2.. The total length of each slab was 3658 mm. The depth of the composite slabs was either 254 mm or 304 mm. The distance between the support and the point load was 1329 mm resulting in shear span ratios of 4.37 and 5.25 for the 304 mm and 254 mm slabs, respectively.

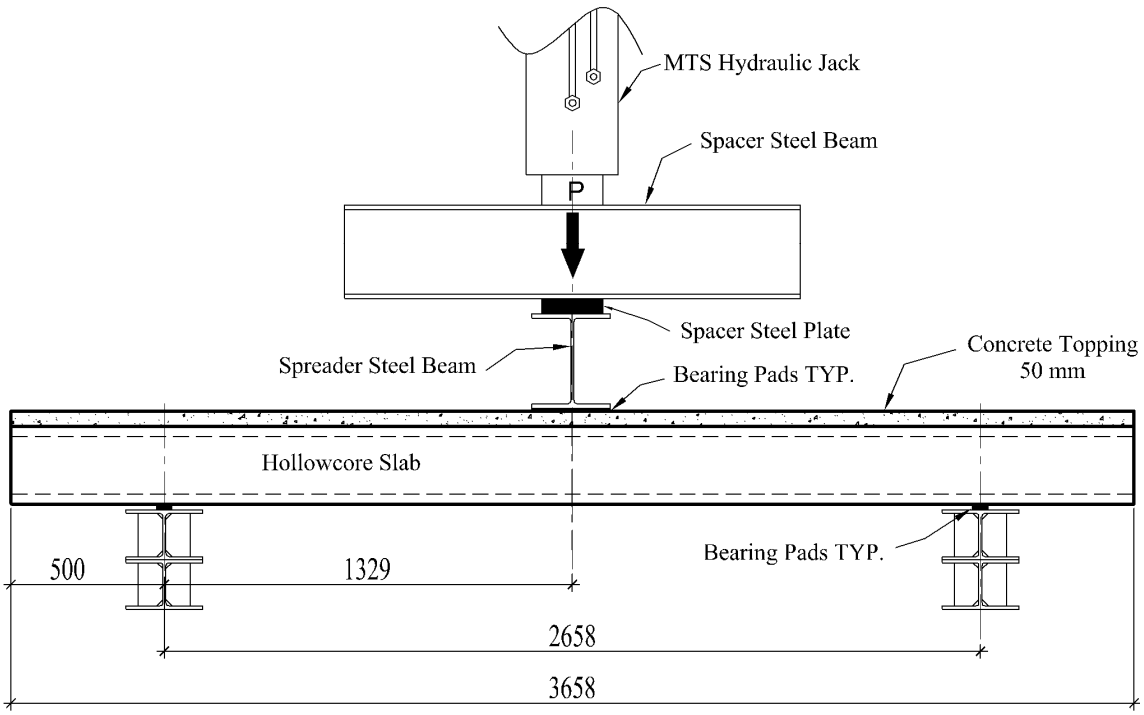

(a) Schematic (dimensions in mm).

(b) Photo.

Fig. 2.20: Full-scale test setup.

The contact surface was reduced for slabs FMA2-2C and FMB2-1C by inducing a separation in the concrete topping. This discontinuity in the concrete topping was achieved by saw cutting as illustrated in Fig. 2.. The saw cut created a 4 mm separation gap in the concrete topping. The four specimens that did not have a gap in their topping were instrumented with six LVDTs as shown in Fig. 2.(a). Two LVDTs (LE and LW) located at mid-span of the slabs measured the vertical deflection. Four LVDTs measured the slip between the concrete topping and the hollowcore slab at the middle of the shear span (SLE1 and SLW1) and near the supports (SLE2 and SLW2). Four strain gauges were also attached to the sides of the concrete topping and the hollowcore slab at the mid-span section. They were installed at a distance of 10 ± 5 mm from the interface line. The distance varied depending on the adequacy of the concrete surface.

Instrumentation layout of slabs FMA2-2C and FMB2-1C is illustrated in Fig. 2.(b). The slip and peel deformations between the hollowcore slabs and the topping were measured using LVDTs (SLCE and SLCW) and (PCE and PCW), respectively.

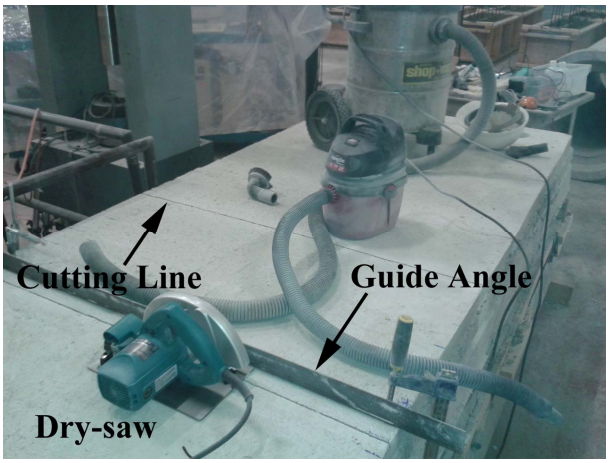

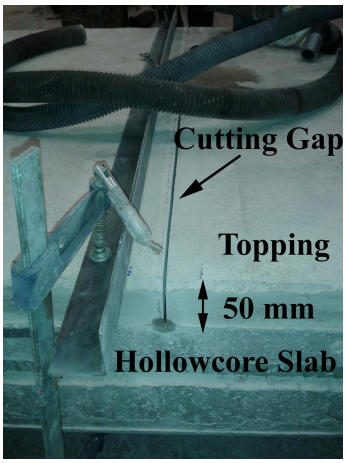

(a) Saw cutting of the concrete topping.

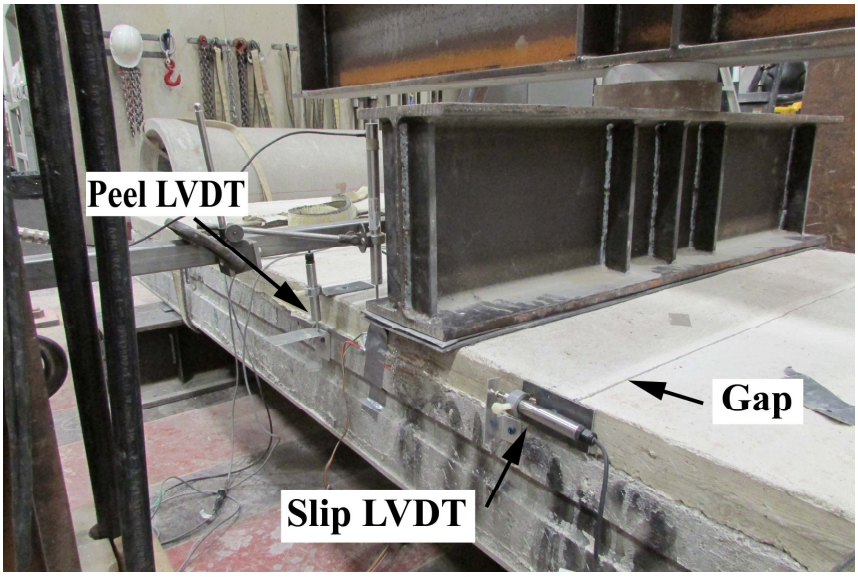

(b) Test setup.

Fig. 2.21: Slabs with gap in their topping (FMA2-2C and FMB2-1C).

Four strain gauges at the mid-span section were also used to monitor concrete strains. Photos of typical LVDTs and strain gauges are given in Fig. 2.. A load rate of 10 kN per

minute was applied for all tests. The instrumentation data were collected through a data acquisition system at a 1 Hz sampling rate.

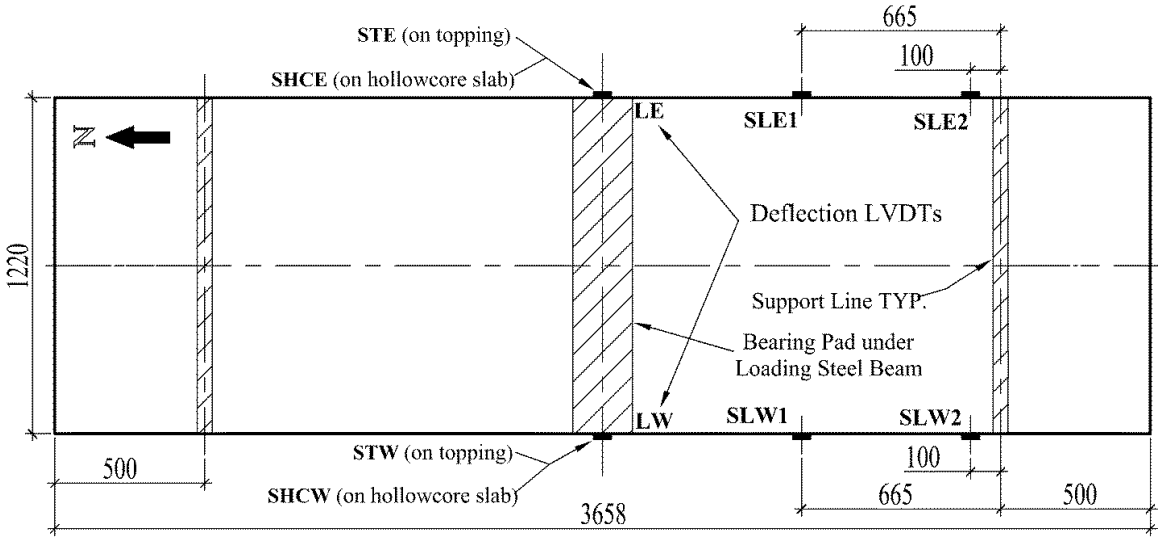

(a) Typical slab.

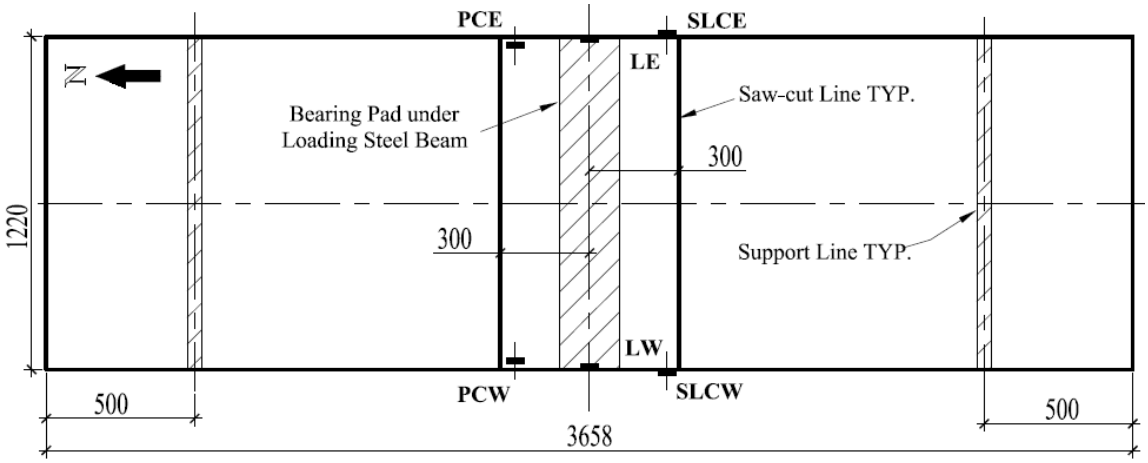

(b) Slabs with gaps in their topping.

Fig. 2.22: Instrumentation layout (dimensions in mm).

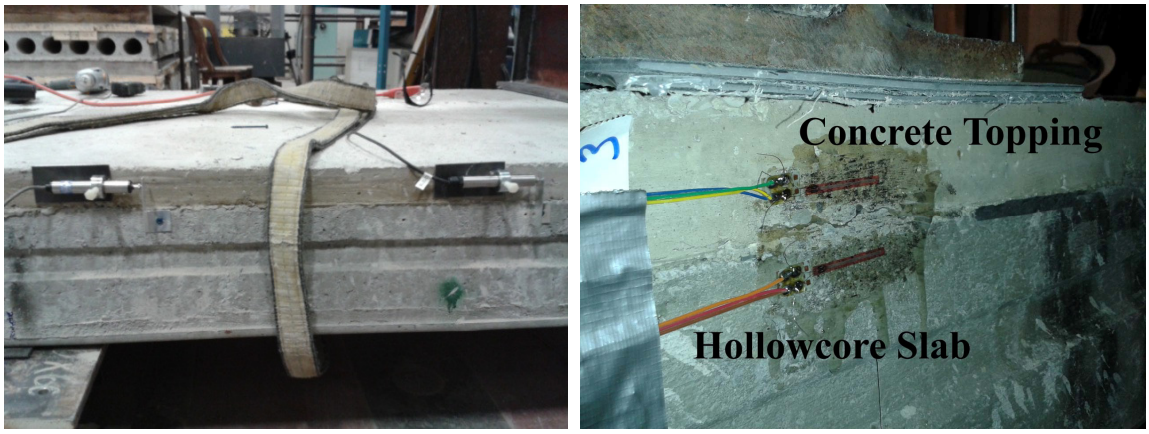

(a) Slip (LVDTs). (b) Concrete strain gauges.

Fig. 2.23: Instrumentation devices.

2.5.1 Test Results

2.5.1.1 Flexural and Vertical Shear Strength Evaluation

The load-deflection graphs are shown in Fig. 2. with the deflection values calculated based on the average of LVDTs LW and LE. The load-deflection curves demonstrate typical flexural behaviour. The initial change in the load-deflection slope is caused by cracking when the tensile stress at the bottom of the hollowcore slab exceeds the cracking stress. The propagation of the existing cracks along with the initiation of new ones continues to affect the load-deflection curve trend.

At a later loading stage close to failure, yielding starts to further affect the load-deflection curve until total failure occurs. Four of the tested slabs failed in flexure-shear mode, where a flexural crack had initiated and then propagated triggering shear failure. Two slabs have failed by strand rupture, FMA2-1 and FMA2-2C. Fig. 2. shows the failure modes for all slabs.

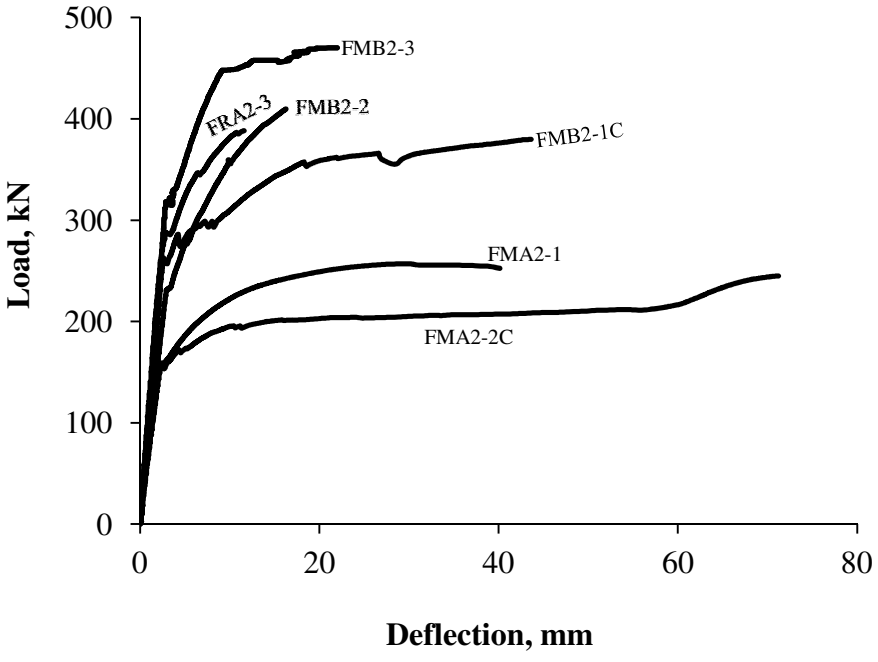

Fig. 2.24: Load-deflection test results.

(a) FMA2-1 (strand rupture).

(b) FMA2-2C (strand rupture).

(c) FMB2-2 (flexure-shear failure).

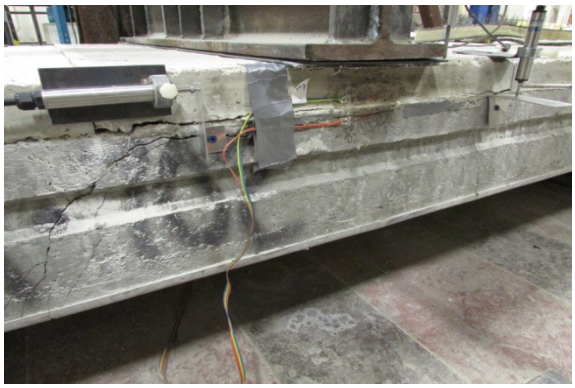

(d) FMB2-1C (flexure-shear failure).

(e) FMB2-3 (flexure-shear failure).

(f) FRA2-3 (flexure-shear failure).

Fig. 2.25: Failure modes.

Table 2.7 summarizes the experimental failure loads along with the predicted failure loads for untopped and topped slabs. The flexural capacity was estimated by assuming a maximum compressive strain of 0.0035. The concrete stress-strain relationship used in the flexural capacity prediction was based on a simple parabola equation, where the strain corresponding to maximum stress is equal to 0.002. The stress-strain relationship for the prestressing strands was developed using the Ramberg-Osgood function (Collins and Mitchell, 1991). Three constants, *A*, *B* and *C* define this function. Those constants were calculated using tensile strength test results of a typical strand for slabs from manufacturer A (Appendix 1), while recommended values from CPCI (2007) and PCI (2004) design handbooks were used for slabs from supplier B. The flexural capacity prediction was executed using strain compatibility as illustrated in Fig. 2..

Table 2.7: Predicted capacity of the tested slabs

Slab Label	**Experimental Failure Load P (kN)**	**Predicted Capacity in terms of Load P, kN**				**Failure Type**
		Shear Failure		**Flexural Failure**		
		topped	**untopped**	**topped**	**untopped**	
FMA2-1	253	270-544	205-444	262	206	strand rupture
FMA2-2C	244	267-536	199-434	260	204	strand rupture
FRA2-3	388	315-639	236-518	451	379	flexure-shear
FMB2-1C	380	288-630	222-535	383	315	flexure-shear
FMB2-2	410	281-619	215-512	382	312	flexure-shear
FMB2-3	512	336-694	256-571	494	428	flexure-shear

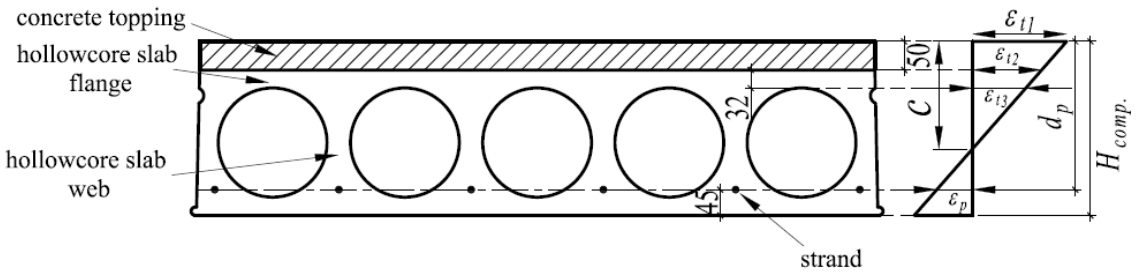

Fig. 2.26: Strain compatibility method

The equivalent rectangular stress block parameters, α_1 and β_1, were calculated as per Eqns. 2.2 and 2.3 below. These equations are based on the integration of the concrete stress-strain curve over the concrete compression area.

$$\frac{\varepsilon_t}{\varepsilon_o} - \frac{1}{3}\left(\frac{\varepsilon_t}{\varepsilon_o}\right)^2 = \alpha_1\beta_1 \qquad 2.2$$

$$\beta_1 = \frac{4-(\varepsilon_t/\varepsilon_o)}{6-(\varepsilon_t/\varepsilon_o)} \qquad 2.3$$

where, ε_t is the top strain and ε_o is 0.002.

The tensile strength of concrete was included in the flexural capacity predictions The area of concrete in tension, A_t, was iterated such that its centroid coincides with the prestressing strand location and its minimum width is less than 15 times the strand diameter, Fig. 2.. The flexural tensile strength of concrete, f_{cr}, was calculated as $0.6\sqrt{f'_{chc}}$ according to A23.3-04 (2004) clause 8.6.4. More details about the strain compatibility method are shown in Appendix 1.

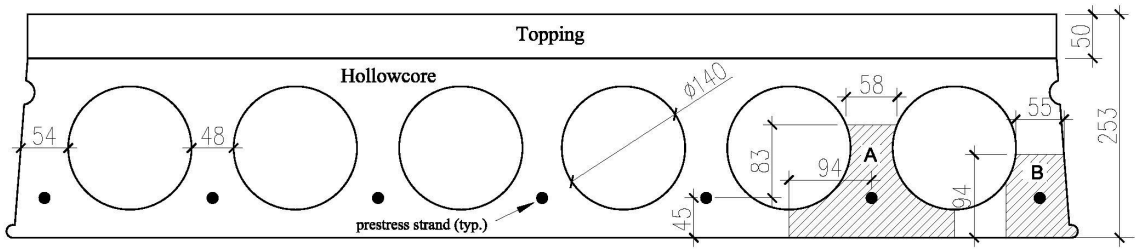

Fig. 2.27: Flexural concrete tensile strength (typical slab)

The shear capacity was estimated based on the general method in CSA A23.3-04 (2004). The effective web width was calculated according to clause 11.2.10.1 as explained in Fig. 2.. The web area encompassed by the 20^{o} tangents to the cores is equal to $b_w d_v$. The effective web width calculations for the topped and untopped slabs are shown in Appendix 1. The predicted shear capacities provided in Table 2.7 are shown as a range, where the minimum value indicates the shear capacity under the applied load and the maximum value represents the shear capacity at d_v from the face of the support.

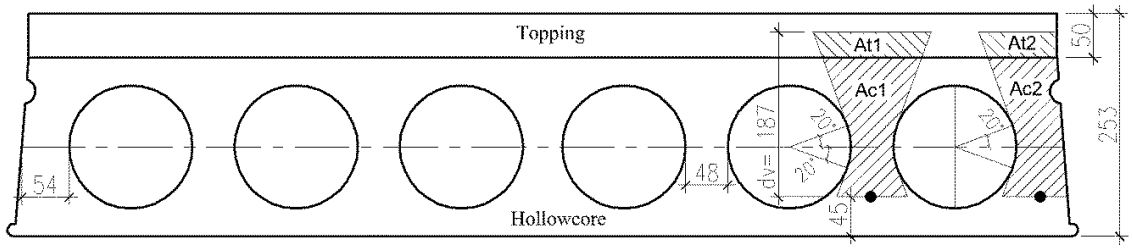

Fig. 2.28: Effective web width.

The experimental failure loads are in good agreement with the predicted failure loads. The slabs from supplier B showed slightly lower predicted flexural capacity than the actual failure loads, which can be attributed to the variation between the actual and the

assumed stress-strain model used for the strands. For slabs that failed by flexure-shear, a flexural crack propagated into a flexure-shear crack that caused failure.

The failure load was within the predicted range of shear capacity for all the slabs. For the two slabs that failed by strands rupture, FMA2-1 and FMA2-2C, the failure load represents the level at which the slab ceased to carry any further load, which occurs approximately at ultimate compressive strain of 0.0035. The strain in the strands at that load level is calculated as 0.0180 and 0.0181 for slabs FMA2-1 and FMA2-2C, respectively, which is lower than the rupture strain of 0.059 reported in the strands tensile test data sheet. The crushing of the extreme compressive fibers did not manifest during the test so the loading was continued until strands rupture.

2.5.1.2 Slip and Peel Deformations

Slip and peel measurements obtained from the displacement LVDTs are illustrated in Fig. 2.. Negative LVDT readings indicate that the LVDT has expanded, which means that slip or peel has occurred. Positive values indicate that the LVDT has compressed, which results from the curvature of the slab specimen due to bending under loading.

Table 2.8 shows the maximum slip and peel deformations for all of the tested slabs. The slip measured for slabs FMA2-1 and FMB2-3 was almost zero suggesting that full composite action was achieved.

Specimen FMA2-2C had better ductility than FMA2-1. This ductility resulted from the observed slip in this specimen. Specimen FMB2-2 had slip values that are higher than FMA2-1 and FMB2-3, which may be due to the lower bond strength between the slab and the concrete topping. However, these slip values were very small and did not affect the overall performance of the specimen.

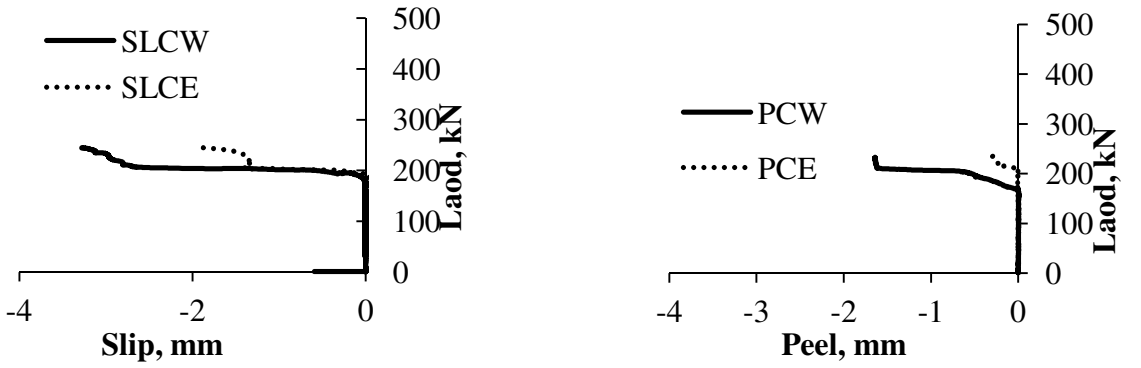

(a) FMA2-2C

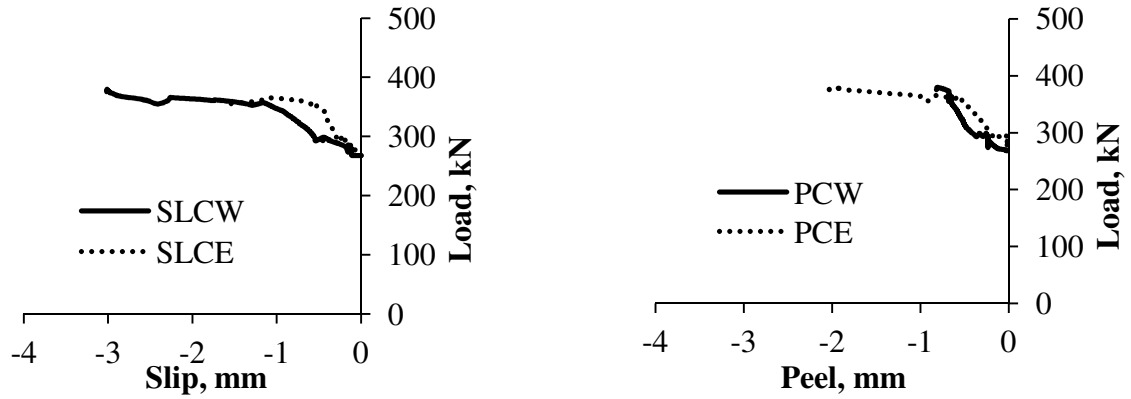

(b) FMB2-1C

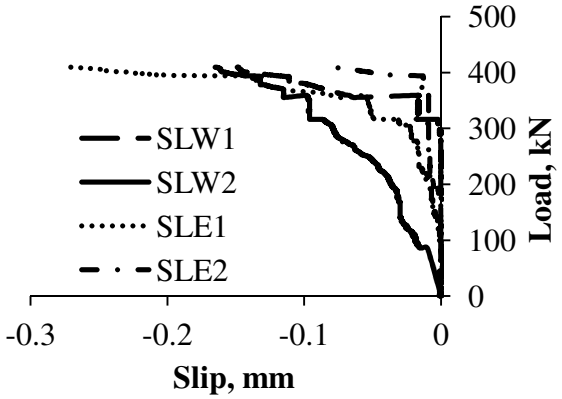

(c) Slab FMB2-2

Fig. 2.29: Slip and peel measurements.

Table 2.8: Full-scale test results at failure loads

Specimen Label	Max. Load P, kN	Max. Slip δs, mm		Max. Peel δp, mm	
		E	W	E	W
FMA2-1	253	0.000	0.004	------	------
FMA2-2C	244	1.949	3.279	0.315	1.643
FRA2-3	388	0.000	0.002	------	------
FMB2-1C	380	1.263	3.018	0.817	2.030
FMB2-2	410	0.270	0.165	------	------
FMB2-3	512	0.021	0.000	------	------

Careful inspection of the slip and peel curves for the cut-slabs illustrated consistency between peel and slip readings. The slip values for specimen FMA2-2C show an initial high horizontal shear stiffness that is significantly reduced at a load of about 186 kN. This might be due to loss of the bond resistance at the interface. The slip measured at the west side was higher than that measured at the east side. This is linked to the peel deformations that show higher values at the west side than the east side. Similar observations can be made about slab FMB2-1C. Strain readings for slab FMB2-1C are shown in Fig. 2.. Near failure, the bond between the concrete topping and the hollowcore slabs was weakened, which triggered slip along the interface and caused the compressive stresses in the concrete topping to unload and the tensile strains in the top of the hollowcore slab to change to compressive strains.

The slip measured for slabs FMA2-1 and FMB2-3 was almost zero suggesting that full composite action was achieved. Specimen FMA2-2C had better ductility than FMA2-1. This ductility resulted from the observed slip in this specimen. Specimen FMB2-2 had slip values that are higher than FMA2-1 and FMB2-3 because of its low bond strength (average of 0.80 MPa with one of the cores having zero bond strength). However, these slip values were very small and did not affect the overall performance of the specimen. Slab FMB2-3 had a thickness of 304 mm including the concrete topping, which is greater than the thickness of slab FMB2-2 but had similar prestressing reinforcement. Horizontal

shear failure was not observed for slab FMB2-3 and the slab acted compositely up to failure. This indicates that the increased thickness did not affect the horizontal shear behaviour.

.

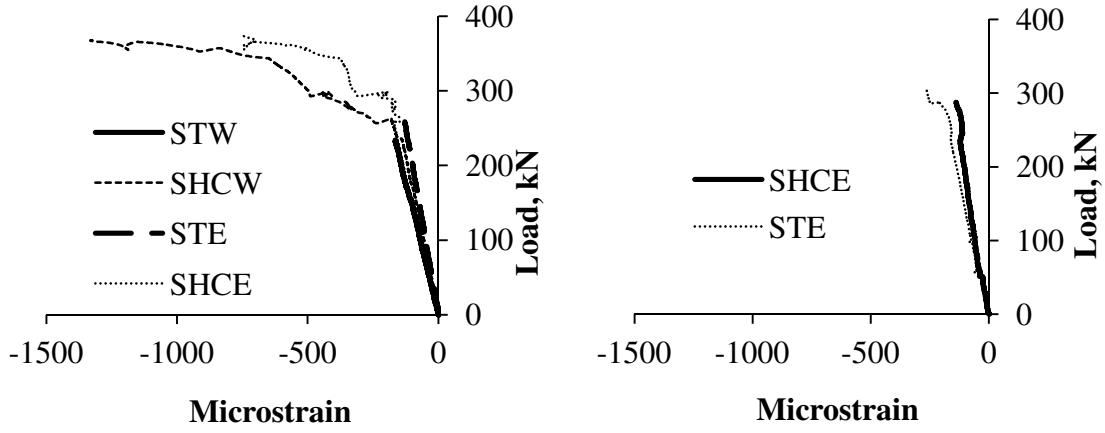

(a) FMB2-1C (b) FRA2-3

Fig. 2.30: Strain readings for all tested slabs.

2.5.1.3 Average Horizontal Shear Strength Evaluation

The average horizontal shear stress at failure, $\tau_{test\ avg.}$, was calculated using the two methods available in A23-04 (2004) and ACI 318-08 (2008). The first method utilizes the maximum shear force as the maximum horizontal shear force applied on the concrete topping, clause 17.5.3 of ACI 318-08 (2008) and clause 17.4.3 of CSA A23.3-04 (2004). The maximum horizontal shear stress is then calculated by dividing the maximum shear force by $b_v d$, where b_v is the width of the interface between the topping and the hollowcore slab and d is the distance from the extreme compression fiber to the centroid of the prestressing strands of the composite slab. The second method is outlined in clause 17.4.4 of A23.3-04 (2004) and clause 17.5.4 of ACI 318-08 (2008) and involves the equilibrium of the internal sectional forces to determine the maximum horizontal shear force at the maximum moment section. This force is then divided by the contact surface

area, A_{cv}, in substitution of $b_v d$. The first method is simple and depends on the shear force diagram of the full-scale test while the second method involves more analysis using the strain compatibility procedure to determine the horizontal shear force in the concrete topping. The equivalent stress block parameters were determined in a similar fashion to the procedure used in the evaluation of the flexural capacity of the composite slabs.

Table 2.9 shows the calculated average shear stress at failure for each of the tested slabs. The results show that both methods generally produce comparable horizontal shear stresses. However, they had significant differences for the case of the cut-slabs, which is expected because the first method does not account for the reduction of the concrete topping area. The allowable horizontal shear strength for composite hollowcore slabs as specified in A23.3-04 (2004) and 318-08 (2008) are 0.70 MPa and 0.55 MPa, respectively. These limits are applicable when the hollowcore slab surface is intentionally roughened to 6 mm and 5 mm amplitudes as per A23.3-04 (2004) and ACI 318-08 (2008), respectively. The tested slabs reached values that are comparable or higher than these limits, which suggests that the used surface roughness can develop a full composite action.

Table 2.9: Shear stress evaluation according to design standards

Slab Label	**Failure Load P, kN**	**Avg. Shear Stress, $\tau_{test\text{-}avg.}$, MPa**	
		Method (1)	Method (2)
FMA2-1	253	0.50	0.53
FMA2-2C	244	NA	2.27
FRA2-3	388	0.61	0.66
FMB2-1C	380	NA	3.67
FMB2-2	410	0.81	0.84
FMB2-3	512	0.81	0.84

2.6 Conclusions

This chapter examined the peel and shear behaviour of the interface between hollowcore slabs with machine-cast surface and concrete topping through pull-off, push-off, and full-scale tests. The work conducted in this study is distinguished from previous work by adapting a comprehensive experimental program, which gave broader understanding of the performance of composite hollowcore slabs. Other manufactures can follow the tests explained in this study to evaluate the adequacy of their products. In view of the presented results and discussions, the following conclusions may be drawn:

Surface roughness and bond strength between hollowcore slabs and topping concrete:

- The surface roughness provided by the machine-cast finish is much lower than the intentional roughness required by North American design standards. High variability of surface roughness was observed for different shipments from the same manufacturer.
- Pull-off test results indicated that if the surface roughness of hollowcore slabs with machine-cast finish exceeds 0.3 mm, their bond strength to the concrete topping is expected to satisfy the 0.9 MPa limit in A23.2 (2009). The loss of bond between the hollowcore slab and the concrete topping decreases the load carrying capacity of the slab, which may cause premature failure in real cases. The suggested surface roughness threshold can be used as a quality control measure. This threshold is valid for the slabs produced by the participating manufacturers.

Shear strength between hollowcore slabs and topping concrete:

- Push-off test results indicated that if the surface roughness of the hollowcore slabs is acceptable and the slab is free from contamination, the shear strength of the interface layer between the slab and the concrete topping can be higher than the minimum acceptable shear stresses specified in North American design standards. The shear strength was found to vary significantly from one manufacturer to another.

Full-scale tests:

- Full-scale three point bending tests have shown that hollowcore slabs with machine-cast finish and acceptable roughness can provide adequate composite action up to

failure. Thus, the horizontal shear strength required by CSA A23.3-04 (2004) and ACI 318-08 (2008) can be met without the need for intentional roughening.

- Two of the slabs had a gap in their concrete topping limiting the effective area of the topping to a small area in the middle of the slab. The topping of the two slabs experienced slip and peel deformations that did not affect the overall behaviour. This might be due to the confining action provided by the load that acts on the topping. This suggests that live loads increase the shear strength provided by the interface layer.

2.7 References

ACI 318, 2008. Building code requirements for structural concrete (ACI 318-08) and commentary. Michigan, United States: American Concrete Institute.

Adawi A, Youssef MA, Meshaly M., 2014. "Analytical modeling of the interface between lightly roughened hollowcore slabs and cast-in-place concrete topping," *ASCE J. Struct Eng*.

ASTM C349, 2008. Standard test method for compressive strength of hydraulic cement mortars (Using Portions of Prisms Broken in Flexure). Pennsylvania, United States: ASTM International.

ASTM C39, 2005. Standard test method for compressive strength of cylindrical concrete specimens. Pennsylvania, United States: ASTM International.

ASTM E965, 2006. Standard test method for measuring pavement macrostructure depth using a volumetric technique. Pennsylvania, United States: ASTM International.

Collins, M.P. and Mitchell, D., "Prestressed Concrete Structures", Prentice-Hall 1991, 760 pp.

CPCI, 2007. CPCI design Manual, 4th edition. Canadian Precast and Prestressed Concrete Institute, Ottawa, Canada.

CSA A23.1, 2009. Concrete materials and methods of concrete construction (A23.1-09). Mississauga, ON, Canada: Canadian Standard Association (CSA).

CSA A23.2, 2009. Test methods and standard practices for concrete (A23.2-09). Mississauga, Canada: Canadian Standard Association (CSA).

CSA A23.3, 2004, Design of concrete structures (A23.3-04). Mississauga, ON, Canada: Canadian Standard Association (CSA).

FIP Commission on Prefabrication, 1982. Shear at the interface of precast and in situ concrete. Sweden: Guide to Good Practice.

PCI, 2004. PCI Design Handbook, 7th Edition. Chicago, IL: Precast/Prestressed Concrete Institute.

CHAPTER THREE

3 Analytical Modeling of the Interface between Hollowcore Slabs and Cast-In-Place Concrete Topping

Hollowcore slabs are precast/prestressed concrete elements that are commonly used in the construction industry. They are manufactured at a precast concrete plant prior to shipping to the job site. After installation, they are typically topped with a 50-mm cast-in-place concrete topping to level the surface. Structural engineers can make use of the concrete topping to increase the load-carrying capacity of the slab. This consideration requires that failure at the interface between the hollowcore slab and the concrete topping does not initiate prior to reaching the ultimate capacity of the composite section.

North American design standards specify that the shear strength of the interface between intentionally roughened hollowcore slab surface and the concrete topping can be taken as 0.70 MPa [CSA A23.3-04 (2004), clause 17.4.3.2] or 0.55 MPa [ACI 318-08 (2008), clause 17.5.3.1]. ACI 318-08 (2008) commentary clause R17.5.3.3 defines intentionally roughened as 6.4 mm of surface roughness, and CSA A23.3-04 (2004) explanatory note N17.4.3.2 defines it as roughness to an amplitude of 5.0 mm. In North America, hollowcore slabs are commonly produced using the extrusion process, which involves the use of zero-slump concrete mix and high vibration augers. The surface of hollowcore slabs manufactured using this process is referred to as machine-cast finish. The roughness of this surface varies depending on a number of factors, including concrete mix design and wear and tear of the concrete extrusion machine. The same variability exists when this surface is roughened. Roughening a hollowcore slab surface to the amplitudes specified in the design standards involves additional time, material, and labor that manufacturers would be keen to avoid. A simple roughening technique that is widely used by manufacturers involves the use of a steel broom. However, the produced roughness does not qualify the slabs to be ranked as intentionally roughened.

This chapter investigates the shear and peel behavior at the interface between hollowcore slabs and cast-in-situ concrete topping. This chapter models the shear and peel stresses

along the interface between the hollowcore slab specimens and the topping concrete. The model is based on the technique presented by El Damatty and Abushagur (2003) to calculate the shear and peel stresses in the adhesive attaching fiber-reinforced polymer (FRP) sheets to the flanges of steel I beams. A closed-form solution of the system equilibrium was used to determine the distribution of the developed shear and peel stresses.

3.1 Push-off Tests

Push-off tests were conducted vertically. While the concrete topping is resting on a steel plate, a downward force was applied to the hollowcore slab. Two steel beams were positioned on the back of the hollowcore slab to provide stability. The concrete topping was instrumented with five strain gauges (S1 to S5), two peel displacement gauges (L1, L2) and two slip displacement gauges (L3, L4). The push-off test setup and instrumentation are shown in Fig. 3.31. The tested hollowcore slabs were 203 mm deep and had a surface area of 1220 mm by 1220 mm. The nominal concrete compressive strength for the hollowcore slabs was 41 MPa. The concrete topping had a surface area of 508 mm by 508 mm, a thickness of 50 mm and a concrete compressive strength of 32 MPa. A total of seven slabs (SMA1-2, SRA1-1, SRA1-3, SRB1-1, SRB1-2, PSMA4-2 and PSMA4-3) were tested.

“M” and “R” refer to the surface finish of the slab as either machine-cast or lightly-roughened, respectively. “A” and “B” refer to the slab manufacturer. Each of the tested slabs had four-½” prestressing strands. Prior to starting the test, a careful visual inspection did not reveal any signs of separation between the concrete topping and the hollowcore slabs. The load was applied via the hydraulic actuator at a rate of 10 kN/minute. Displacement and strain readings were collected throughout the tests.

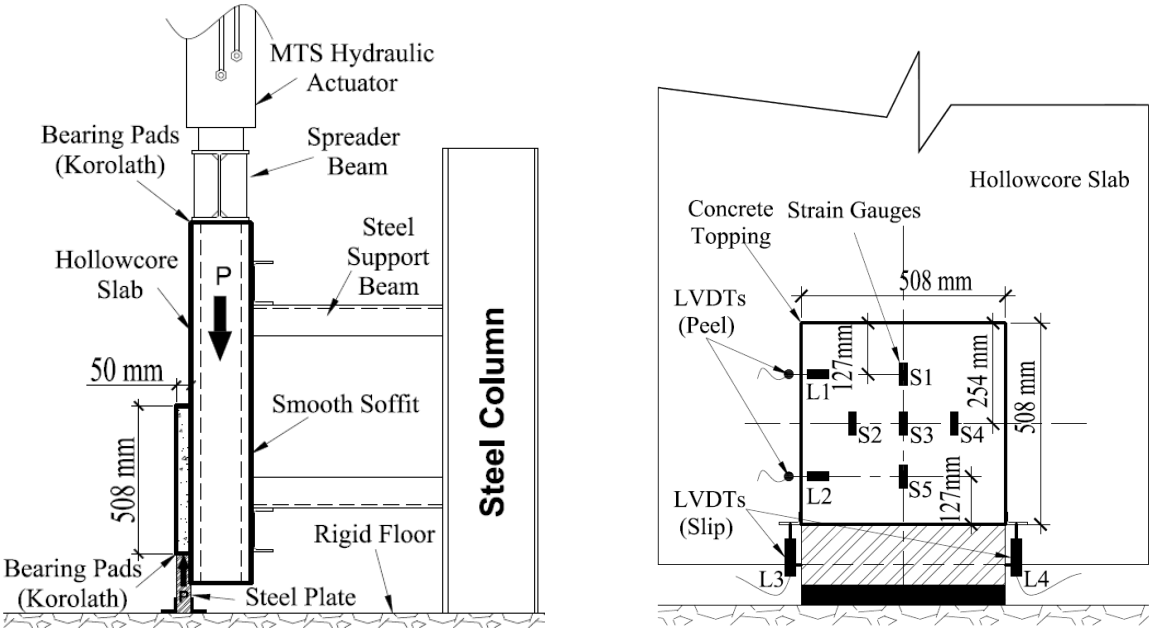

Fig. 3.31: Push-off test setup and instrumentation.

The ultimate load, at which the concrete topping separates from the hollowcore slab, and the corresponding average shear strength, $v_{h\ avg.}$, are shown in Table 3.1. To obtain a conservative estimate of $v_{h\ avg.}$, the effect of slippage on the contact area was not accounted for and, thus, $v_{h\ avg.}$ was directly calculated by dividing the failure load by the contact area. The ultimate load accounts for the weight of the slab and the steel spreader beam.

The average horizontal shear strength for all of the tested slabs was higher than the limit of 0.7 MPa and 0.55 MPa required by CSA A23.3 (2004) and ACI 318 (2008), respectively. Slabs from manufacturer A demonstrated considerably higher shear strength than those from manufacturer B except for PSMA4-3 because it had a very low surface roughness. This difference might be due to the initial surface roughness and/or the roughening pattern.

Table 3.1: Push-off test results

Specimen Label	**Failure load, kN**	**Average shear strength, $v_{h\ avg.}$, MPa**	**Calculated yielding horizontal shear stress, $v_{h\ max.}$, MPa**
SMA1-2	354	1.37	1.69
SRA1-2	504	1.95	6.19
SRA1-3	554	2.15	7.24
SRB1-1	223	0.86	1.24
SRB1-2	182	0.71	1.01
PSMA4-2	308	1.19	2.47
PSMA4-3	66	0.26	0.26

While the interface capacity in the pre-yielding stage depends on the bond between the concrete topping and the hollowcore slab, the post-yielding behavior is governed by shear friction between the slab and the topping. The abrupt failure type that was observed for all tested specimens emphasizes that the horizontal stress transferred along the interface layer did not have the ability to fully redistribute over the contact area once failure was initiated. This observation suggests that the reported values of average shear stresses are lower than the actual shear stresses that were reached.

3.2 Analytical Model

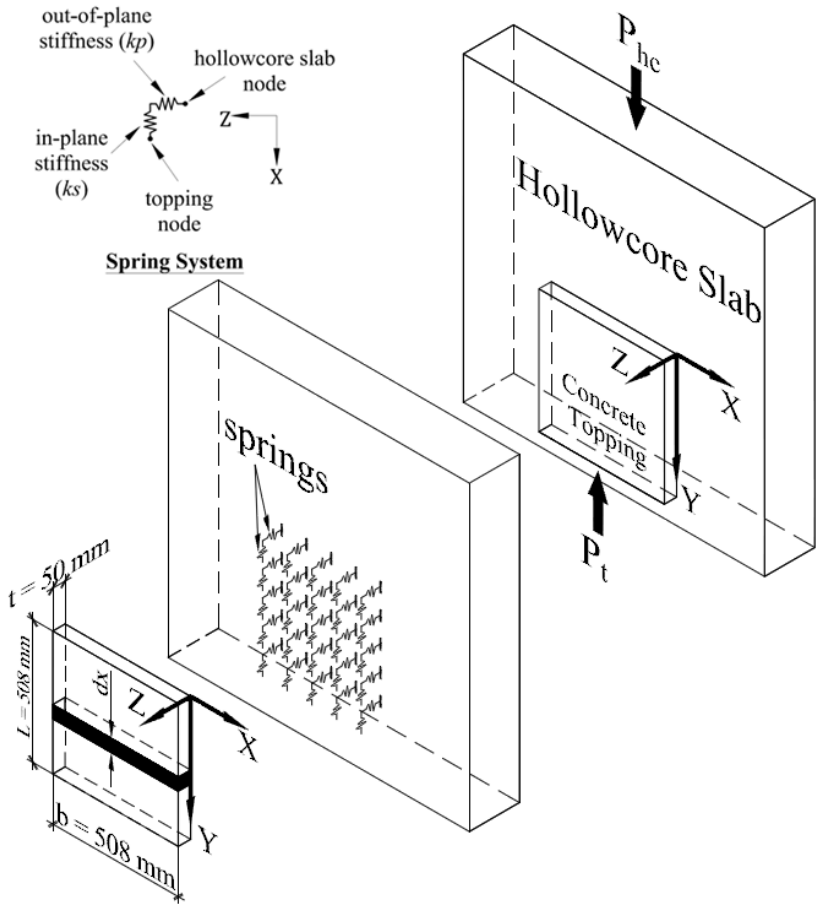

Fig. 3.32: General layout of the push-off test spring model.

The hollowcore slabs are modeled as rigid elements. Two continuous spring systems were used to simulate the stiffness of the interface layer as illustrated in Fig. 3.32. Similar modeling technique was used by El Damatty and Abushagur (2003) while modeling the adhesive attaching FRP sheets to steel I beams. The first set of springs depicts the in-plane stiffness k_s in the direction of the applied load (parallel to the X axis). They allow modeling the horizontal shear stress behavior. The out-of-plane stiffness k_p models the peel behavior using another set of springs that are parallel to the Z axis. The shear stress profile $v_h(x)$ acting along the interface between the hollowcore slab and the concrete

topping can be calculated using Eq. 3.1, where *u(x)* is the in-plane displacement profile of the concrete topping along the X axis.

$$v_h(x) = k_s \times u(x) \qquad 3.1$$

The in-plane and out-of-plane equilibrium are explained in the following sections on an infinitesimal segment of the concrete topping "element T", Fig. 3.33, to evaluate the shear and peel stiffness (k_s) and (k_p).

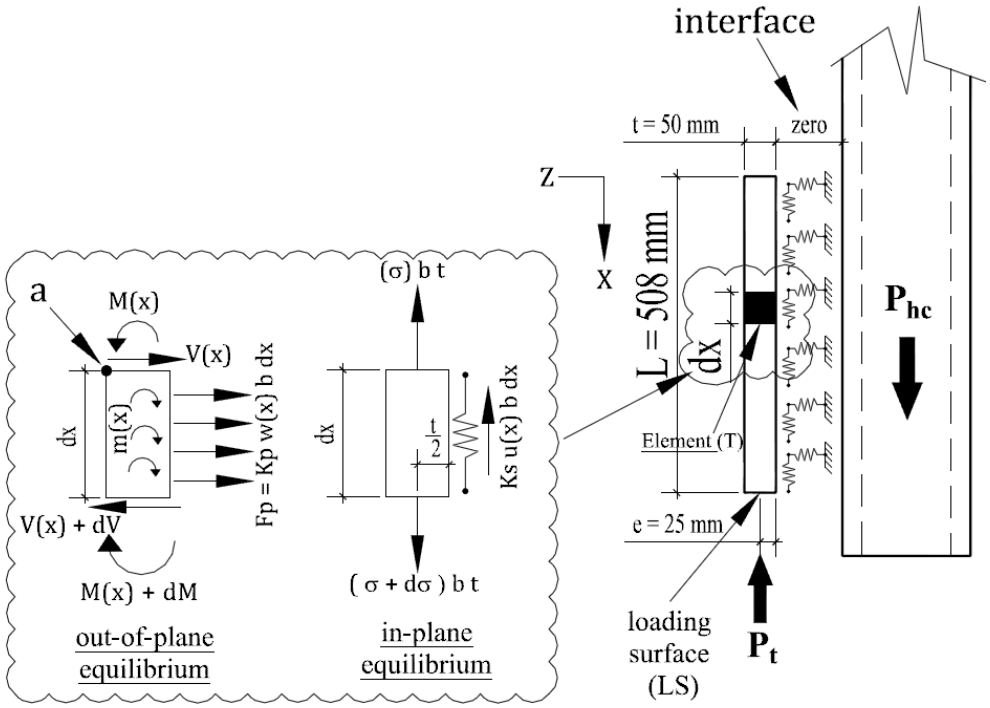

Fig. 3.33: Free body diagram of element T.

3.2.1 In-Plane Equilibrium

When the hollowcore slab is pushed downward by the applied force P_{hc}, an equivalent reaction force P_t is generated in the concrete topping, Fig. 3.33. The resultant of the developed axial stresses in the concrete topping, σ, is acting at its centroid. σ has a value

of zero at the top point of the topping ($x = 0$) and a maximum value at the bottom point (x = 508 mm).

Considering the in-plane equilibrium of an infinitesimal element T, the increase in axial stresses $d\sigma$ is in equilibrium with the developed shear stresses at the interface. The force in the in-plane spring, F_s, represents the shear force along the interface between the hollowcore slab and the concrete topping. This force can be calculated from the summation of forces along the X axis as given by Eq. 3.2. F_s can also be calculated as a function of the shear spring stiffness as given by Eq. 3.3.

$$F_s = btd\sigma \tag{3.2}$$

$$F_s = K_s u(x) b dx \tag{3.3}$$

The relationship between σ and the in-plane displacement $u(x)$ can be obtained from Eqns. 3.2 and 3.3 and Hook's Law as illustrated in Eqns. 3.4 and 3.5.

$$\frac{d\sigma}{dx} = \frac{k_s u(x)}{t} \tag{3.4}$$

$$\sigma = E_c \frac{du}{dx} \tag{3.5}$$

where (du/dx) is the strain in the concrete topping, and E_c is the modulus of elasticity of concrete. Since the concrete topping is made of normal density concrete and have a compressive strength f'_c of 30 MPa, E_c is calculated using clause 8.6.2.3 of CSA A23.3-4 (2004). The differential equation that governs the state of stresses in the concrete topping is:

$$\frac{d^2 u}{dx^2} - \omega^2 u(x) = 0 \tag{3.6}$$

where

$$\omega^2 = \left(\frac{k_s}{tE_C} \right) \tag{3.7}$$

Eq. 3.6 is a second order differential equation and can be solved by defining the following boundary conditions:

1) At $x = 0 \rightarrow \frac{du}{dx} = 0$ (strain = 0)

2) At $x = L \rightarrow \frac{du}{dx} = -\frac{P_t}{btE_c}$ (strain from Hook's Law)

Solving Eq. 3.6 using the defined boundary conditions leads to the following in-plane displacement profile.

$$u(x) = -\frac{P_t}{btE_C \omega \sinh(\omega L)} \cosh(\omega x) \tag{3.8}$$

The relationship between the load P_t and the measured displacement at the bottom surface of the concrete topping when x is equal to L can be expressed by Eq. 3.9.

$$P_t = -btE_C \omega \tanh(\omega L) u(L) \tag{3.9}$$

where *u(L)* is the average in-plane displacement *measured* using LVDTs L3 and L4. The measured P_t - *u(x)* is simplified to a bilinear curve as shown in Fig. 3.34 for slab SRB1-1. The slope k_{sm} was obtained such that areas A1 and A2 are equal. The coordinates of points C for all specimens are reported in Table 2 and were used to define P_t and *u(L)* and then evaluate ω using Eq. 3.9.

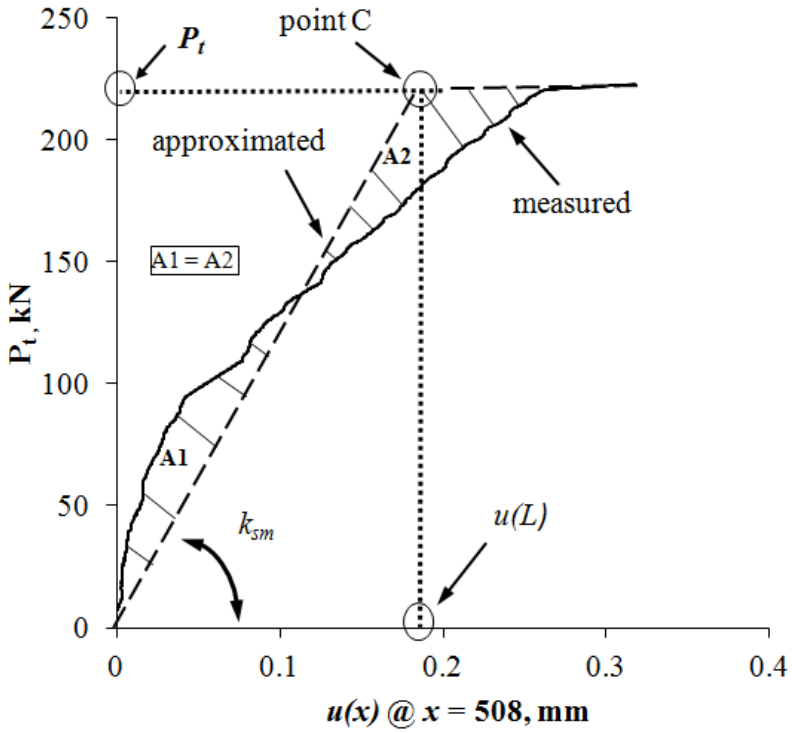

Fig. 3.34: Approximate load-slip relationship for slab SRB1-1.

Table 3.2: Values of P_t and $u(L)$ at the yielding points, C.

Slab label	**P_t, kN**	**$u(L)$, mm**
SMA1-2	354	0.49
SRA1-2	504	0.13
SRA1-3	554	0.13
SRB1-1	223	0.18
SRB1-2	182	0.15
PSMA4-2	308	0.13
PSMA4-3	66	1.9

3.2.2 Maximum Shear Stress ($v_{h\,max}$)

The in-plane displacement distribution along the X axis of the concrete topping can be obtained using Eq. 3.8. The horizontal shear stress distribution, v_h, can be then evaluated using Eq. 3.1. Fig. 3.35 illustrates the horizontal shear stress distribution along the X axis. Fig. 3.36 compares the calculated horizontal shear stress profile for slab SRB1-1 and the average measured horizontal shear stress at failure.

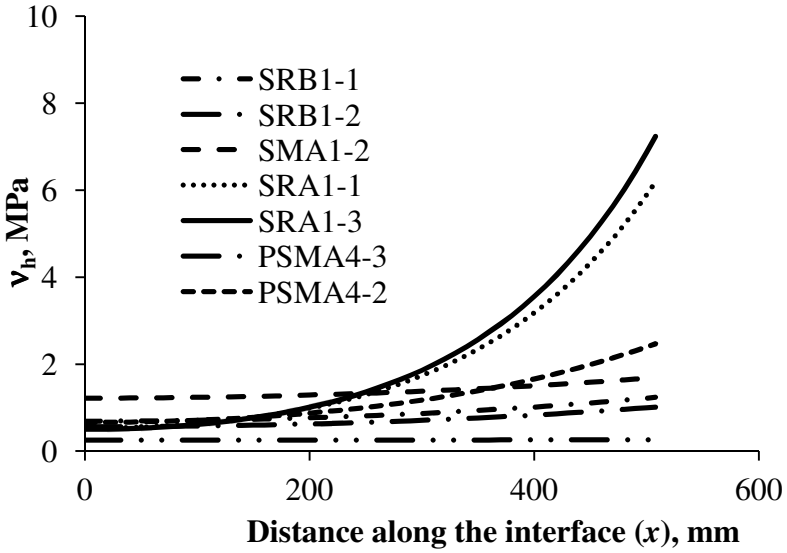

Fig. 3.35: Horizontal shear stress distribution.

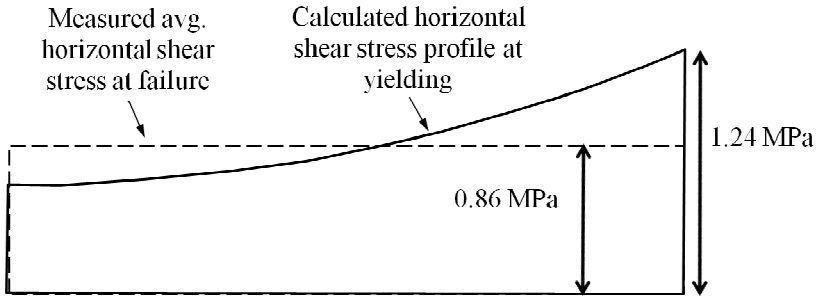

Fig. 3.36: Comparison of shear stress for slab SRB1-1.

The actual horizontal shear profile shows a concentration of the shear stresses near the applied load P_t. This observation indicates that the tested slabs sustained higher stresses than the average value. Table 3.1 shows the average and the calculated horizontal shear stress values at yielding. For all of the tested slabs, the shear strength at the interface between the hollowcore slabs and the concrete topping reached values that are much higher than the values specified in North American design standards.

3.2.3 Out-of-Plane Equilibrium

Fig. 3.33 illustrates the forces and stresses acting on element T in the out-of-plane direction. The external applied moment, *m(x)*, results from the eccentric force in the shear spring, F_s, and can be found by multiplying the force F_s by half the thickness of the concrete topping. The applied moment, *m(x)*, can be defined using Eq. 3.10.

$$m(x) = \frac{1}{2} k_s b t u(x) \tag{3.10}$$

The force, F_p, is developed in the out-of-plane springs as a result of the applied moment *m(x)* and is responsible for the peel behavior of the concrete topping. F_p can be calculated from the equilibrium of forces along the Z axis and the equilibrium of the external and the internal moments acting on the element, Eqns. 3.11 and 3.12.

$$\frac{dV}{dx} = -k_p b w(x) \tag{3.11}$$

$$\frac{dM}{dx} = V + m(x) \tag{3.12}$$

Utilizing the moment-curvature relationship, Eq. 3.13, the differential equation governing the peel behavior, Eq. 3.14, can be derived.

$$M(x) = EI \frac{d^2 w}{dx^2}(x) \tag{3.13}$$

$$\frac{d^4 w(x)}{dx^4} + \lambda^4 w(x) = \frac{1}{EI}\frac{dm}{dx} \qquad 3.14(a)$$

where $\lambda^4 = \frac{bk_p}{EI}$ 3.14(b)

The homogenous and particular solutions of Eq. 14 are given by Eq. 15.

$$\begin{aligned} w(x) = {} & A\cos(\lambda x)\cosh(\lambda x) + B\cos(\lambda x)\sinh(\lambda x) \\ & + C\sin(\lambda x)\cosh(\lambda x) + D\sin(\lambda x)\sinh(\lambda x)\cos(\lambda x) - F\sinh(\omega x) \end{aligned} \qquad 3.15(a)$$

where $F = \frac{\mathrm{P_t} k_s}{E_c{}^2 I \sinh(\omega L)(\lambda^4 + \omega^4)}$ 3.15(b)

The constants *B* and *D* can be determined by applying the following boundary conditions at the free end of the concrete topping (*x = 0*).

(1) $\frac{d^2 w}{dx^2} = 0$ (M = 0).

(2) $\frac{d^3 w}{dx^3} = 0$ (V = 0).

Substituting with the evaluated constants, Eq. 15 reduces to the following form:

$$\begin{aligned} w(x) = {} & A\cos(\lambda x)\cosh(\lambda x) + C[\cos(\lambda x)\sinh(\lambda x) + \sin(\lambda x)\cosh(\lambda x)] \\ & + \frac{F}{2}\frac{\omega}{\lambda}\cos(\lambda x)\sinh(\lambda x) + F\sinh(\omega x) \end{aligned} \qquad 3.16$$

Eq. 3.16 represents the calculated out-of-plane displacement profile of the concrete topping, *w(x)*, and contains three unknowns *A*, *C* and λ. The load and displacement defining point C in Fig. 3.34 and the corresponding strains (point D in Fig. 3.37) are used to evaluate these constants as follows:

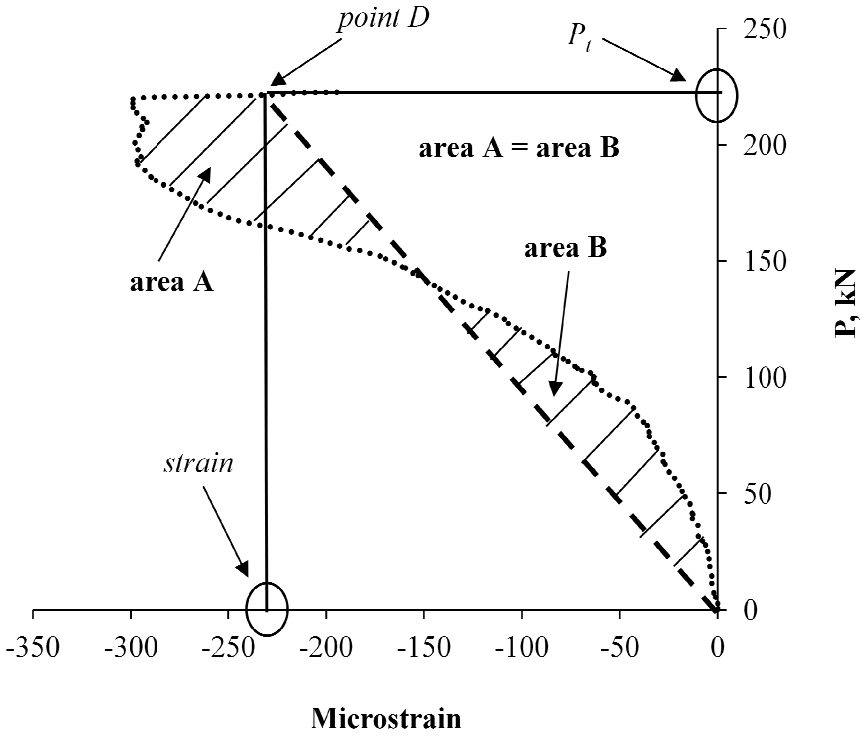

Fig. 3.37: Approximate load-S3 strain relationship for slab SRB1-1 (typical)

1- The values of $(du/dx)_{mid}$, Fig. 3.38, are evaluated at the locations of S1, S3 and S5 by differentiating Eq. 3.8.

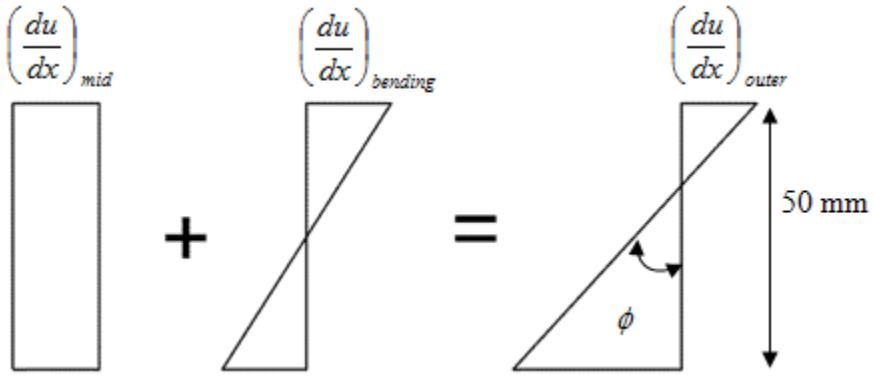

Fig. 3.38: State of strains in the concrete topping.

2- Readings of S1, S3, and S5 represent the measured strain at the surface of the concrete topping, $(du/dx)_{outer}$, Fig. 3.38.

3- $(du/dx)_{bending}$ is evaluated at the locations of S1, S3, and S5 using Eq. 3.17.

$$\left(\frac{du}{dx}\right)_{bending} = \left(\frac{du}{dx}\right)_{outer} - \left(\frac{du}{dx}\right)_{mid} \qquad 3.17$$

4- The curvature of the concrete topping at the locations of S1, S3 and S5 is evaluated using Eq. 3.18.

$$\left(\frac{d^2w}{dx^2}\right) = -\frac{2}{t}\left(\frac{du}{dx}\right)_{bending} \qquad 3.18$$

5- The cubic function that best fits the calculated curvature in step 4 is then evaluated. Fig. 3.39 shows a typical cubic function.

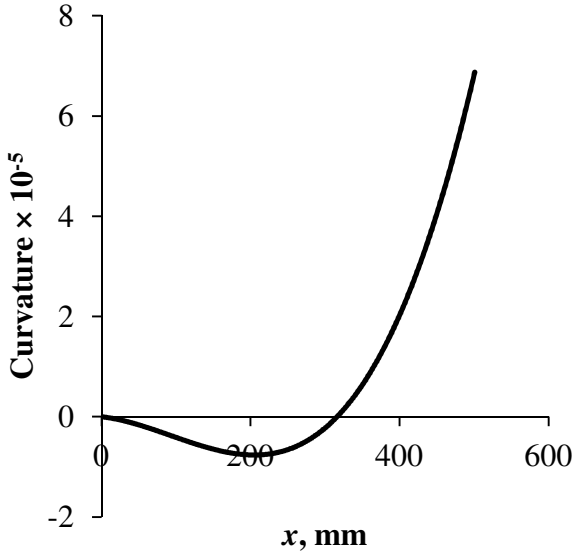

Fig. 3.39: Curvature best fit cubic curve.

6- The out-of-plane measured displacement profile $w(x)_m$ was obtained by double integration of Eq. 3.18. The two integration constants were then evaluated using the out-of-plane displacement readings from LVDTs L1 and L2.

7- Nonlinear regression analysis was conducted to match the calculated out-of-plane displacement profile $w(x)$ with the displacement profile $w(x)_m$ evaluated in step 6. This analysis allowed determining constants A, C and λ. The out-of-plane profile, $w(x)$, is shown in for all tested slabs.

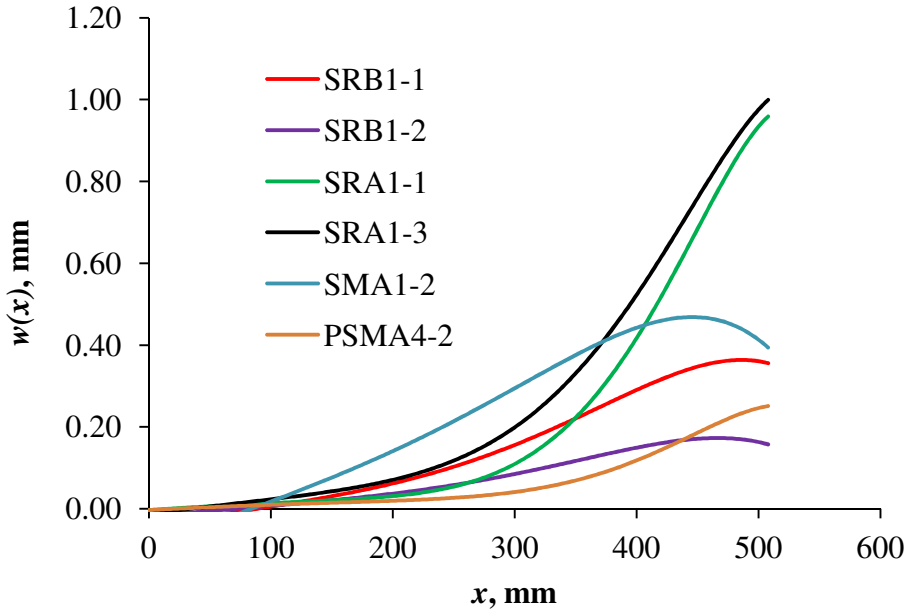

Fig. 3.40: Out-of-plane displacement profiles.

3.3 Shear and Peel Stiffnesses

The peel stiffness k_p is calculated using Eq. 3.14(b) by substituting with the value of λ. The shear stiffness (k_s) is calculated using Eq. 3.6. Table 3.3 shows the calculated shear and peel stiffnesses for all slab specimens. (k_p) is considerably smaller than (k_s) for all slabs.

Table 3.3: Shear and peel stiffness values.

Specimen Label	Horizontal shear stiffness k_s, (N/mm)/mm^2	Peel stiffness k_p, (N/mm)/mm^2
SMA1-2	3.48	0.50
SRA1-2	47.6	5.69
SRA1-3	54.0	8.67
SRB1-1	6.72	2.07
SRB1-2	6.85	1.92
PSMA4-2	19.0	4.50
PSMA4-3	0.26	NA

Average shear stiffness (k_s) of 31.0 (N/mm)/mm^2 and 6.8 (N/mm)/mm^2 and average peel stiffness (k_p) of 6.3 (N/mm)/mm^2 and 2.0 (N/mm)/mm^2 were calculated for slabs from manufacturer A and B, respectively. Slab PSMA4-3 was not included in the average value of (k_s) and its peel stiffness (k_p) was not calculated because of its significantly low readings. Peel stiffness (k_p) was not calculated for slabs SMA1-2 because it was not instrumented with strain gauges. Manufacturers A and B can use these values to predict the composite behavior of their hollowcore slabs.

3.4 Conclusions

An analytical model that simulates the interface between the hollowcore slab and the concrete topping using continuous springs was presented. The springs depicted the interfacial shear and peel behaviors. The actual shear stresses were evaluated using the analytical model and found to be higher than the average measured values for all of the

tested slabs. The actual values are much higher than the specified code limits. The shear and peel stiffnesses, (k_s) and (k_p), of the interface between hollowcore slabs and concrete topping were then estimated using the presented analytical model. The reported (k_s) and (k_p) values are unique for the tested slabs. The presented method can be repeated to evaluate these stiffnesses for slabs from different manufacturers. Structural engineers can then use (k_s) and (k_p) values to evaluate the actual shear stresses developed at the interface between hollowcore slabs and their concrete topping and judge on the appropriateness of using the composite action.

3.5 References

ACI 318, 2008. "Building Code Requirements for Structural Concrete (ACI 318-08) and Commentary." American Concrete Institute, Michigan, United States.

CSA A23.1, 2009. "Concrete materials and methods of concrete construction. (CSA A23.1-09)" Canadian Standard Association, Mississauga, Canada.

CSA A23.3, 2004. "Design of concrete structures." Canadian Standard Association (CSA A23.3-04)", Mississauga, Canada.

El Damatty A.A. and Abushagur M., 2003. "Testing and modeling of shear and peel behavior for bonded steel/FRP connections." Thin-Walled Structures, 41, 987-1003.

Girhammar U.A. and Pajari M., 2008. "Tests and analysis on shear strength of composite slabs of hollow core units and concrete topping." Construction and Building Materials, 22, 1708-1722.

Ibrahim I. S. and Elliot K. S., 2006. "Interface Shear Stress of Hollow Core Slabs with Concrete Toppings." Sixth International Conference on Concrete Engineering and Technology, (CONCET 2006), Institution of Engineers Malaysia, Kuala Lumpur, 104-116

Technical Bulletin 74-B6, 1974. “Composite Systems Without roughness.” Concrete Technology Association (CTA), CTA 35, pp 271-316.

Technical Bulletin 76-B4 (1976). “Composite Systems without Ties.” Concrete Technology Association (CTA), CTA 36, pp 317-360.

CHAPTER FOUR

4 Analytical Evaluation of the Composite Behavior of Hollowcore Slabs with Concrete Topping

Retrofitting reinforced concrete beams with plates is a common practice to increase their load capacity. The plates are usually bonded to the soffit of the beams using a bonding agent such as epoxy. The design aim is reaching the ultimate capacity of the beam prior to delamination of the plate. Vilnay (1988) presented an analytical method to estimate the shear and peel stresses between a reinforced concrete beam and a steel plate bonded to its soffit. Vilnay's method (1988) does not account for the effects of axial deformations of the beam, bending deformations of the plate and shear deformations of the epoxy layer. It assumes zero shear stress under the load and is only applicable for the case of a point load applied at mid-span. Smith and Teng (2001) proposed an analytical solution to determine the shear and peel stress distributions in the adhesive layer connecting beams and retrofitting plates made of any material. Smith and Teng's approach (2001) accounts for the effect of the bending deformation of the strengthening plate and the axial deformation of the beam. The interfacial shear stress is assumed to be continuous at the point load. This approach can also be applied to general load scenarios.

Analytical evaluation of the interfacial shear and peel stresses for composite hollowcore slabs with concrete topping does not exist in the literature. Adawi et al. (2014) estimated the shear and peel stiffness coefficients, (k_s) and (k_p), that govern the behaviour of the interface between hollowcore slabs and the concrete topping by providing closed form solutions for the differential equations governing the push-off tests. However, the push-off tests do not resemble the actual state of the interfacial stresses in composite hollowcore slabs systems. This chapter provides closed form solutions for the differential equations governing the behavior of a simply supported composite hollowcore slabs. Two analytical solutions, simplified and modified, developed based on the deformation compatibility of the composite section are developed and validated. The simplified solution follows the approach of Vilnay (1988) while the methodology of Smith and

Teng (2001) is utilized to develop the modified solution. The simplified solution is easier to derive and implement compared to the modified solution because it neglects the bending deformations of the concrete topping. The modified solution on the other hand includes the bending deformation of the concrete topping and can be applied to any load case. The peel stresses are evaluated using the modified solution only. Details of the analytical solutions are explained in the following sections.

4.1 Full-scale Tests

Adawi et al. (2015) tested five machine-cast hollowcore slabs that were topped with 50 mm concrete. Chapter 2 presented the results for an additional slab that was lightly-roughened before casting of the topping concrete. The surface roughness of the machine-cast hollowcore slabs ranged between 0.297 mm and 0.325 mm, which is considerably lower than the 6.35 mm and 5.00 mm roughness amplitudes required by CSA A23.3-04 (2004) and ACI 318-08 (2008), respectively, to allow for composite action. The area of the concrete topping was reduced for slabs FMA2-2C and FMB2-1C to increase the horizontal shear stresses.

The full-scale tests were conducted using the three point bending test setup. The span was 2658 mm and the concentrated load was applied at mid-span using a steel spreader beam. The slabs were instrumented with gauges to measure strains in the hollowcore slabs and the concrete topping during the test. Shear and peel displacements were measured using four LVDTs that were distributed symmetrically along the slab. All slabs showed adequate composite performance up to failure. The slabs with reduced concrete topping area suffered significant slip and peel deformations, however, they were able to achieve the predicted capacity for the composite section.

4.2 Evaluation of Interfacial Stresses Using Analytical Solutions

Fig. 4.41 shows the forces acting on a segment (*dx*) of a simply supported composite hollowcore slab.

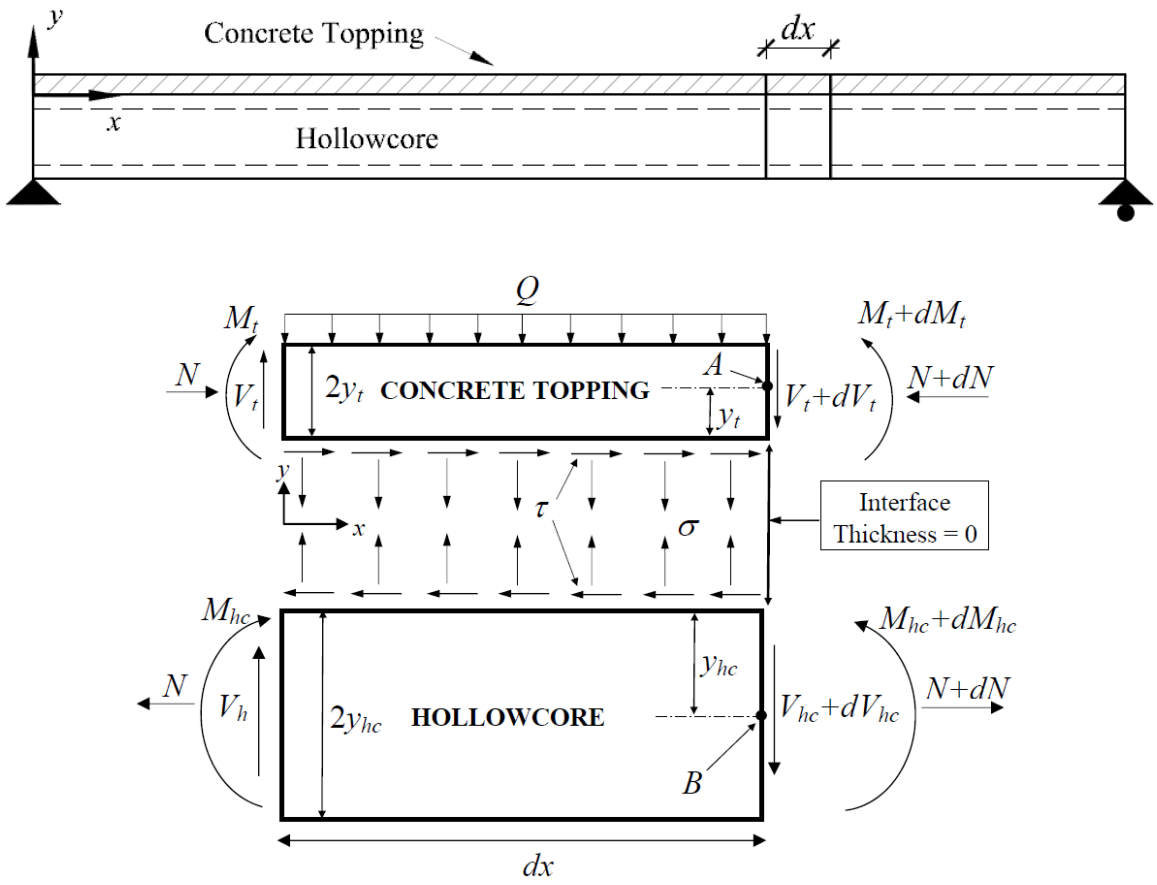

Fig. 4.41 : Equilibrium forces of segment (*dx*)

The figure shows the concrete topping connected to the hollowcore slab at the interface, which has a thickness of zero. $N(y_{hc} + y_t)$ represents the moment component resisted by the composite section. (M_{hc}, V_{hc}) and (M_t , V_t) are the moment and vertical shear resisted by the hollowcore slab and the concrete topping, respectively. (Q) is the generalized uniformly distributed load on the composite slab.

From the equilibrium of the forces and moments shown in Fig. 4.41,

$$\frac{dN}{dx} = b\tau \tag{4.1}$$

$$\frac{dM_{hc}}{dx} = V_{hc} - b\tau y_{hc} \tag{4.2}$$

$$\frac{dM_{t}}{dx} = V_{t} - b\tau y_{t} \tag{4.3}$$

$$dN = K(u_{hc} - u_{t}) \tag{4.4}$$

where (K) is the general shear stiffness of the interface in N/mm and ($u_{hc} - u_t$) is the relative displacement between the top of the hollowcore slab (u_{hc}) and the bottom of the concrete topping (u_t). By dividing Eq. 4.4 by (bdx), differentiating with respect to (x) and noting that the total strain at the bottom of the concrete ($\varepsilon_t = du_t / dx$) and at the top of the hollowcore slab ($\varepsilon_{hc} = du_{hc} / dx$), the following equation can be reached.

$$\frac{d\tau}{dx} = k_s(\varepsilon_{hc} - \varepsilon_t) \tag{4.5}$$

Where (k_s) is the interfacial shear stiffness in (N/mm)/mm^2 and (b) is the width of the concrete topping. ε_t and ε_{hc} can be determined based on the moments and normal forces in the hollowcore slabs and the concrete topping as described by Eqns. 4.6 and 4.7 below.

$$\varepsilon_t = \frac{M_t y_t}{E_t I_t} - \frac{N}{E_t A_t} \tag{4.6}$$

$$\varepsilon_{hc} = \frac{-M_{hc} y_{hc}}{E_{hc} I_{hc}} + \frac{N}{E_{hc} A_{hc}} \tag{4.7}$$

In the following sections, the differential equations governing the shear stresses acting on the element shown in Fig. 4.41 are first derived using the two proposed methods: simplified and modified. They are then solved for the case of an applied point load at

mid-span to obtain the shear stress distribution along the interface between the hollowcore slabs and the concrete topping. The peel stress distribution is determined by solving the differential equations developed using the modified method.

4.2.1 Interfacial Shear Stress

4.2.1.1 Simplified Method

Vilnay's approach (1988) assumes that the strain at the bottom of the beam is due to bending of the beam, ignoring the bending rigidity of the steel retrofitting plate. The simplified method is developed based on Vilnay's assumptions (1988) while accounting for: (1) location of the concrete topping relative to the slabs and (2) effect of the axial deformations of the hollowcore slab. Eq. 4.6 is reduced to:

$$\varepsilon_t = \frac{N}{E_t A_t} \tag{4.8}$$

Substituting Eqns. 4.7 and 4.8 in Eq. 4.5 yields:

$$\frac{d\tau}{dx} = k_s \left[\left(\frac{-M_{hc} y_{hct}}{E_{hc} I_{hc}} + \frac{N}{E_{hc} A_{hc}} \right) - \frac{N}{E_t A_t} \right] \tag{4.9}$$

Rearranging Eq. 4.9 and differentiating it with respect to (x):

$$\frac{d^2\tau}{dx^2} = \left(\frac{k_s}{E_t A_t} \frac{dN}{dx} \right) - \left(\frac{k_s y_{hc}}{E_{hc} I_{hc}} \frac{dM_{hc}}{dx} \right) + \left(\frac{k_s}{E_{hc} A_{hc}} \frac{dN}{dx} \right) \tag{4.10}$$

Substituting Eqns. 4.1 and 4.2 into Eq. 4.10 gives the following relationship:

$$\frac{d^2\tau}{dx^2} = \left(\tau \frac{k_s}{E_t A_t} \right) - \left(\frac{k_s y_{hc}}{E_{hc} I_{hc}} \left(V_{hc} - \tau y_{hc} \right) \right) + \left(\tau \frac{k_s}{E_{hc} A_{hc}} \right) \tag{4.11}$$

Considering the case of the one point load applied at mid-span and substituting with $V_{hc}=P/2$, the second order differential equation that governs the shear stress distribution is shown below.

$$\frac{d^2\tau}{dx^2} + \tau A - B = 0 \qquad 4.12$$

where

$$A = k_s\left(\frac{1}{E_t A_t} + \frac{1}{E_{hc} A_{hc}} + \frac{y_{hc}^{\ 2}}{E_{hc} I_{hc}}\right) \qquad 4.13$$

$$B = \frac{k_s y_{hc} P}{2E_{hc} I_{hc}} \qquad 4.14$$

4.2.1.2 Modified Method

The modified solution follows Smith and Teng's approach (2001). It includes the effect of bending deformation of the concrete topping. The ratio between the moment resisted by the slab and the topping can be based on their relative rigidity as follows.

$$M_{hc} = \frac{E_{hc} I_{hc}}{E_t I_t} M_t = RM_t \qquad 4.15$$

The moment equilibrium of the infinitesimal segment implies that:

$$M_T = M_{hc} + M_t + \left[N\left(y_t + y_{hc}\right)\right] \qquad 4.16$$

Solving Eqns. 4.15 and 4.16 for (M_{hc}) and (M_t) and differentiating with respect to (x):

$$\frac{dM_{hc}}{dx} = \frac{R}{R+1}\left[V_T - b_t \tau (y_t + y_{hc})\right] \qquad 4.17$$

$$\frac{dM_t}{dx} = \frac{1}{R+1}\left[V_T - b_t\tau(y_t + y_{hc})\right] \quad 4.18$$

where, (M_T) and (V_T) are the total moment and vertical shear. By differentiating Eqn. 4.5 with respect to (x) and substituting Eqns. 4.6, 4.7, 4.17 and 4.18, the second order differential equation that governs the interfacial shear stress can be obtained.

$$\frac{d^2\tau}{dx^2} = k_s b_t \tau\left[\frac{(y_{hc}+y_t)^2}{E_{hc}I_{hc}+E_tI_t} + \frac{1}{E_{hc}A_{hc}} + \frac{1}{E_tA_t}\right] - k_sV_T\left[\frac{(y_{hc}+y_t)}{E_{hc}I_{hc}+E_tI_t}\right] \quad 4.19$$

4.2.2 General Solutions

4.2.2.1 Simplified Method

The general solution of Eq. 4.12 is given by the following form:

$$\tau(x) = C_1e^{x\sqrt{A}} + C_2e^{-x\sqrt{A}} + \frac{B}{A} \quad 4.20$$

Considering the general case of a partial concrete topping subjected to one point load at mid-span, Fig. 4.42, the constants (C_1) and (C_2) can be determined using the following boundary conditions:

1) $\tau = 0$ at $x = L/2$ (symmetry)
2) $M_{hc} = Pa/2$ at $x = 0$ (total moment is resisted by the hollowcore slab)
3) $N = 0$ at $x = 0$ (end of concrete topping)
4) $\frac{d\tau}{dx} = \frac{-k_sPay_{hc}}{2E_{hc}I_{hc}}$ at $x = 0$ (after applying boundary conditions 2 and 3 in Eq. 4.9)

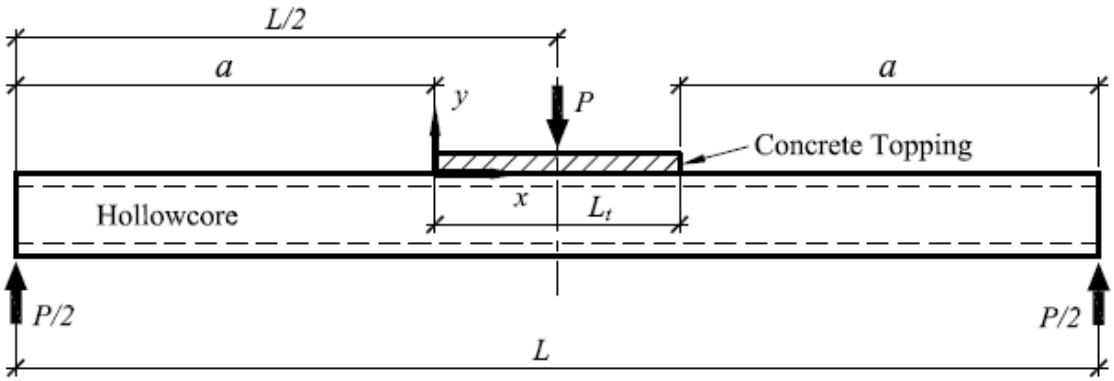

Fig. 4.42 : Boundary conditions for the simplified solution

4.2.2.2 Modified Method

The general solution of Eq. 4.19 is given by:

$$\tau = B_1 \cosh(\lambda x) + B_2 \sinh(\lambda x) + m_1 V_T \qquad 4.21$$

where

$$\lambda^2 = k_s b_t \left[\frac{(y_{hc} + y_t)^2}{E_{hc} I_{hc} + E_t I_t} + \frac{1}{E_{hc} A_{hc}} + \frac{1}{E_t A_t} \right] \qquad 4.22$$

$$m_1 = \frac{k_s}{\lambda^2} \left[\frac{(y_{hc} + y_t)}{E_{hc} I_{hc} + E_t I_t} \right] \qquad 4.23$$

The constants are evaluated for the general case of hollowcore slab with partial concrete topping. The boundary conditions and the corresponding constants for all potential locations of the load (P) relative to the concrete topping are as follows:

- For $a < b$, Fig. 4.43(a)

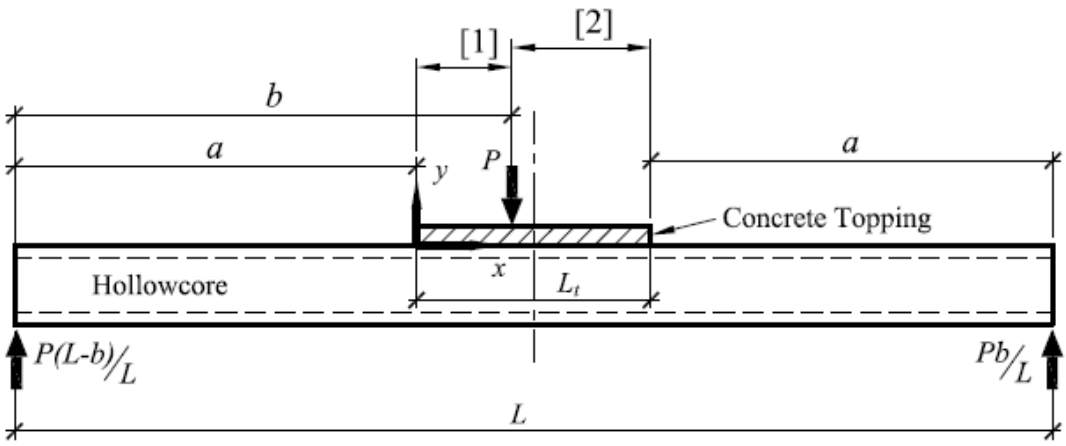

(a) $a < b$

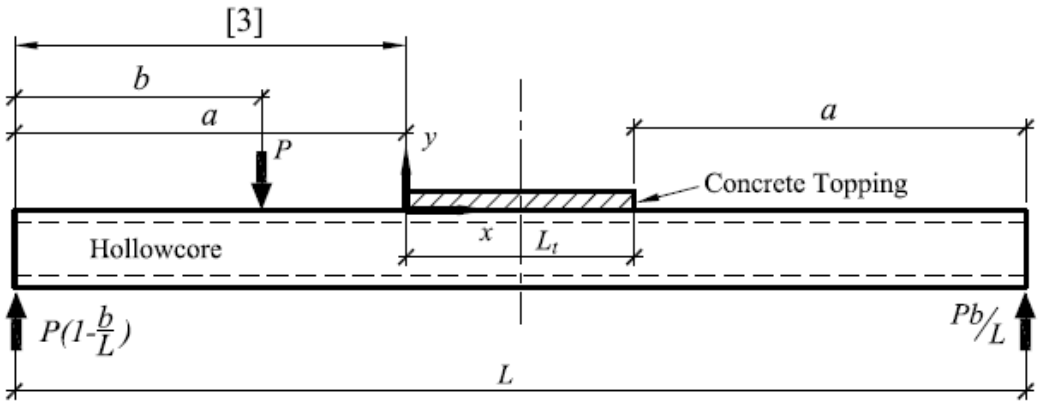

(b) $a > b$

Fig. 4.43 : Boundary conditions for the modified solution.

Boundary conditions:

- at $x = 0$, $M_T = M_{hc} = Pa\left(1 - \frac{b}{L}\right)$
- at $x = L_t$, $M_{hc} = M_T = P\frac{ab}{L}$
- at $x = (b - a)$, $\tau(x)$ and $\frac{d\tau}{dx}(x)$ are continuous functions.

[1] for $0 \le x \le (b-a)$ and $a < b$:

$$\tau(x) = B_3 \cosh(\lambda x) + B_4 \sinh(\lambda x) + m_1 P\left(1 - \frac{b}{L}\right) \quad 4.24$$

where

$$B_3 = \frac{m_2}{\lambda} Pa\left(1 - \frac{b}{L}\right) - m_1 P e^{-k} \quad 4.25$$

$$B_4 = \frac{-m_2}{\lambda} Pa\left(1 - \frac{b}{L}\right) \quad 4.26$$

[2] for $(b-a) \le x \le L_t$ and $a < b$:

$$\tau(x) = B_4 \cosh(\lambda x) + B_5 \sinh(\lambda x) + m_1 P\left(1 - \frac{b}{L}\right) \quad 4.27$$

where

$$B_5 = \frac{m_2}{\lambda} Pa\left(1 - \frac{b}{L}\right) + m_1 P \sinh(k) \quad 4.28$$

$$B_6 = \frac{-m_2}{\lambda} Pa\left(1 - \frac{b}{L}\right) - m_1 P \sinh(k) \quad 4.29$$

- For $a > b$, Fig. 4.43(b):

Boundary conditions:

at $x = 0$, $M_T = M_{hc} = Pb\left(1 - \frac{a}{L}\right)$

at $x = L_t$, $M_T = M_{hc} = P\dfrac{ab}{L}$

For $0 \le x \le L_t$

$$\tau(x) = B_7 \cosh(\lambda x) + B_8 \sinh(\lambda x) - \left(m_1 P \frac{b}{L}\right) \tag{4.30}$$

where

$$B_7 = \frac{m_2}{\lambda} Pb\left(1 - \frac{a}{L}\right) \tag{4.31}$$

$$B_8 = \frac{-m_2}{\lambda} Pb\left(1 - \frac{a}{L}\right) \tag{4.32}$$

For all of the above equations,

$$m_2 = \frac{k_s y_{hc}}{E_{hc} I_{hc}} \tag{4.33}$$

$$k = \lambda(b - a) \tag{4.34}$$

4.2.3 Interfacial Peel Stress (σ)

The differential equation governing the equilibrium is derived and solved based on the work of Smith and Teng (2001) after accounting for the location of the concrete topping relative to the hollowcore slab. Equilibrium of forces along *y* axis in Fig. 4.41 yields the following equations:

$$\frac{dV_t}{dx} = -b_t\sigma(x) - \frac{P}{L_t} \tag{4.35}$$

$$\frac{dV_{hc}}{dx} = b_t\sigma(x) \tag{4.36}$$

where (b_t) is the width of the concrete topping and (P/L_t) is the average uniformly distributed load that results from the applied load (P) on the partial concrete topping and represent (Q) in Fig. 4.41. The peel stress can be defined by using the stiffness of the interface layer:

$$\sigma(x) = k_p\left[w(x)_{hc} - w(x)_t\right] \tag{4.37}$$

where k_p is the peel stiffness of the interface and $w(x)$ is the displacement profile in the Y direction. By differentiating Eq. 4.37 twice, Eq. 4.38 can be obtained.

$$\frac{d^2\sigma}{dx^2} = k_p\left(\frac{d^2w_{hc}}{dx^2} - \frac{d^2w_t}{dx^2}\right) \tag{4.38}$$

The relationship between the moments and curvatures for the hollowcore slab and the topping are:

$$\frac{d^2w_{hc}}{dx^2} = \frac{-M_{hc}}{E_{hc}I_{hc}} \tag{4.39}$$

$$\frac{d^2w_t}{dx^2} = \frac{-M_t}{E_tI_t} \tag{4.40}$$

By taking moment around points A and B in Fig. 4.1:

$$\frac{dM_{hc}}{dx} = V_{hc} - \left(b_t y_{hc}\tau(x)\right) \tag{4.41}$$

$$\frac{dM_t}{dx} = V_t - \left(b_t y_t\tau(x)\right) \tag{4.42}$$

By differentiating Eqns. 4.38 two times and substituting with Eqns. 4.39 - 4.42, the following fourth-order differential equation can be obtained:

$$\frac{d^4\sigma}{dx^4}+\left[k_p b_t \sigma(x)\left(\frac{1}{E_{hc}I_{hc}}+\frac{1}{E_t I_t}\right)\right]+\left[\frac{d\tau}{dx}k_p b_t\left(\frac{y_t}{E_t I_t}-\frac{y_{hc}}{E_{hc}I_{hc}}\right)\right]+\frac{k_p P}{E_t I_t L_t}=0 \qquad 4.43$$

The general solution of Eq. 4.43 is given as follows:

$$\sigma(x)=\left[e^{-\beta x}\left(C_1\cos(\beta x)+C_2\sin(\beta x)\right)\right]+$$
$$\left[e^{\beta x}\left(C_3\cos(\beta x)+C_4\sin(\beta x)\right)\right]-\left[-n_1\frac{d\tau}{dx}\right]-\left[n_2\frac{P}{L_t}\right] \qquad 4.44$$

By assuming that the peel stress approaches zero for large (x) values (Smith and Teng, 2001), the constants C_3 and C_4 are equal to zero. The constants (C_1) and (C_2) are determined using the following boundary conditions:

1) at $x = 0$, $M_t = 0$, $N = 0$ and $M_T = M_{hc}$ (end of the concrete topping), where (M_T) is the total external moment. Implementing this boundary condition in Eq. 4.38 yields the following expression:

$$\frac{d^2\sigma}{dx^2}=\frac{k_p}{E_{hc}I_{hc}}M_T(0) \qquad 4.45$$

2) at $x = 0$, $V_t = 0$ and $V_T = V_{hc}$ (end of concrete topping), where (V_T) is the total external shear force. By differentiating Eq. 4.38 once with respect to (x) and substituting Eqns. 4.41 and 4.42, this boundary condition can be expressed as:

$$\frac{d^3\sigma}{dx^3}=\frac{k_p}{E_{hc}I_{hc}}V_T(0)-n_3\tau(0), \qquad 4.46$$

where

$$n_3=k_p b_t\left(\frac{y_t}{E_t I_t}-\frac{y_{hc}}{E_{hc}I_{hc}}\right). \qquad 4.47$$

Multiple differentiation of the peel stress general solution given in Eq. 4.44 yields the following second and third derivatives at the end of the concrete topping ($x = 0$):

$$\frac{d^2\sigma}{dx^2} = -2\beta^2 C_2 - n_1 \frac{d^3\tau}{dx^3} - n_2 \frac{d^2Q}{dx^2} \tag{4.48}$$

$$\frac{d^3\sigma}{dx^3} = -2\beta^3 C_1 + 2\beta^3 C_2 - n_1 \frac{d^4\tau}{dx^4} - n_2 \frac{d^3Q}{dx^3} \tag{4.49}$$

The second and third order derivative of the load (Q) can be eliminated because it is limited to either uniformly distributed or point load type (Smith and Teng, 2001). By substituting the boundary conditions described above into Eqns. 4.48 and 4.49, the constants (C_1) and (C_2) can be determined as follows:

$$C_1 = \left[\frac{k_p}{2\beta^3 E_{hc} I_{hc}}\left(V_T(0) + \beta M_T(0)\right)\right] - \left[\frac{n_3}{2\beta^3}\tau(0)\right] + \left[\frac{n_1}{2\beta^3}\left(\frac{d^4\tau(0)}{dx^4} + \frac{\beta d^3\tau(0)}{dx^3}\right)\right] \tag{44.50}$$

$$C_2 = \left[\frac{-k_p}{2\beta^2 E_{hc} I_{hc}} M_T(0)\right] - \left[\frac{n_1}{2\beta^2}\frac{d^3\tau(0)}{dx^3}\right] \tag{44.51}$$

where

$$n_1 = \frac{y_t E_{hc} I_{hc} - y_{hc} E_t I_t}{E_{hc} I_{hc} + E_t I_t} \tag{44.52}$$

$$n_2 = \frac{E_{hc} I_{hc}}{b_t (E_{hc} I_{hc} + E_t I_t)} \tag{44.53}$$

$$\beta = \sqrt[4]{\frac{k_p b_t}{4}\left(\frac{1}{E_{hc} I_{hc}} + \frac{1}{E_t I_t}\right)} \tag{44.54}$$

4.2.4 Analytical Solution Results

4.2.4.1 Interfacial Shear Stress Distribution

Using the simplified and the modified methods explained in the previous sections, the shear stress distribution along the interface between the concrete topping and the hollowcore slab was evaluated for the full-scale test slabs at yielding. (k_s) values evaluated by Adawi et al. (2014) were utilized. For slabs with machine-cast surface, (k_s) ranged from 3.48 to 19 (N/mm)/mm^2. For slabs with lightly-roughened surface finish (k_s) was 6.75 (N/mm)/mm^2. The resulting distributions are given in Fig. 4.44 through Fig. 4.46.

Considering slabs with full concrete topping, the shear stress distribution calculated using the modified solution is lower than that calculated using the simplified solution with an average percentage difference of 51%. Both solutions produced higher interfacial shear stresses for higher shear stiffness coefficient (k_s). For the slabs with reduced topping area, the assumption of the modified method that the shear stress is continuous at (x) = L_t/2 produced a finite shear stress value at mid-span. Smith and Teng (2001) mentioned that this error does not significantly affect the shear stress distribution at the ends of the concrete topping. The simplified solution enforces zero shear stress under the point load as a boundary condition, so this behavior was not a concern.

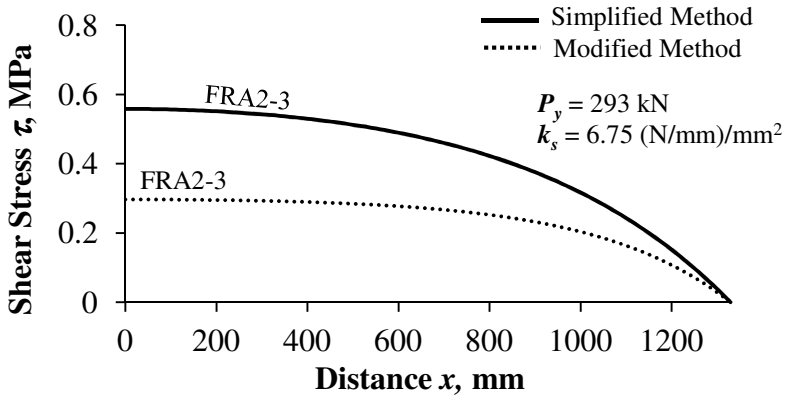

Fig. 4.44 : Shear stress distribution of slab FRA2-3 (full concrete topping).

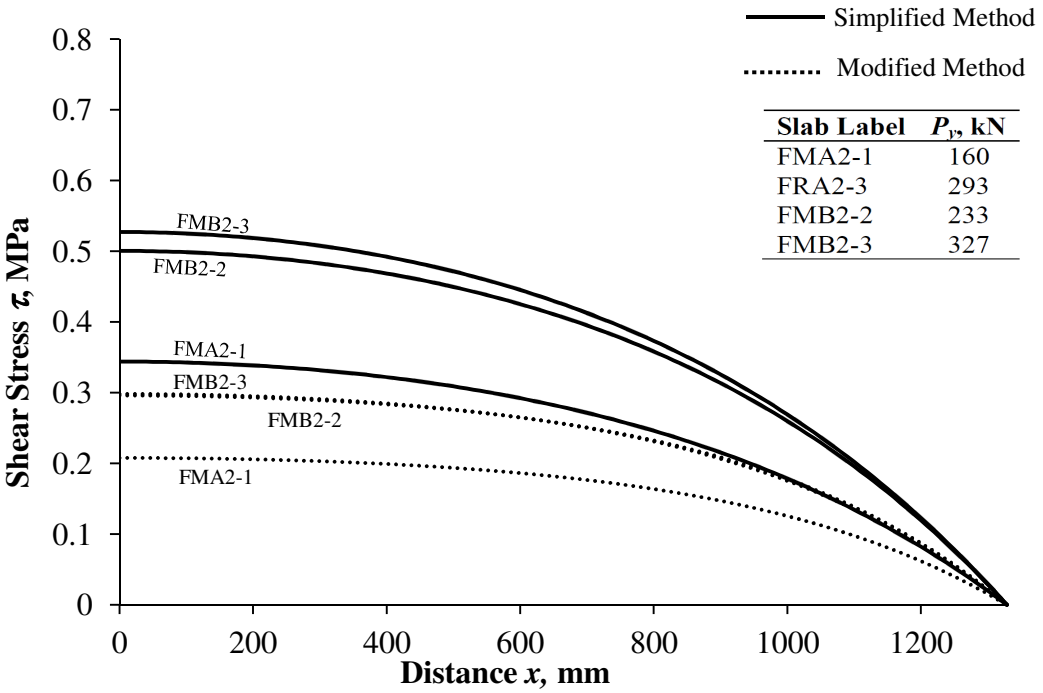

(a) k_s = 3.48 (N/mm)/mm^2

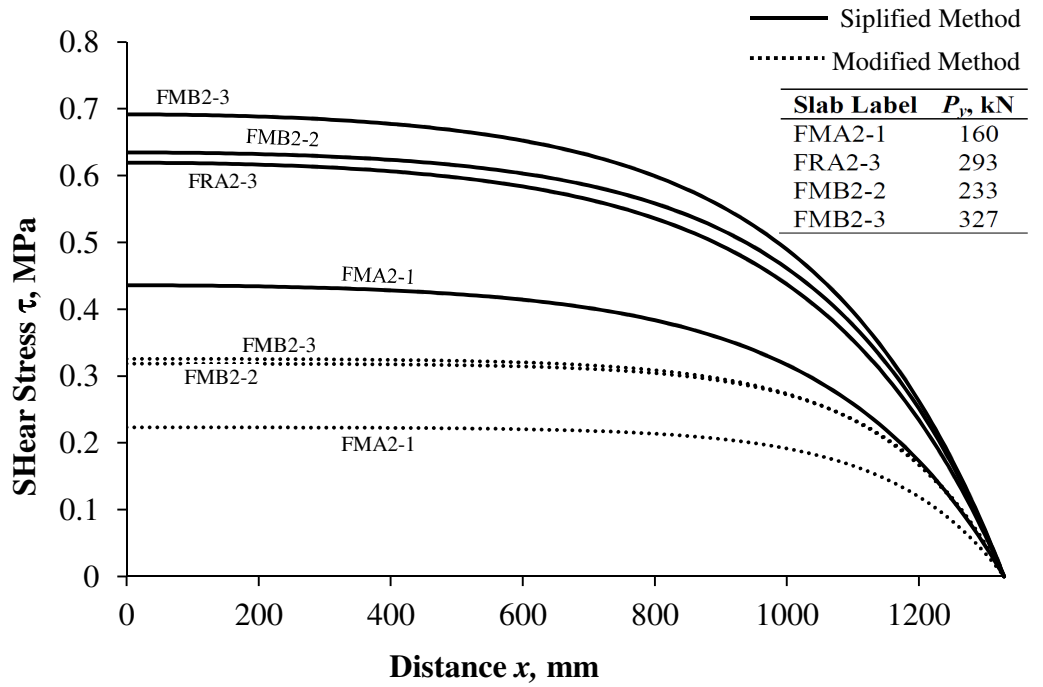

(b) k_s = 19 (N/mm)/mm^2

Fig. 4.48 : Shear stress distribution of the full-scale tests (full concrete topping).

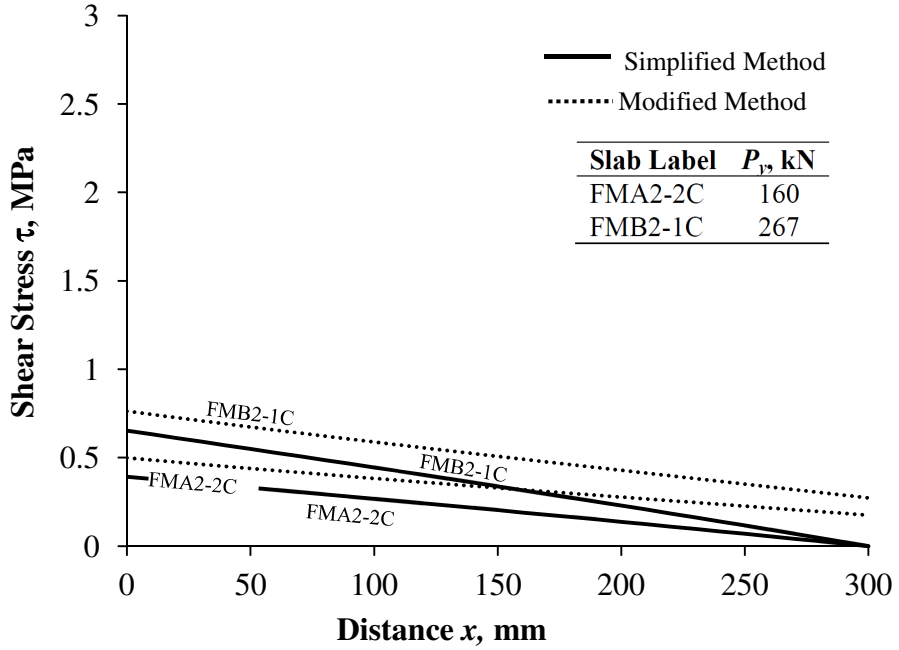

(a) k_s = 3.48 (N/mm)/mm^2

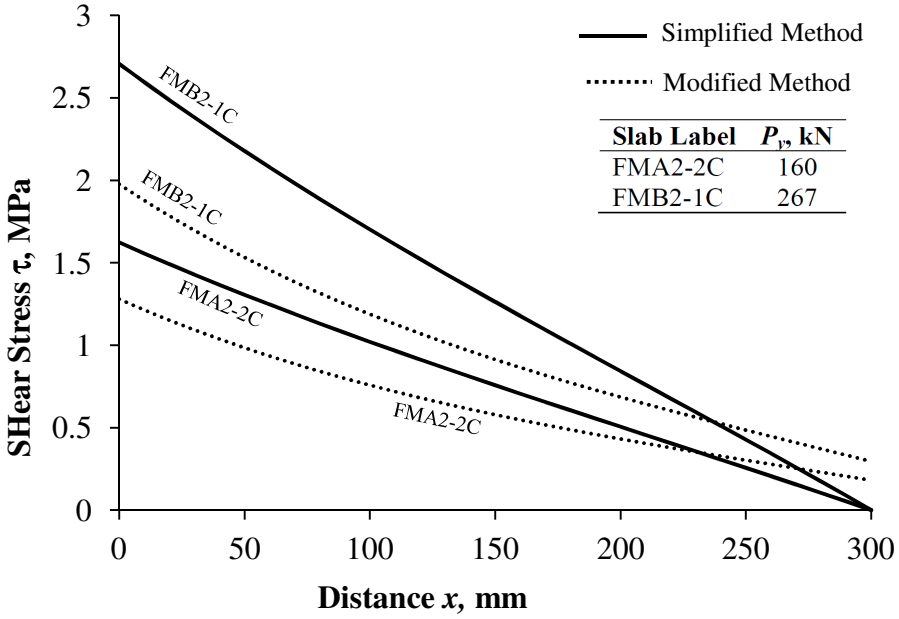

(b) k_s = 19 (N/mm)/mm^2

Fig. 4.46 : Shear stress distribution of the full-scale tests (reduced concrete topping).

The average horizontal shear stress at yielding ($\tau_{test\text{-}avg.}$) is calculated using the two methods available in the North American design standards, CSA A23.3-04 (2004) and ACI 318-08 (2008). The first method depends on the shear force diagram of the full-scale test and does not take into account the length of the concrete topping hence could not be used to evaluate the horizontal shear stress for the cut-slabs. The second method requires the use of strain compatibility to determine the horizontal shear force in the concrete topping. Table 4.1 summarizes ($\tau_{test\text{-}avg.}$) along with the results from the simplified and modified analytical solutions.

Table 4.1: Interfacial shear stress results

Slab Label	**Yield Load P_y, kN**	**Max. Shear Stress τ_f, MPa**									**Avg. Shear Stress (North American Standards), $\tau_{f\text{-}avg.}$ MPa**	
		Machine-cast Surface Finish						**Lightly-roughened Surface Finish**				
		k_s = 3.48 (N/mm)/mm^2			**k_s = 19 (N/mm)/mm^2**			**k_s = 6.75 (N/mm)/mm^2**			**Method (1)**	**Method (2)**
		SM	**MM**	**FE**	**SM**	**MM**	**FE**	**SM**	**MM**	**FE**		
FMA2-1	**160**	0.34	0.21	0.17	0.44	0.22	0.22	NA	NA	NA	0.32	0.34
FMA2-2C	**160**	0.39	0.50	0.38	1.62	1.28	1.00	NA	NA	NA	NA	1.49
FRA2-3	**293**	NA	NA	NA	NA	NA	NA	0.56	0.3	0.24	0.46	0.49
FMB2-1C	**267**	0.65	0.76	0.4	2.71	1.98	1.22	NA	NA	NA	NA	2.53
FMB2-2	**233**	0.50	0.30	0.24	0.63	0.32	0.33	NA	NA	NA	0.46	0.50
FMB2-3	**327**	0.53	0.30	0.24	0.69	0.33	0.30	NA	NA	NA	0.52	0.56

Note: SM: simplified method, **MM**: modified method, **FE**: linear finite element analysis.

Considering the slabs with full concrete topping, it can be observed that the shear stress values calculated using the modified solution were the lowest. Results of the simplified solution were more comparable with the design standards.

4.2.4.2 Validation of the Proposed Methods using Linear Finite Element Analysis

A linear finite element analysis was performed to judge on the accuracy of both methods.

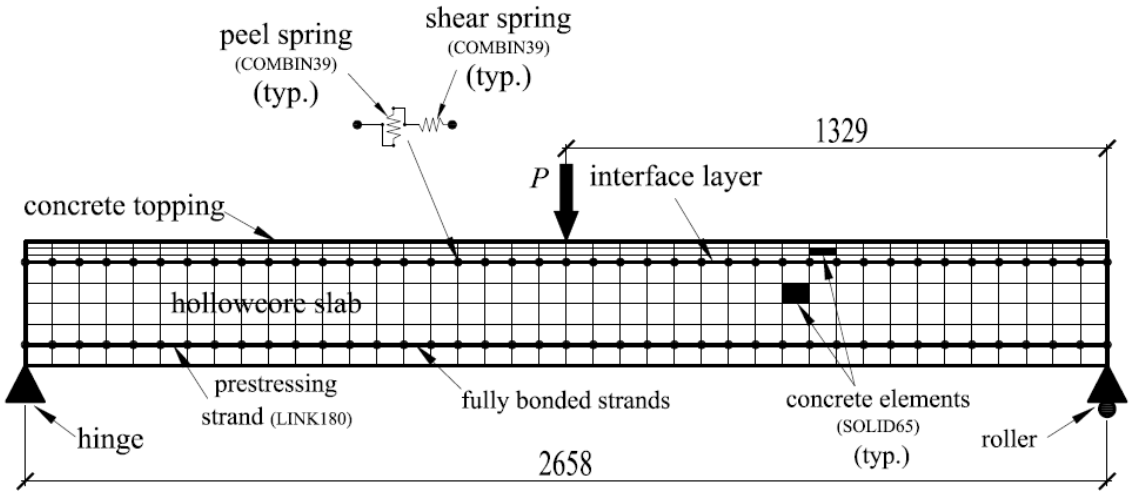

Fig. 4.50 : Idealization of the linear FE model.

The FE modeling was conducted using ANSYS R15 (2013) and idealized as illustrated in Fig. 4.50. Element SOLID65 was used to model the hollowcore slab and the concrete topping. LINK180 elements were used to model the prestressing strands and full bond was assumed between the strands and the surrounding concrete.

The interfacial shear and peel stiffness between the hollowcore slabs and the topping concrete were modeled using spring elements (COMBIN39) utilizing the linear stiffness

values used in the analytical models. A general 3-D view of the loaded slab is given in Fig. 4.51.

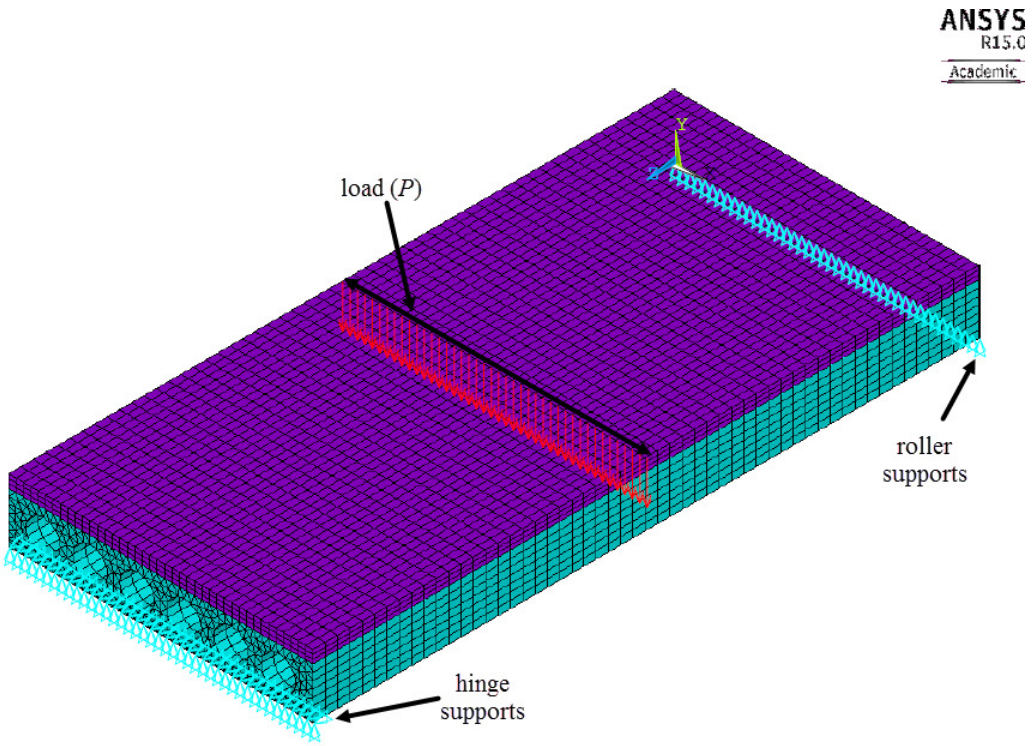

Fig. 4.51 : General 3-D view.

Similar to the analytical models, linear material properties were used in the FE model utilizing the Young's modulus for the hollowcore slab, the concrete topping and the prestressing strands (E_{hc}, E_t and E_p), respectively. The results of the FE analysis are shown in Table 4.1.

It can be observed that the finite element analysis yielded the lowest shear stress values among the presented methods. The modified method appear to be consistent with the FEA when used with the upper bound (k_s) value, 19 (N/mm)/mm^2 with an average difference of 16%.

4.2.4.3 Peel Stress Distribution

The peel stress distribution evaluated is shown in Fig. 4.52.

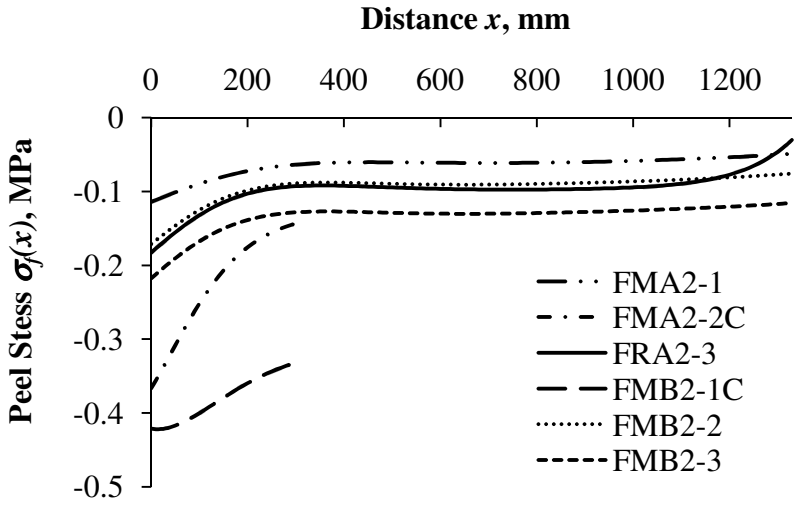

Fig. 4.52 : Peel stress distribution.

The approximate peel stiffness coefficient (k_p = 2.0 (N/mm)/mm^2) determined from analytical modeling of the push-off tests was used. As can be noticed, negative peel stress was calculated at the interface layer for all of the tested slabs. This implies that the interface layer was under compression, thus peel failure was not a concern. This result is consistent with the experimental data from the cut-slabs where the peel deformation gauges did not record any movement up to the yielding loads.

The behavior of the peel stress is consistent for all of the slabs where the maximum negative peel stress occurs at the end of the concrete topping and then decrease towards the mid-span point where the load (P) is applied. Additionally, the magnitude of the negative peel stress increases with the increase in the bending rigidity (EI) and the concrete compressive strength, f'_c, of the slab. The linear finite element analysis conducted in the previous section also produced negative peel stresses for all slabs. This

corroborates the results obtained using the proposed analytical model for the peel behavior.

4.2.5 Conclusions

Two analytical methods, simplified and modified, were developed to evaluate the interfacial shear stress distribution along the interface between the concrete topping and the hollowcore slab during the full-scale tests. The simplified method ignores the moment and shear resistances of the concrete topping while they are considered in the modified method. Additionally, the simplified method assumes zero interfacial shear stress under the point load whereas the modified method retains continuity at that location.

The analytical solutions are applicable up to the yielding load level where the composite slab is behaving in the linear elastic zone. The interfacial shear stress levels obtained from the methods existing in the North American codes were shown to be conservative in comparison with the proposed analytical solutions. Considering the slabs with reduced concrete topping, the analytical solutions revealed higher interfacial shear stresses than the limits mentioned in CSA A23.3-04 (2004), 0.7 MPa, and ACI 318-08 (2008), 0.55 MPa. However, those slabs exhibited reliable composite action up to the predicted failure loads. The interfacial shear stiffness (k_s) did not seem to significantly affect the interfacial shear stress except when the concrete topping is reduced. Higher (k_s) values appear to produce better results for this case. Peel stresses did not have any tangible effect considering the linear analysis presented in this chapter.

In comparison with linear finite element analysis, it can be concluded that the modified method is the most adequate technique in evaluating the interfacial shear and peel stresses in composite hollowcore slabs. This method can be conveniently used by designers regardless of the concrete topping length. The shear and peel stiffness coefficients can be estimated using the analytical modeling explained in Chapter 3.

4.3 References

ACI 318, 2008. Building code requirements for structural concrete (ACI 318-08) and commentary. Michigan, United States: American Concrete Institute.

Adawi A, Youssef MA, Meshaly M., 2014. “Analytical modeling of the interface between lightly roughened hollowcore slabs and cast-in-place concrete topping”. ASCE J Struct Eng 2014.

ANSYS® Academic Research, Release 15.0, 2013, ANSYS, Inc.

CSA A23.3, 2004, Design of concrete structures (A23.3-04). Mississauga, ON, Canada: Canadian Standard Association (CSA).

Smith, S.T., Teng, J.G., 2001. Interfacial stresses in plated beams. Engineering Structures 23 (7), 857–871.

Vilnay O., 1988. “The analysis of reinforced concrete beams strengthened by epoxy bonded steel plates”, Int J Cement Compos Lightweight Concrete;10(2):73–8.

CHAPTER FIVE

5 Finite Element Analysis of the Composite Action between Hollowcore Slabs and the Topping Concrete

The vast majority of previous literature on composite action of flexural elements is related to steel beams, where the concrete topping is attached to the top flange of the steel beam using shear connectors. Those connectors can be modeled using spring elements, (Salari et al., 1998) and (Queiroz et al., 2006). Springs can also be used to model bond strength between concrete and the asphalt overlays in roads, (Taizo et al., 2005). Mones (2012) modeled composite hollowcore slabs using 2-D plane stress elements. Spring elements resembled the interfacial shear stress. The analysis assumed linear elastic behaviour and did not account for the peel behaviour. The shear stiffness of the spring elements was determined using push-off tests. Results of the finite element analysis were not validated.

The behaviour of the concrete material becomes highly nonlinear after cracking, which greatly affects its overall response. Therefore, it is necessary to investigate the behaviour of the composite hollowcore slabs in the post-cracking zone (nonlinear). This chapter starts by summarizing the push-off and full-scale tests that were conducted on composite hollowcore slabs. Finite element modeling of the push-off tests allowed determining the interfacial shear and peel stiffness for each slab. These were used as initial values while modeling the full-scale tests, which allowed evaluating the final interfacial shear and peel stiffness of the composite slabs.

5.1 Push-off and Full-scale tests

Push-off tests were conducted in the vertical orientation. The concrete topping was resting on a steel plate, and a downward force was applied to the hollowcore slab. Two steel beams were positioned on the back of the hollowcore slab to provide stability. The

concrete topping was instrumented with five strain gauges (S1 to S5), two peel displacement gauges (L1, L2) and two slip displacement gauges (L3, L4). The push-off test setup and instrumentation are shown in Fig. 5.1.

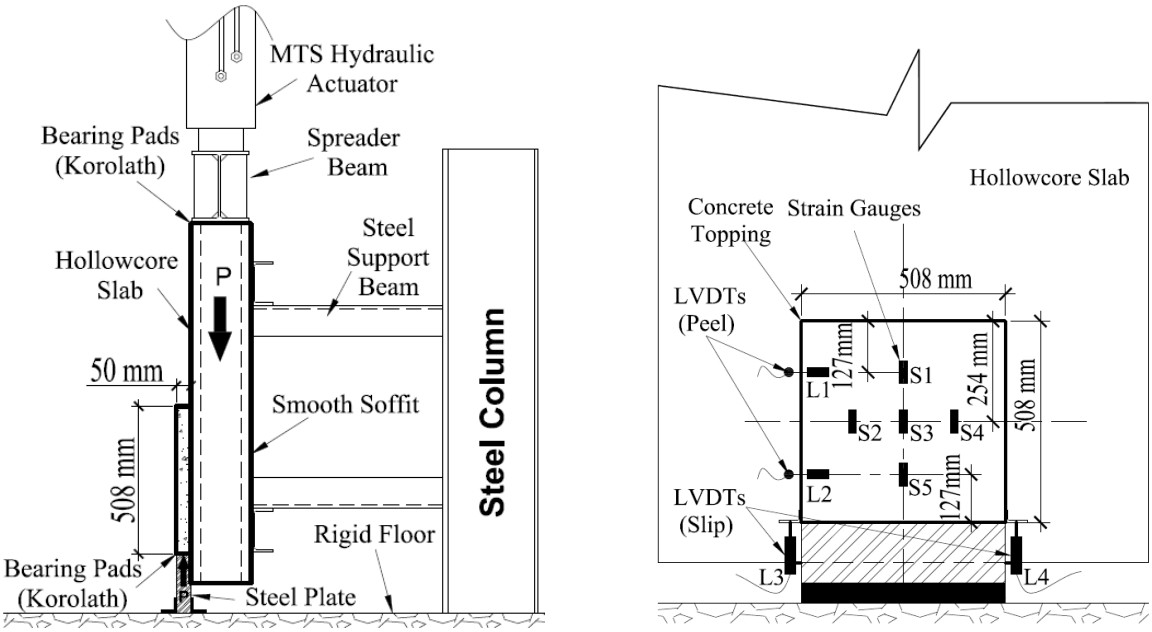

Fig. 5.1: Push-off test setup and instrumentation.

The tested hollowcore slabs were 203 mm deep and had a surface area of 1220 mm by 1220 mm. The nominal concrete compressive strength for the hollowcore slabs was 41 MPa. The concrete topping had a surface area of 508 mm by 508 mm, a thickness of 50 mm and a concrete compressive strength of 32 MPa. A total of seven slabs (SMA1-2, SRA1-1, SRA1-3, SRB1-1, SRB1-2, PSMA4-2 and PSMA4-3) were tested. “M” and “R” refer to the surface finish of the slab as either machine-cast or lightly-roughened, respectively. “A” and “B” refer to the slab manufacturer.

Table 5.1 provides details about the full-scale test slabs. Five of the slabs (FMA2-1, FMA2-2C, FMB2-1C, FMB2-2 and FMB2-3) had machine-cast surface finish. Slab FRA2-3 had a lightly-roughened surface finish. The length and width of the slabs were

approximately 3658 mm and 1220 mm, respectively. The concrete topping had a thickness of 50 mm and a concrete compressive strength of 30 MPa.

Table 5.1: Full-scale test slabs

Slab Label	**Concrete Compressive Strength f'_c (MPa)**	**Thickness, mm**	**Prestressing Strands**
FMA2-1	53	203	203, 4- ½" strands
FMA2-2C	50	203	203, 4- ½" strands
FRA2-3	51	253	253, 6- ½" strands
FMB2-1C	62	203	203, 7- ½" strands
FMB2-2	58	203	203, 7- ½ " strands
FMB2-3	60	203	203, 7- ½" strands

Fig. 5.2 shows a typical full-scale test. The load (*P*) was applied at mid-span using a steel spreader beam. The figure also shows the instrumentations for slabs (FMA2-1, FRA2-3, FMB2-2 and FMB2-3) that had full concrete topping and slabs (FMA2-2C and FMB2-1C) for which the concrete topping was discontinuous. Vertical deflection was measured at mid-span using displacement gauges (LE and LW).

Slip was measured using displacement gauges (SLE1 and SLE2) at the east side and (SLW1 and SLW2) at the west side for composite slabs that had full concrete topping. Peel deformations were not measured for those slabs. For slabs that had a cut in their concrete topping, slip was measure on both sides of the concrete topping using displacement gauges (SLCW and SLCE). Peel deformations were measured using

displacement gauges (PCW and PCE). Strain gauges were attached to the hollowcore slabs (SHCE and SHCW) and the concrete topping (STE and STW) at mid-span as close as possible to the interface layer. More details about the push-off and full-scale tests are given by Adawi et al. (2014) and in Chapter 2.

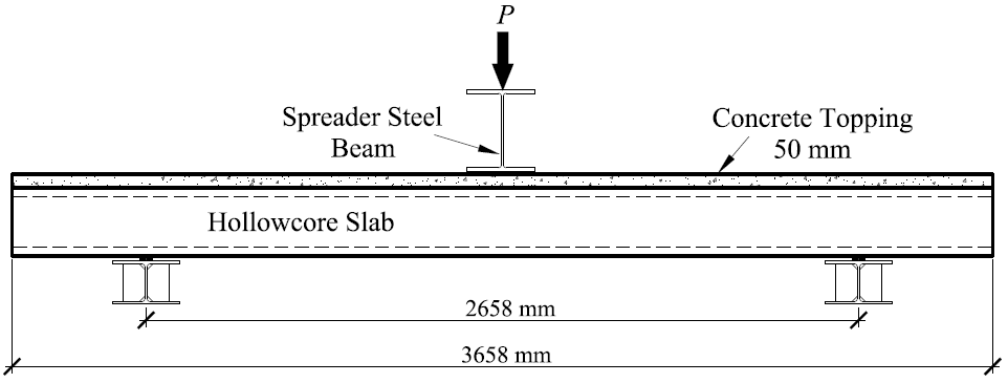

Typical full-scale test setup.

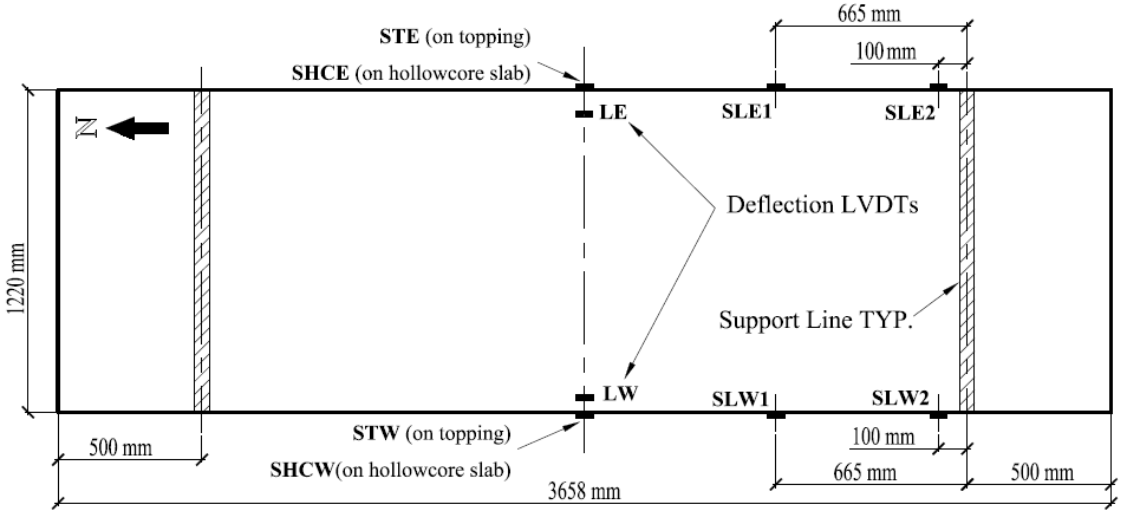

Instrumentation of slabs with full concrete topping

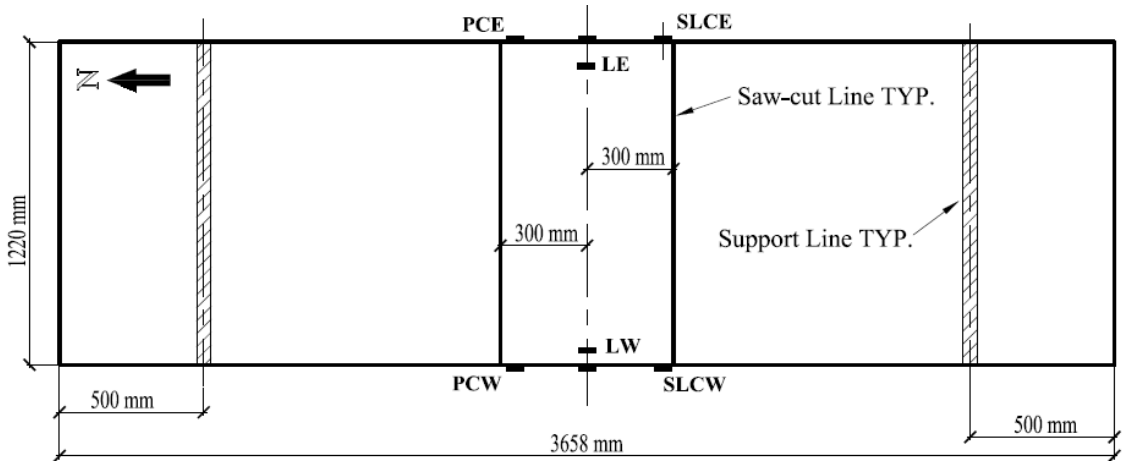

Instrumentation of the slabs with discontinued concrete topping

Fig. 5.2: Full-scale test setup and instrumentation.

5.2 Finite Element Modeling

ANSYS R15.0 (2013) was utilized to model the push-off and the full-scale tests. This section explains the modeling techniques including modeling of the prestressing force and the staged construction process. The material models used in the analysis will then be presented.

5.2.1 Push-off Test

The finite element idealization of the push-off test is illustrated in Fig. 5.3. The concrete and the hollowcore slab were modeled using 4-noded plane stress elements (PLANE182) that has two translation degrees of freedom per node. An element size of 12.7 mm by 12.7 mm resulted in a total of 40 common nodes along the interface layer. While a finer mesh size did not improve the results, a coarser mesh was not deemed necessary since the processing time was quite reasonable. The width of the concrete element in the out-of-plane direction is equal to 508 mm.

Two coincident set of nodes were used at the interface, one for the bottom surface of the topping slab and the other for the top surface of the hollowcore slab. At every node, two contact elements (COMBIN39) were used to attach the hollowcore slab to the concrete topping in the X and Z directions. COMBIN39 is unidirectional nonlinear spring element where its generalized force-displacement relationships can be defined independently for tension and compression. The tributary area associated with each spring depends on its location. Thus, the springs were divided in two groups: edge springs with a tributary area of 6.35 mm by 508 mm and interior springs with a tributary area of 12.7 mm by 508 mm.

Roller supports were used at the loaded end of the hollowcore slab. The lateral deformation of the hollowcore slab was experimentally prevented using the steel frame shown in Fig. 5.3. This frame was modeled using compression only springs. The load was applied on the concrete topping in a force controlled manner.

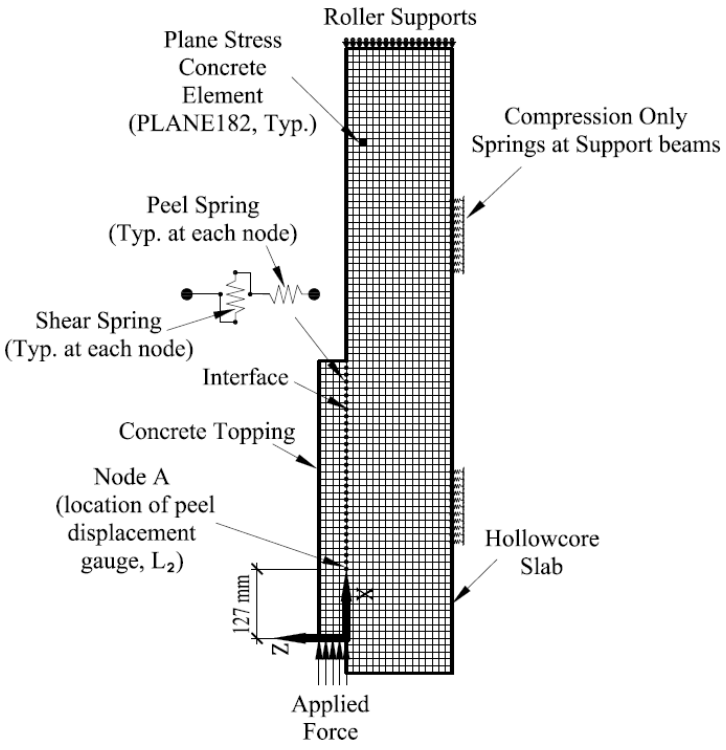

Fig. 5.3: Finite element idealization of the push-off test.

5.2.2 Full-scale Test

The full-scale test was conducted using a three-point bending test setup as shown in Fig. 5.2. The finite element idealization of the test is demonstrated in Fig. 5.4.

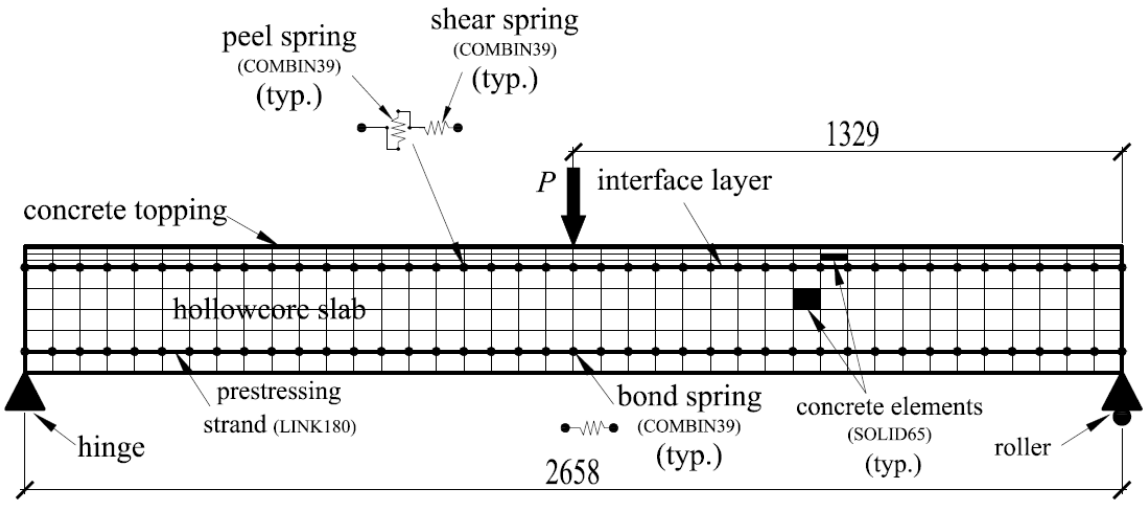

Fig. 5.4: FE idealization of the full-scale test.

Similar to the push-off test, the main components of the full-scale test are: the hollowcore slab, the concrete topping and the interface between the hollowcore slab and the concrete topping. 6-noded and 8-noded 3-D solid elements (SOLID65) were used to model the hollowcore slab and the concrete topping, respectively.

The interface layer between the hollowcore slab and the concrete topping was modeled using nonlinear spring elements. A typical 3-D model for the composite hollowcore slab is shown in Fig. 5.5.

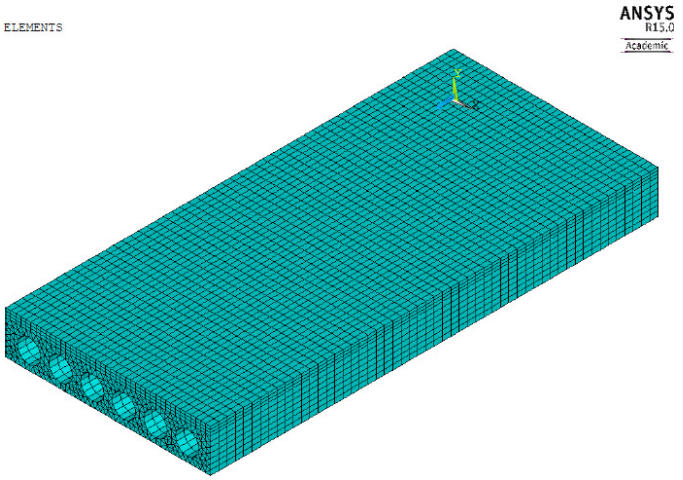

(a) General 3-D view of the composite hollowcore slab.

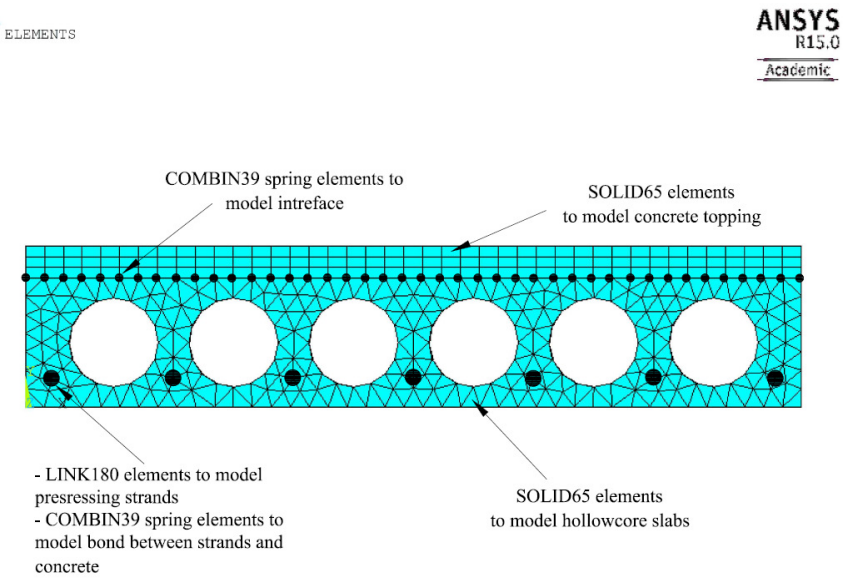

(b) Cross section of the composite slab.

Fig. 5.5: Finite element model of the full-scale test

The prestressing strands of the hollowcore slab were modeled using a 3-D truss element (LINK180) that is defined by two nodes with three degrees of freedom in translation at each node.

The geometry of a typical composite hollowcore slab was initially created by using block shapes. Several ANSYS geometry tools including “BOOLEANS” were used to create the voids in the hollowcore slab. The meshing was first conducted on the cross section area

using the generic area element (MESH200) as shown in Fig. 5.6. The meshed cross section was then swept over the entire hollowcore slab's using the (SOLID65) concrete element. Nodes at the strands location were forced during meshing in order to coincide with the strands nodes that will be created later. Aspect ratio adequacy was verified automatically using the ANSYS recommended built-in criteria.

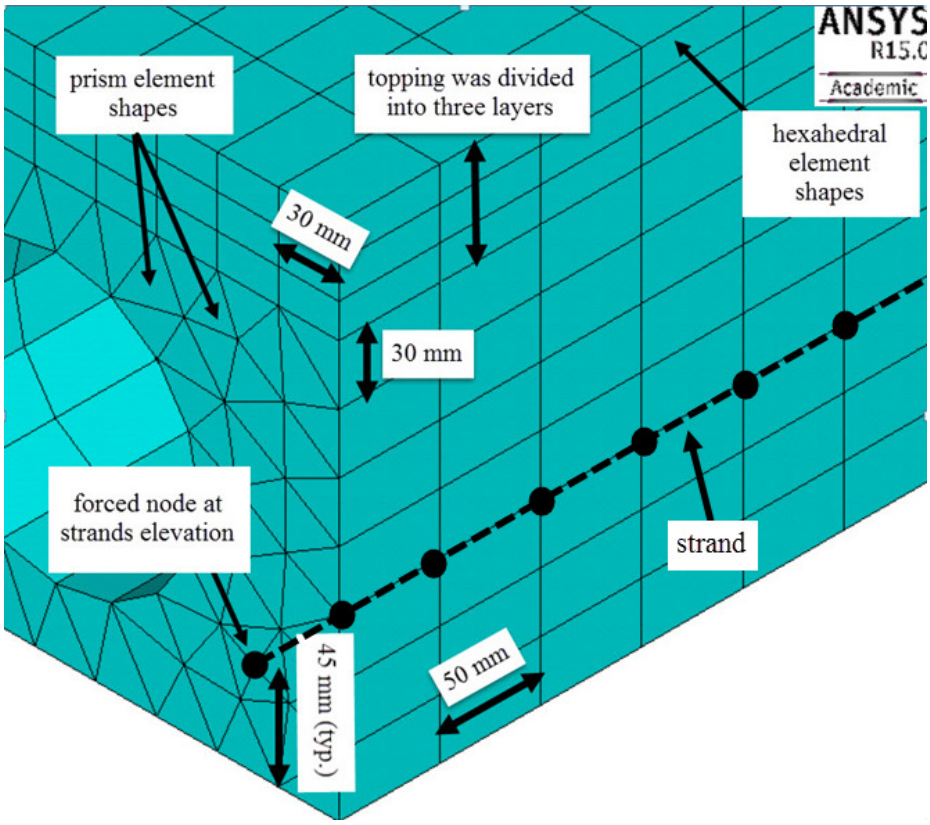

Fig. 5.6: Meshing layout.

The coincident nodes at the interface were connected using the nonlinear spring elements (COMBIN39) in the three directions X, Y and Z. The boundary conditions were assigned such that they simulate the actual support conditions of the composite slab in the full-scale test, Fig. 5.4. The bottom nodes at the hinged end of the slab were restricted in the Z and Y directions while the nodes at the roller support were restricted in the Y direction.

The load, (*P*), was applied at the nodes located on top of the concrete topping at mid-span of the slab.

Each strand consisted of (LINK180) elements that have the same length as the concrete elements along the Z direction, Fig. 5.6. Accordingly, coincident nodes from the concrete and strands elements were created along the length of each strand. Those coincident nodes were used to model the bond between the strands and the surrounding concrete as explained in the following section.

5.2.3 Special Modeling Techniques

Modeling the composite hollowcore slab involves dealing with two complex issues: modeling the transfer of the prestressing force and the strain discontinuity between the hollowcore slab and the concrete topping. The concrete topping is cast after the hollowcore slab. This implies that the strains, and stresses, in the concrete topping were equal to zero before applying the concentrated load (*P*) shown in Fig. 5.4. The following sections explain how those two issues were addressed.

5.2.3.1 Prestressing Force

The prestressing force was modeled using the "initial state" (INISTATE) command. This command can be used to apply specific strain values to element (LINK180) that resembles the strands. The strain in the prestressed strands at the time of testing was estimated. The jacking stress was 70% of the strand's ultimate tensile strength. Prestress losses were estimated to be 15% of the jacking stress. Bond between the hollowcore slab and the prestressing strands was modeled using nonlinear spring elements (COMBIN39), as shown in Fig. 5.7.

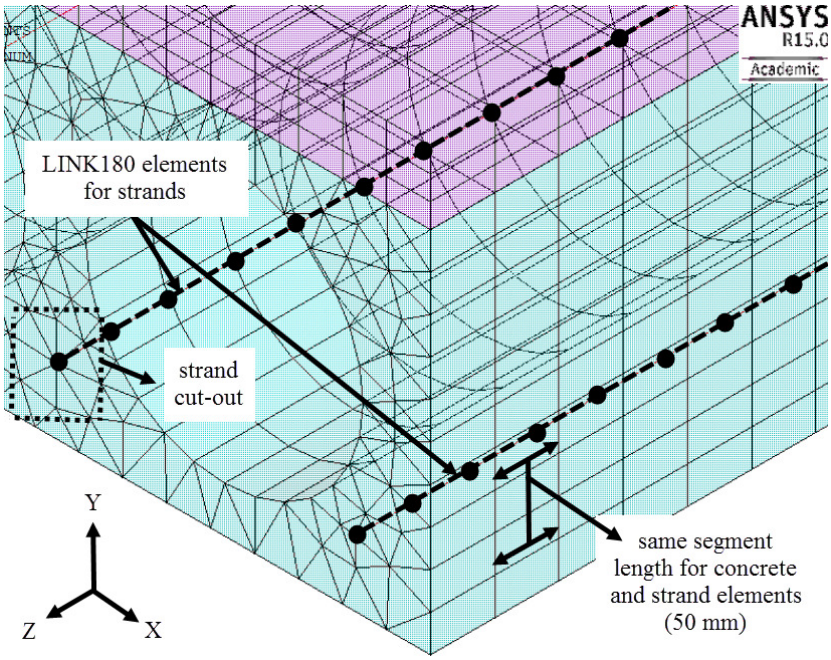

(a) Modeling of strands.

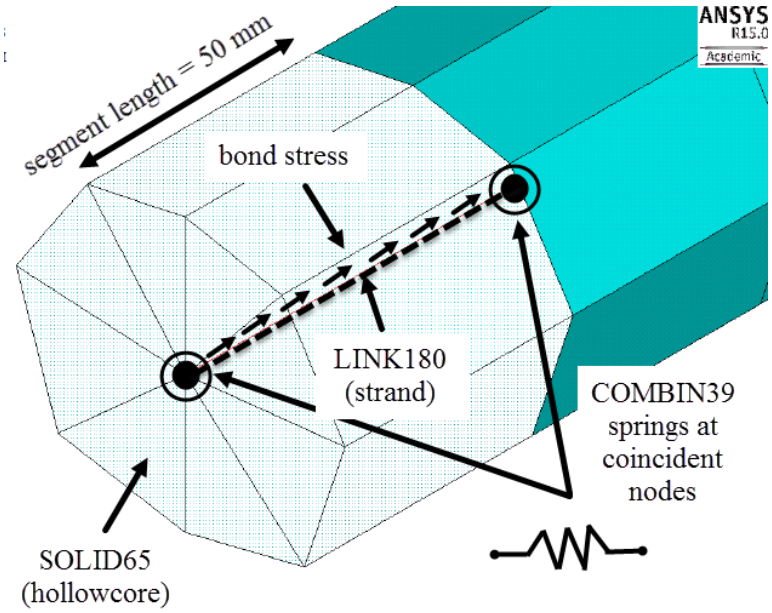

(b) Strand cut-out.

Fig. 5.7: Illustration of the bond stress modeling.

The constitutive force-displacement curve for those springs was developed using the bond-slip model by Balázs (1992), Eq. 5.1.

$$\tau_b = 2.324 \times \sqrt{f'_{ch}(s)^{1/2}} \text{ (MPa)} \qquad 5.1$$

where (τ_b) is the bond stress in the direction of slip direction, (f'_{ch}) is the concrete compressive strength of the hollowcore slab and (s) is the slip between the strand and the surrounding concrete in millimeters. The bond stress (τ_b) is multiplied by the cylindrical circumferential area of the strand along the segment length to define the spring force at different slip values. For illustration, the force-displacement relationship of the bond springs used for slab FMA2-1 is shown in Fig. 5.8.

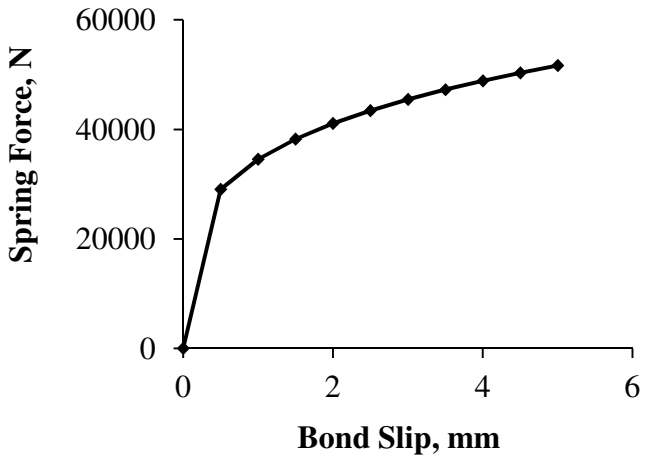

Fig. 5.8: Bond-slip relationship for slab FMA2-1

5.2.3.2 Strain Discontinuity

The concrete topping was cast after prestressing the hollowcore slab. Accordingly, the strains and stresses in the concrete topping were equal to zero before applying the external load (P). The interfacial shear and peel stresses were also equal to zero at that stage. Fig. 5.9 illustrates the typical staged construction for the composite slab. To model

the staged construction process, the initial stiffness of the concrete topping elements was significantly reduced such that it does not contribute to the overall stiffness. This was achieved by using the "Kill" feature. The prestressing force was then applied as an initial strain using the "Initial State" feature in ANSYS. The stiffness of the concrete topping elements was finally adjusted to reflect its actual value using the feature "Birth" in ANSYS.

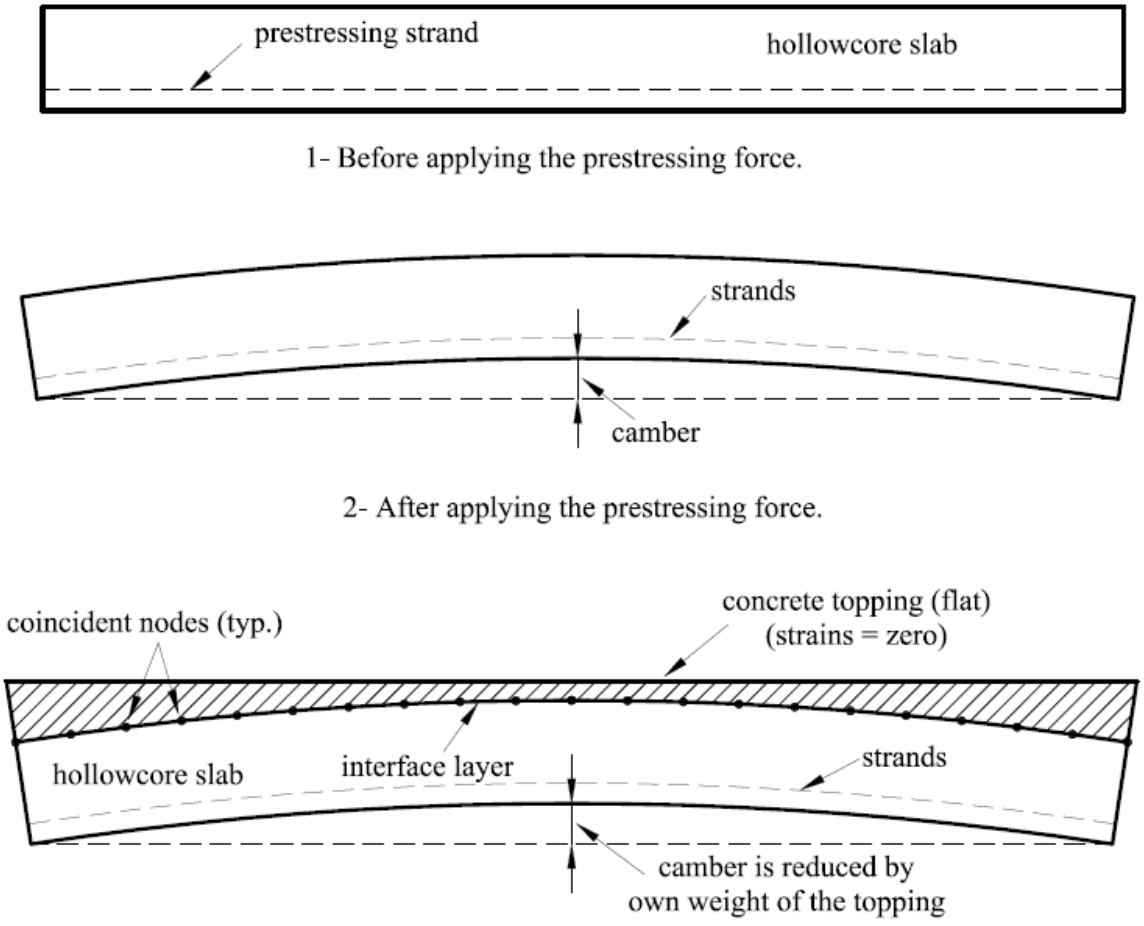

Fig. 5.9: Staged construction steps.

The concrete topping and the interface springs were checked at the mid-span section to ensure that they did not experience any stresses. The load (P) was then applied along the entire width of the composite slab as shown in Fig. 5.10.

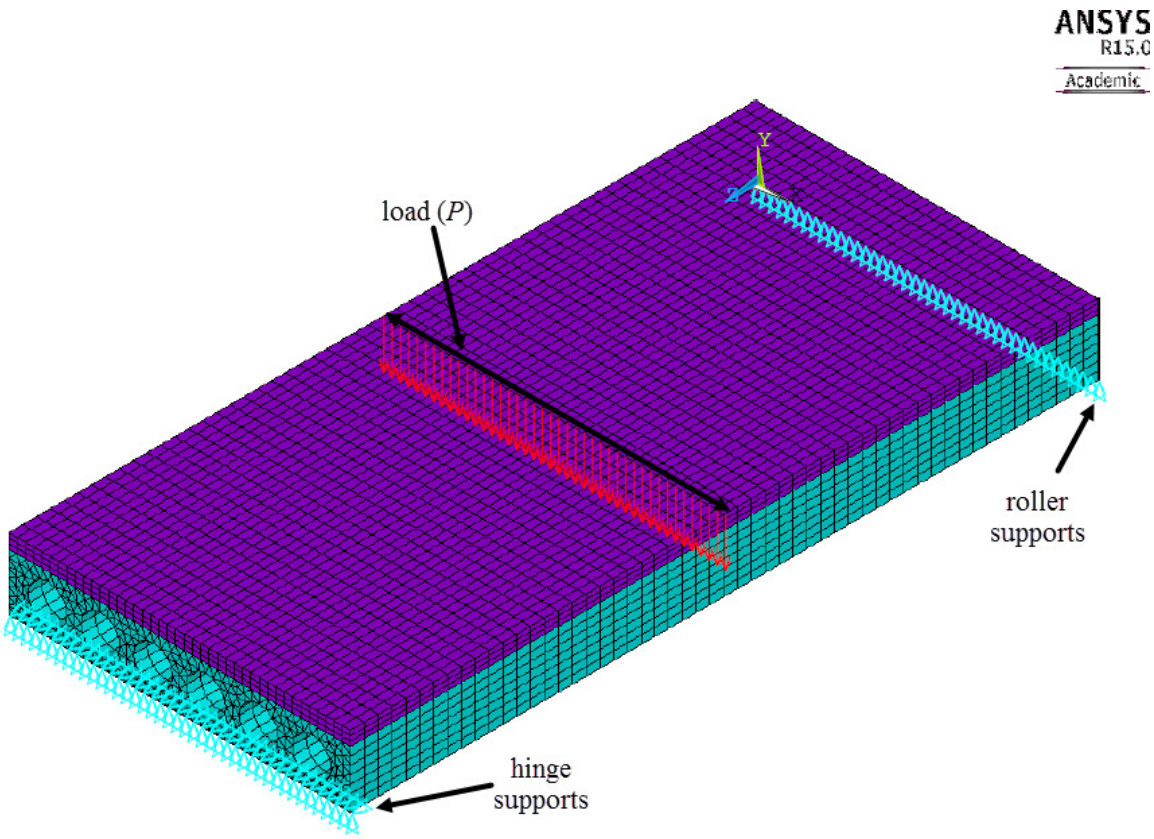

Fig. 5.10: Loaded composite slab

5.2.4 Material Models

5.2.4.1 Concrete

The concrete material model is implemented in ANSYS by three components: (1) linear isotropic component, (2) multilinear kinematic hardening properties of concrete and (3) William and Warnke (1974) concrete model, which describes the constitutive behaviour of concrete under triaxial conditions.

The linear isotropic component is defined by the concrete initial tangent stiffness (E_c) that was determined using Eqn. 5.5, recommended by Collins (1991), and the Poisson's ratio of 0.2. The unconfined concrete stress-strain relationship proposed by Popovics (1973) and calibrated by Porasz (1989) was used to define the multilinear stage using Eqns. 5.2 to 5.4:

$$f_c = f'_c \frac{n(\varepsilon_c/\varepsilon'_c)}{n-1+(\varepsilon_c/\varepsilon'_c)^{nk}} \text{ (MPa)} \qquad 5.2$$

$$n = 0.8 + \frac{f'_c}{17} \qquad 5.3$$

$$k = 1 \text{ for } (\varepsilon_c/\varepsilon'_c) < 1.0 \qquad 5.4$$
$$= 0.67 + \frac{f'_c}{62} \text{ for } (\varepsilon_c/\varepsilon'_c) > 1.0$$

where,

f_c: concrete compressive stress

ε_c: concrete compressive strain

f'_c: peak cylinder compressive strength

ε'_c: strain at peak compressive stress

n: curve fit parameter

k: factor to account for the post peak ductility for high strength concrete

(ε'_c) can then be calculated using Eqn. 5.6

$$E_c = 3320\sqrt{f'_c} + 6900 \text{ (MPa)} \qquad 5.5$$

$$\varepsilon'_c = \frac{f'_c\, n}{E_c (n-1)} \qquad 5.6$$

For illustration, the concrete stress-strain curve for the hollowcore slab SMA1-2 and its concrete topping are shown in Fig. 5.11.

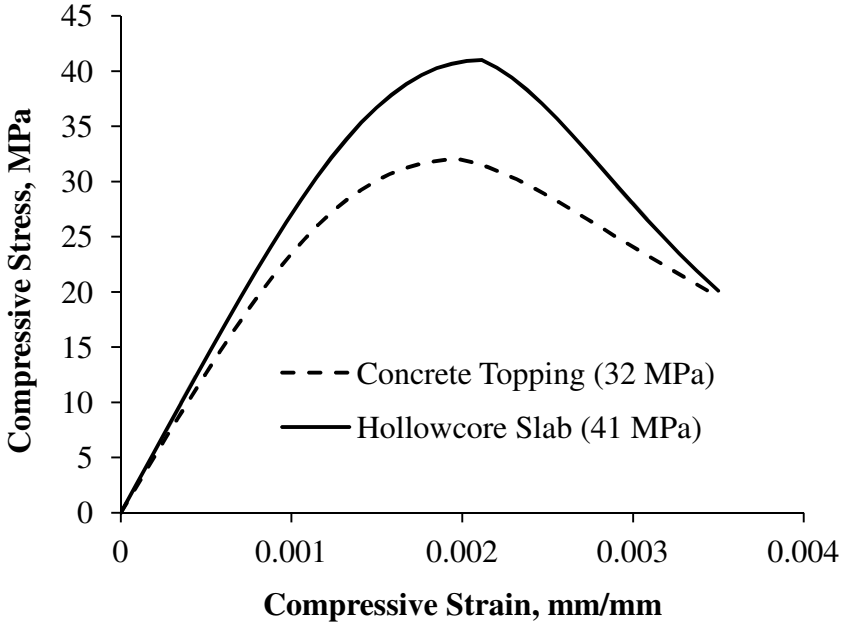

Fig. 5.11: Concrete stress-strain curve for hollowcore slab SMA1-2.

The concrete triaxial behaviour is defined by assigning shear transfer coefficients of 0.3 and 0.95 for open and closed cracks, respectively (Cheng and Wang, 2010). The uniaxial tensile cracking stress (f_t) was calculated using the formula recommended by Bentz (2000), Eq. 5.7.

$$f_t = 0.45\left(f'_c\right)^{0.4} \qquad 5.7$$

where, (f'_c) is the concrete compressive strength

5.2.4.2 Prestressed Reinforcement

The tensile test results for the prestressing strands for slabs from manufacturer A were conducted in accordance with ASTM standard A416/A416M-02 (2002). The ultimate strength (f_{pu}), rupture strain (ε_{pr}) and average modulus of elasticity (E_p) were 1965 MPa, 0.0059 and 199,948 MPa, respectively. The complete stress-strain curve is shown in Fig. 5.12.

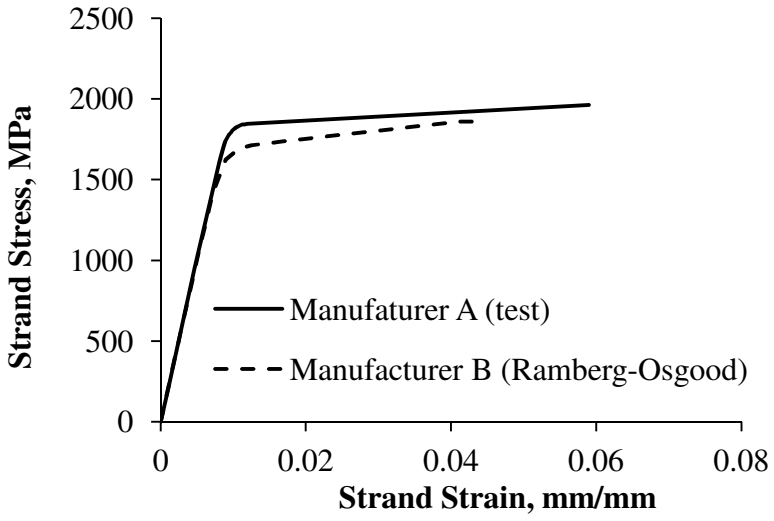

Fig. 5.12: Stress-strain curves for the prestressed strands.

The tensile test results were not available for strands used by manufacturer B, thus, stress-strain curve for those strands was constructed using the Ramberg-Osgood formulation, Eq. 5.8 (Collins, 1991).

$$f_p = E_p \varepsilon_p \left\{ A + \frac{1 - A}{\left[1 + \left(B\varepsilon_p\right)^C\right]^{\frac{1}{C}}} \right\} \leq f_{pu} \qquad 5.8$$

where (f_p) and (ε_p) are the stress and strain in the prestressing strand, respectively. The constants *A*, *B* and *C* were taken as 0.025, 118 and 10.0, respectively, as recommended in the 4th edition of the Canadian Precast/Prestressed Institute (CPCI) design manual (2007). The modulus of elasticity (E_p) was taken as 200 GPa.

5.2.5 Failure Criteria

The failure criteria were: (1) maximum principal concrete strain reaching 0.002, which indicates shear failure; (2) compressive strain in concrete exceeding 0.0035 indicating flexural failure; (3) maximum stress in the strands reaching 1860 MPa and 1965 MPa for the slabs from manufacturers A and B, respectively; (4) interface shear failure when shear springs reach their ultimate capacity and (5) interface peel failure when peel springs reach their ultimate capacity.

5.3 Finite Element Analysis

5.3.1 Push-off Tests

5.3.1.1 Force-Displacement Curves of the Spring Elements

The assumed force-displacement curve for a typical shear spring is illustrated in Fig. 5.13(a), which shows three main regions: elastic, inelastic and failure. In the elastic region, the shear resistance is provided by chemical bond and mechanical friction. The chemical bond is lost at the yielding load, (P_{yx}). Sudden failure occurs when mechanical friction diminishes at load pf (P_{ux}). For the peel springs, Z direction, the resistance is only provided by the chemical bond as shown in Fig. 5.13(b).

5.3.1.2 Solution Strategy

Determination of the parameters defining the force-displacement curves for the spring elements involves an iterative procedure. The results obtained from the pull-off and the push-off tests of slab SRB1-1 are used to explain the solution strategy.

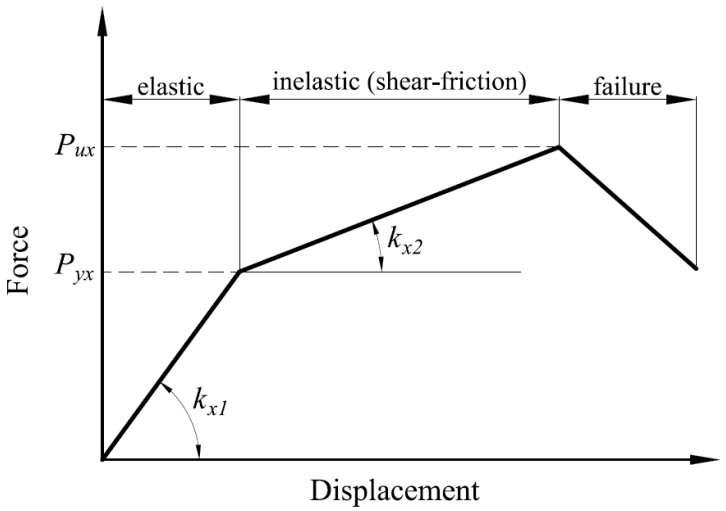

(a) Shear spring.

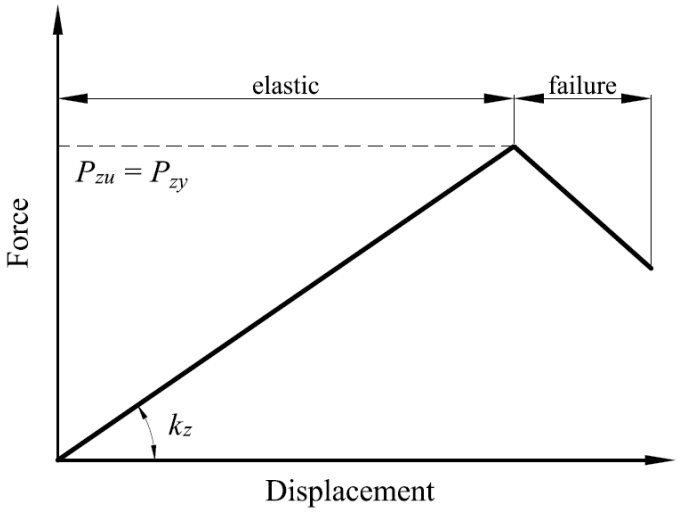

(b) Peel spring.

Fig. 5.13: Concept force-displacement curves of the interfacial spring elements.

The push-off test average load-displacement graph, P-UX, for slab SRB1-1 is shown in Fig. 5.14. The P-UX curve can be reasonably approximated using multi-linear segments. The linear segments are plotted such that the error areas above and below each segment are equal. The approximated P-UX curve was used to define the initial parameters of the shear springs force-displacement curve. By taking into account the number of springs, the following initial parameters can be obtained k_{x1}=373.3 × 10^3 N/mm, k_{x2}=73.4 ×10^3 N/mm, P_{yx} =2073 N and P_{ux} =5650 N.

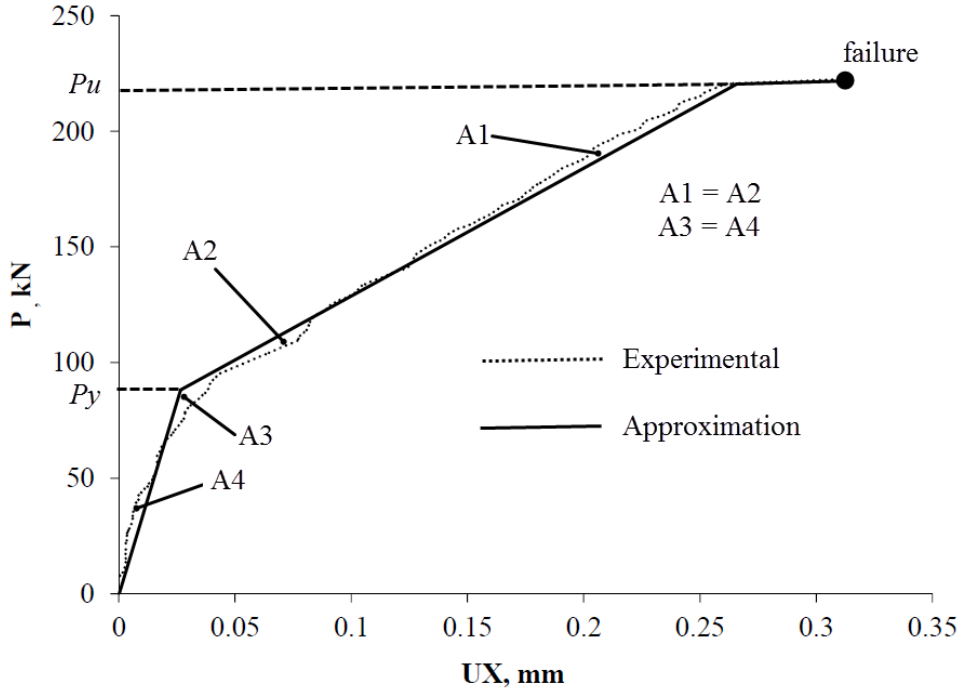

Fig. 5.14: Approximation of the P-UX graph for slab SRB1-1.

The initial parameters for the peel springs could not be drawn from the push-off tests. They were established using the pull-off test results. The bond strength for slab SRB1-1 was estimated to be 1.86 MPa, which is the average bond strength of similar slabs from the same manufacturer. The tributary area for an interior spring is equal to 6452 mm^2, thus, its maximum tensile force, (P_{yz}), can be calculated as 12 kN. The peel stiffness, k_z,

could not be determined experimentally because of the extremely small displacements. Adawi at al. (2014) provided a closed form solution of the differential equations governing the push-off tests, which allowed evaluating, k_p, as 2.1 (N/mm)/mm^2. Accordingly, the stiffness of an interior peel spring, k_z, is equal to 12.9 kN/mm. Peel springs were assumed to have very high stiffness in compression (120 kN/mm) to model the rigid compressive behaviour between the topping concrete the hollowcore slab.

The finite element analysis was conducted in a force-control fashion using automatic load stepping to enhance convergence. The obtained peel and slip deformations were compared to the experimental results. Suitable adjustments were then made to the properties of the shear and peel springs and the analysis was repeated.

The iterative process for slab SRB1-1 illustrated in Fig. 5.15. The initial properties for the shear and peel springs resulted in slip and peel values that are higher than the experimental results. In addition, it can be observed that the peel response was showing a linear behaviour that is not consistent with the experimental curve. Thus, the stiffness of the shear springs (k_x) was increased in the subsequent trials until a satisfactory match was obtained. A nonlinear force-displacement curve was used in to describe the peel behaviour. The above procedure was repeated for the rest of the push-off slabs and their final results are shown in Appendix 2.

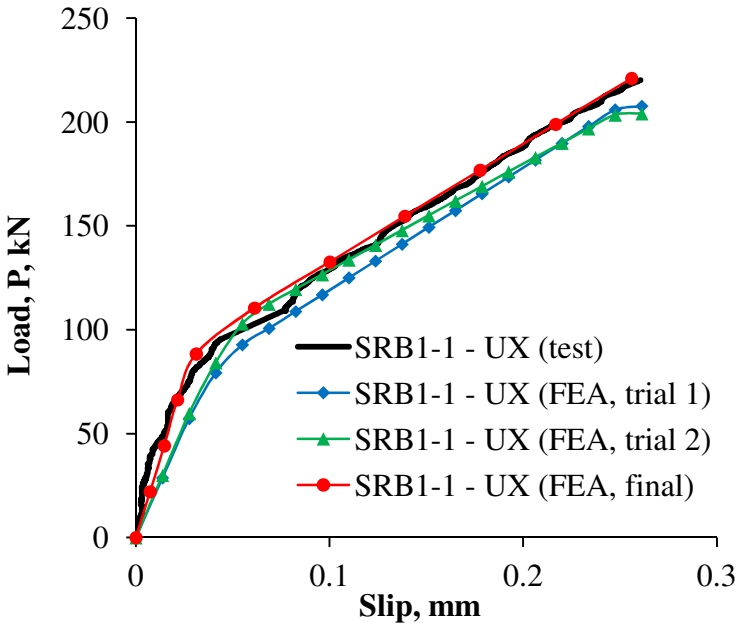

(a) Shear springs.

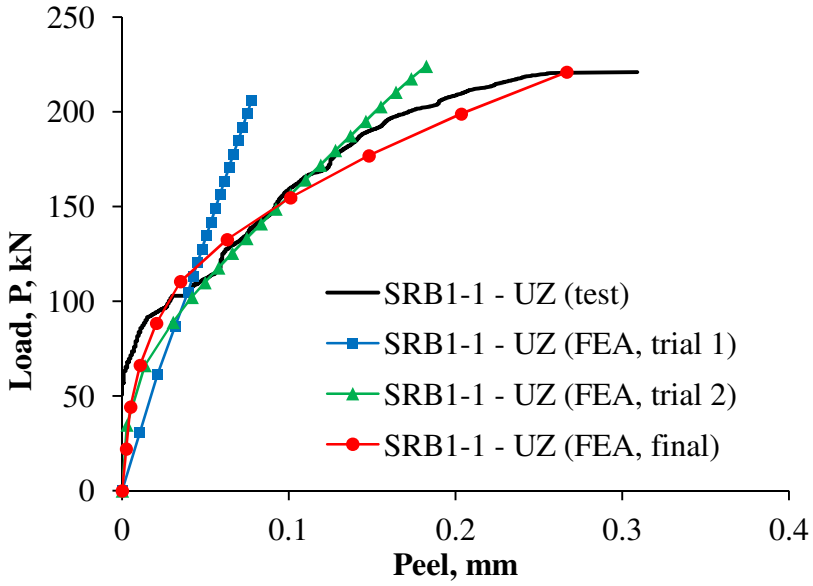

(b) Peel springs.

Fig. 5.15: Iterations for slab SRB1-1.

The parameters defining the force-displacement curves for the shear and peel springs are summarized in Table 5.2. Those values govern the nonlinear behaviour of the interfacial shear and peel responses in the push-off tests. The final force-displacement curves for the peel and shear springs are shown in Fig. 5.16 for slab SRB1-1. The final curves for the rest of the slabs are shown in Appendix 2.

Table 5.2: Force-displacement curves parameters of the push-off tests

Slab Label	**Shear Stiffness**				**Peel Stiffness**			
	yield		**ultimate**		**yield**		**ultimate**	
	P_{yx}, **kN**	k_{x1}, **kN/mm**	P_{ux}, **kN**	k_{x2}, **kN/mm**	P_{yz}, **kN**	k_{z1}, **kN/mm**	P_{uz}, **kN**	k_{z2}, **kN/mm**
SMA1-2	2.0	333	9.2	12.1	0.45	225	1.15	1.8
SRA1-1	7.0	700	12.7	5.8	1.0	100	1.6	3.2
SRA1-3	8.0	1600	15.0	23.7	1.7	170	2.1	0.8
SRB1-1	2.3	115	6.3	14.3	0.4	20	0.6	0.7
SRB1-2	3.8	38	4.8	12.5	0.6	12	0.75	3.0
PSMA4-2	6.5	650	7.35	6.5	1.3	130	1.35	2.5
PSMA4-3	1.0	200	1.7	0.4	0.15	150	0.19	0.5

Considering the slabs from manufacturer (A), k_{x1}, k_{x2}, P_{yx}, P_{ux}, k_{z1}, k_{z2}, P_{uz} and P_{uz} were found to range from: 200 to 650 kN/mm, 0.4 to 12.1 kN/mm, 1.0 to 6.5 kN, 1.7 to 9.2 kN, 130 to 225 kN/mm, 0.5 to 1.8 kN/mm, 0.15 to 1.3 kN and 0.19 to 1.35 kN for the slabs with machine-cast finish and: 700 to 1600 kN/mm, 5.8 to 23.7 kN/mm, 7.0 to 8.0 kN,

12.7 to 15 kN, 100 to 170 kN/mm, 0.8 to 3.2 kN/mm, 1.0 to 1.7 kN and 1.6 to 2.1 kN for lightly-roughened slabs. For lightly-roughened slabs from manufacturer (B), the variables were: 38 to 115 kN/mm, 12.5 to 14.3 kN/mm, 2.3 to 3.8 kN, 4.8 to 6.3 kN, 12 to 20 kN/mm, 0.7 to 3.0 kN/mm, 0.4 to 0.6 kN and 0.7 to 3.0 kN.

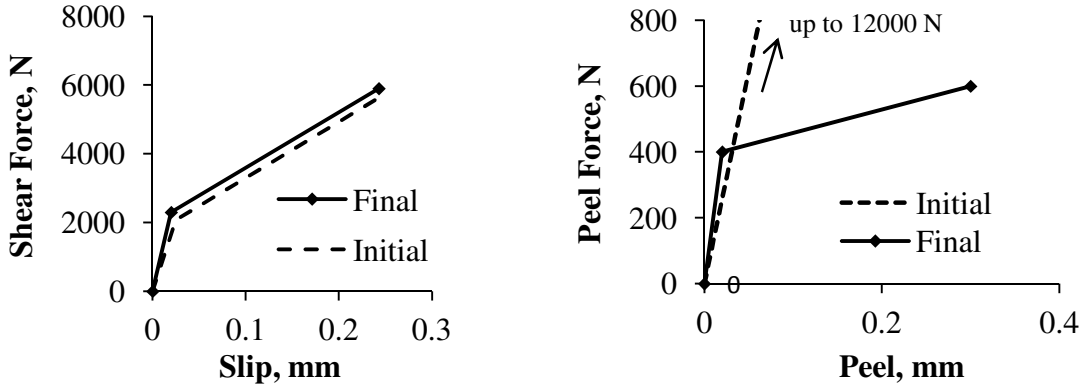

(a): Shear spring (SRB1-1). (b) Peel spring (SRB1-1).

Fig. 5.16: Force-displacement curves of the springs of slab SRB1-1.

The ultimate peel force (P_{zu}) was found to be much less than the peel strength evaluated the pull-off tests, which indicates a reduction in bond strength in the Z direction. This reduction is related to interaction between the shear and peel stresses along the interface. The peel springs experienced yielding behaviour when the chemical bond between the concrete topping and the hollowcore slab is lost due to shear. A comparison between the linear shear and peel stiffness evaluated by Adawi et al. (2014) and the nonlinear stiffness evaluated in this chapter is provided in Fig. 5.17 for slab SRB1-1. The shear and peel interfacial stiffness are shown in Appendix 2 for the rest of the slabs.

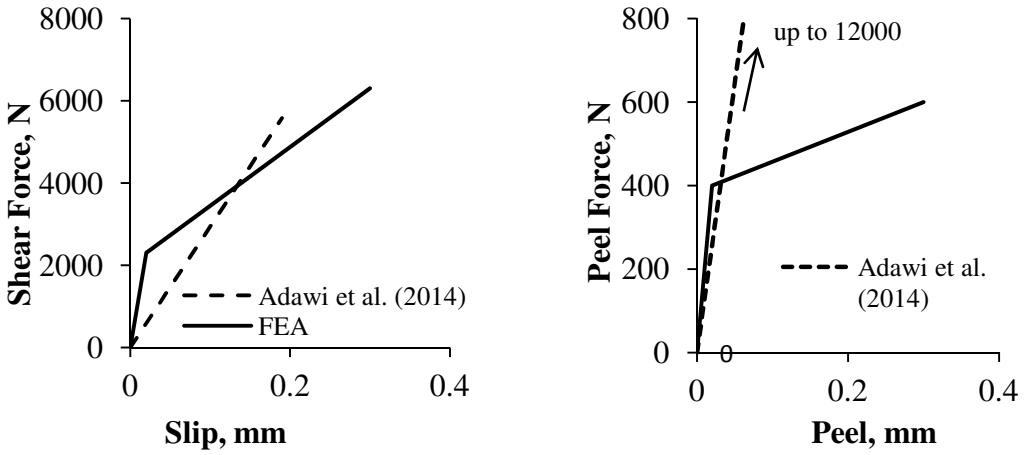

Fig. 5.17: Interfacial shear and peel stiffness for slab SRB1-1

Fig. 5.18 compares the strains obtained experimentally and using the finite element analysis for slab SRB1-1. The strain graphs for the rest of the slabs are shown in Appendix 2.

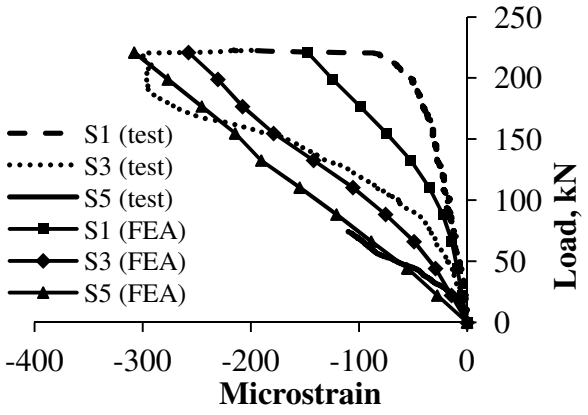

Fig. 5.18: Strain results for slab SRB1-1

The linear analytical modeling presented by Adawi et al. (2014) and used in Chapter 3 concluded that the shear stress is not uniformly distributed over the interface layer. The

maximum shear stress evaluated using the finite element analysis is compared with the results obtained from the push-tests and the analytical model in Table 5.3.

Table 5.3: Maximum shear stress comparison

Slab Label	**Maximum shear stress, MPa**		
	Linear Analytical Solution, Adawi et al. (2014)	**Nonlinear Finite Element Analysis**	**Average Shear Strength (tests), $v_{h\ avg.}$**
SMA1-2	1.69	1.43	1.39
SRA1-1	1.95	1.97	1.95
SRA1-3	2.15	2.33	2.15
SRB1-1	1.24	0.98	0.860
SRB1-2	1.01	0.75	0.710
PSMA4-2	2.47	1.2	1.19
PSMA4-3	0.26	0.26	0.256

Similar to the linear analytical modeling, the finite element analysis revealed higher shear stresses than the average values. However, the finite element results appear to be closer to the average shear stresses than the analytical. It is clear that the use of the nonlinear shear springs has resulted in redistributing the shear stresses, thus, reducing the values of the maximum shear stresses.

5.3.2 Full-Scale Tests

Results of the finite element analysis for the full-scale tests are presented in this section.

5.3.2.1 Load-deflection Response

A summary of the load-deflection results obtained from the experimental tests and the FEA analysis is shown in Table 5.4.

Table 5.4: Load-deflection results

Slab Label	Analysis Type.	Cracking load, kN	Failure load, kN	Deflection at failure, mm	Failure Type
FMA2-1	Exp.	157	253	29.4	strands rupture
	FEA	152	257	19.7	strand rupture
FMA2-2C	Exp.	152	244	49.6	strands rupture
	FEA	164	206	18.4	concrete crushing
FRA2-3	Exp.	275	388	12	flexure-shear
	FEA	278	386	11.1	shear failure
FMB2-1C	Exp.	254	380	44	flexure-shear
	FEA	250	376	23	shear failure
FMB2-2	Exp.	231	410	16.3	flexure-shear
	FEA	225	408	15.7	shear failure
FMB2-3	Exp.	315	512	19.8	flexure-shear
	FEA	338	500	16	shear failure

The results are also shown graphically in Fig. 5.19 and Fig. 5.20. It can be noticed that the finite element analysis was fairly successful in capturing the behaviour of the slabs in

terms of stiffness and failure load. The ductility was accurately predicted for slabs FRA2-3, FMB2-2 and FMB2-3, which failed in shear. Although the failure mechanism for slab FMA2-1 was accurately predicted as strand rupture, the ductility was underestimated by 30%. Same behaviour was observed for FMB2-1C.

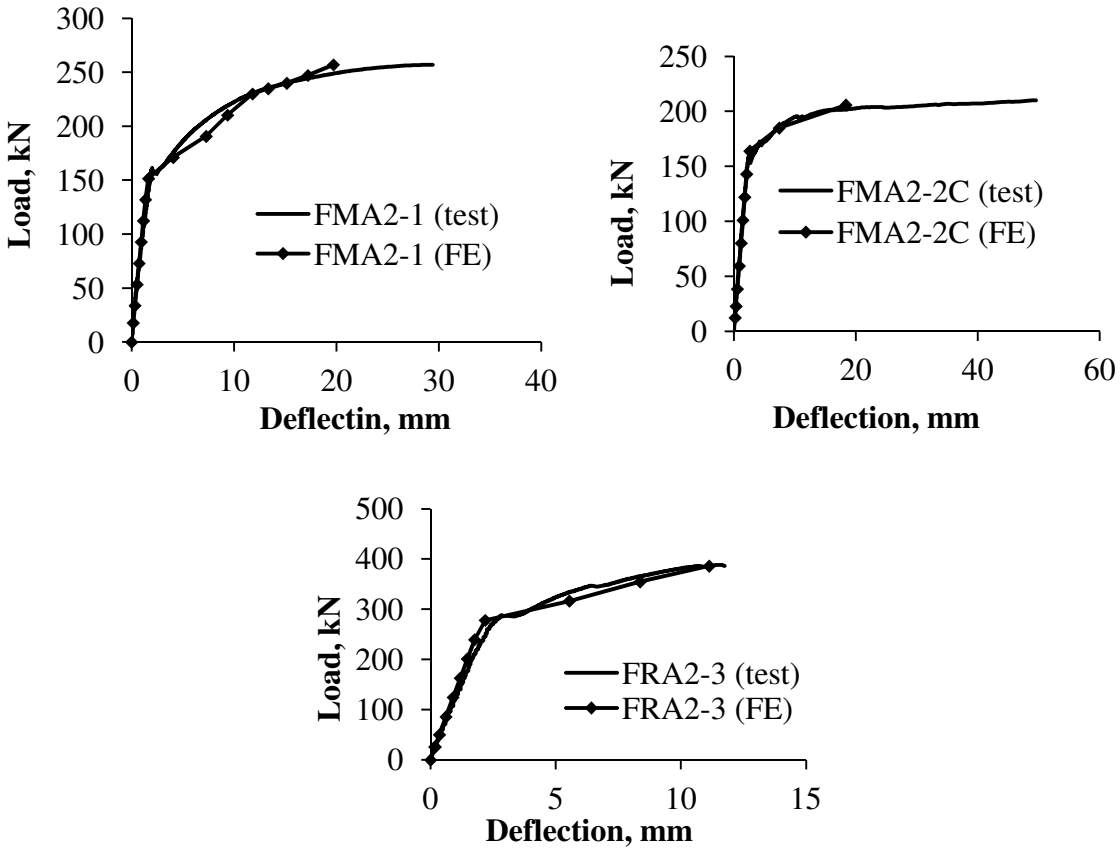

Fig. 5.19: Load-deflection results for slabs from manufacturer A

Slab FMA2-2C that had a cut in its concrete topping failed because the compressive strains in the hollowcore slab exceeded the limit of 0.0035. This failure indicates that horizontal shear failure had taken place and the composite action was lost. The difference between this failure and that observed experimentally is due to the confining effect of the applied load.

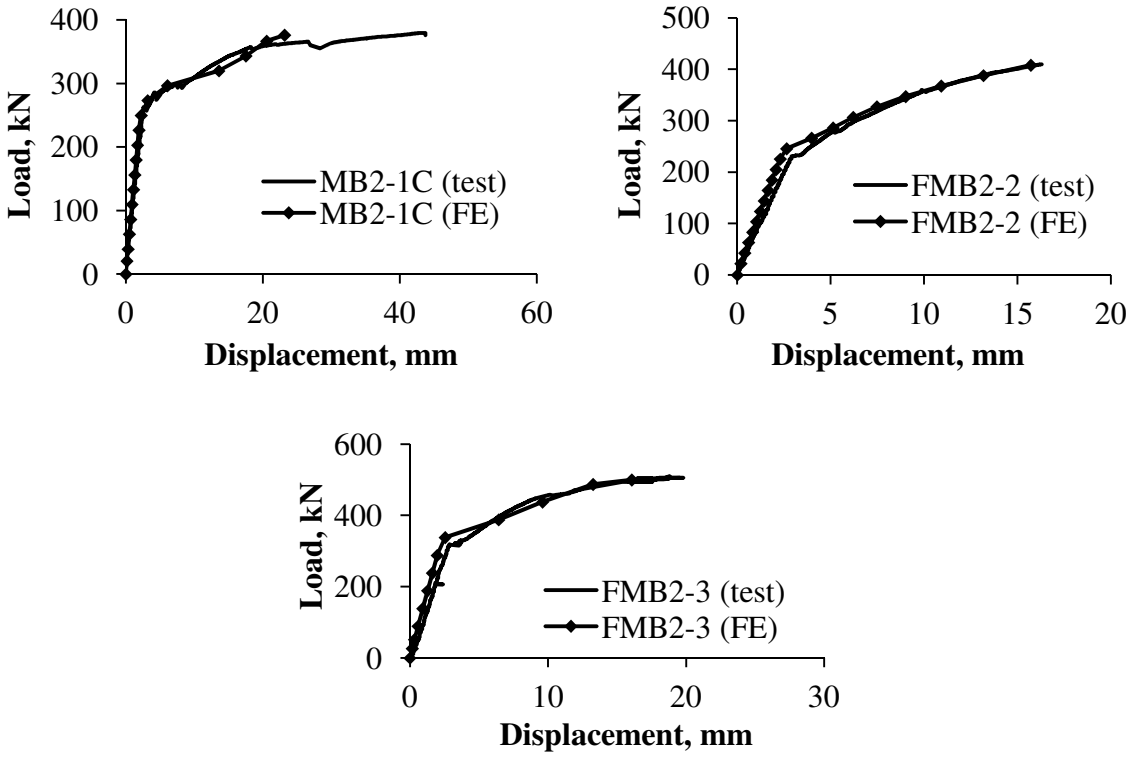

Fig. 5.20: Full-scale results for slabs from manufacturer B

5.3.2.2 Strain Results at the Mid-span Section

The strain results for slabs FMA2-1, FMA2-2C, FMB2-1C, FMB2-2 and FMB2-3 show good agreement between the experimental and the FEA results as shown in Fig. 5.21. The strain relaxation in the concrete topping after cracking was successfully captured in the FEA as shown in the graphs.

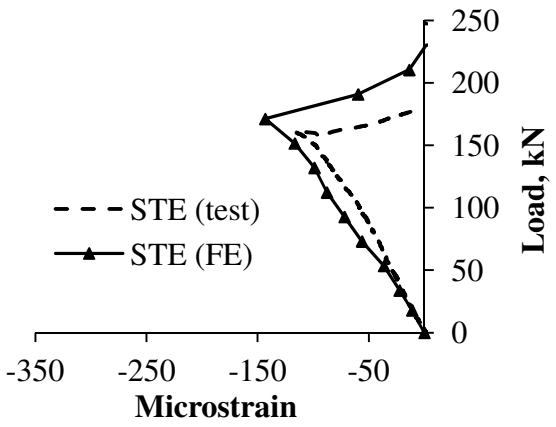

(a) FMA2-1

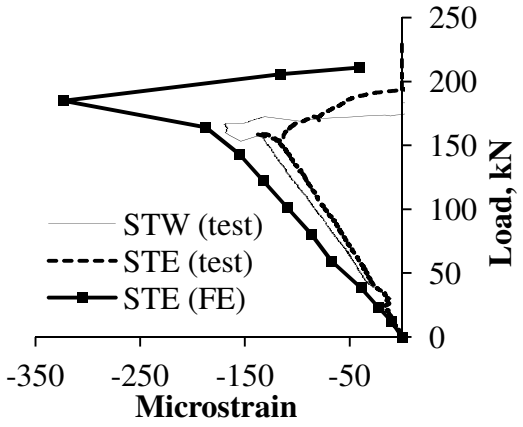

(b) FMA2-2C

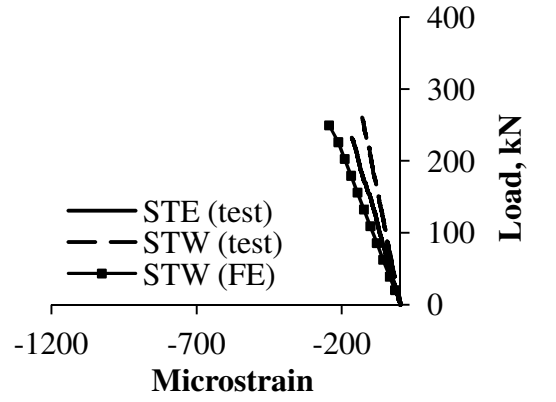

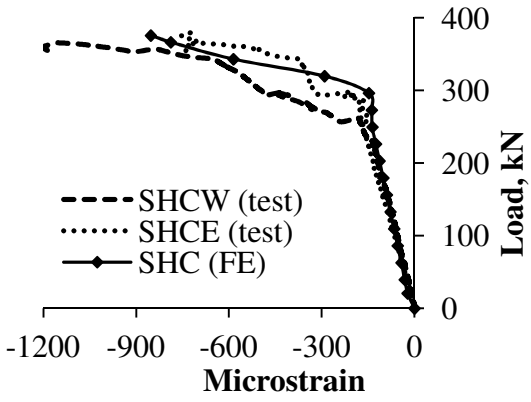

(c) MB2-2C

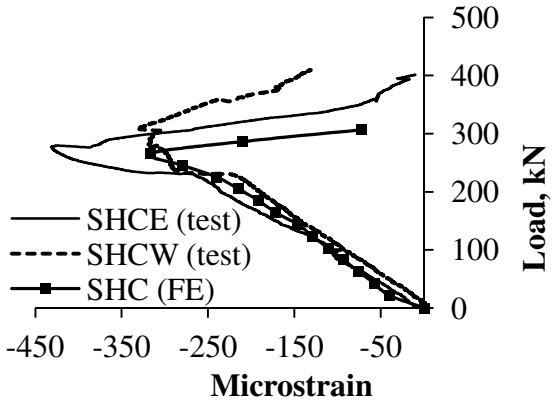

(d) FMB2-2

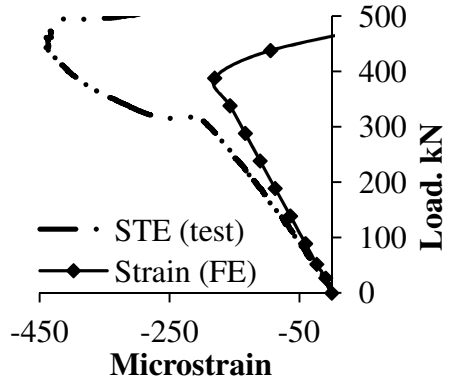

(e) FMB2-3

Fig. 5.21: Mid-span strain Results

5.3.2.3 Interfacial Slip and Peel Results

The slip results are compared with the experimental measurements for slab FMB2-2 in Fig. 5.22. Readings from LVDT SLW2 were found to be in good agreement with the FEA results. Visual inspection of this slab revealed hair cracks in the concrete topping that extend to the interface level and sporadic delamination spots between the concrete topping and the hollowcore slab along the interface, Adawi et al. (2015). This translated in significant slip measured for this slab compared with the rest of slabs that had a full concrete topping.

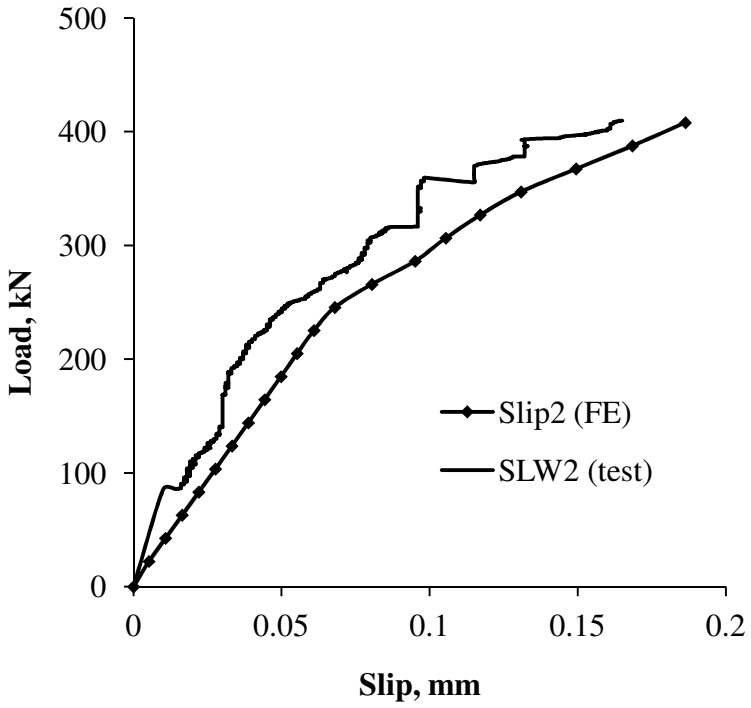

Fig. 5.22: FEA slip results for slab FMB2-2.

5.3.2.4 Constitutive Relationships of the Interfacial Springs

The stiffness of the nonlinear springs (COMBIN39) simulating the interface between the hollowcore slab and the concrete topping was crucial in controlling the composite slabs response in the FEA. The constitutive force-displacement curves were initially based on the FEA results of the push-off tests. The final force-displacement curves were determined using an extensive iteration process to match the full-scale experimental results. The final shear and peel stiffness results along with the parameters defining the force-displacement curves for the interface springs are show in Table 5.5 and Fig. 5.23. Difference between these values and the push-off test values can be attributed to confinement of the interface layer in the region of the applied load in the full-scale test and interaction between the shear and peel stresses along the interface layer.

Table 5.5: FEA shear and peel stiffness results for the full-scale test slabs

Slab Label	**Shear Stiffness**				**Peel Stiffness**			
	yield		**ultimate**		**yield**		**ultimate**	
	P_y, N	**Slip, mm**	**P_u, N**	**Slip, mm**	**P_y, N**	**Peel, mm**	**P_u, N**	**Peel, mm**
FMA2-1	200	0.02	1100	0.12	200	0.1	200	0.1
FMA2-2C	2740	0.007	6170	0.24	1000	0.5	1000	0.5
FRA2-3	480	0.18	675	0.3	1000	0.5	1000	0.5
FMB2-1C	4000	0.01	6000	0.24	1000	0.5	1000	0.5
FMB2-2	1440	0.24	1440	0.24	2000	1	2000	1
FMB2-3	1050	0.35	1050	0.35	2000	1	2000	1

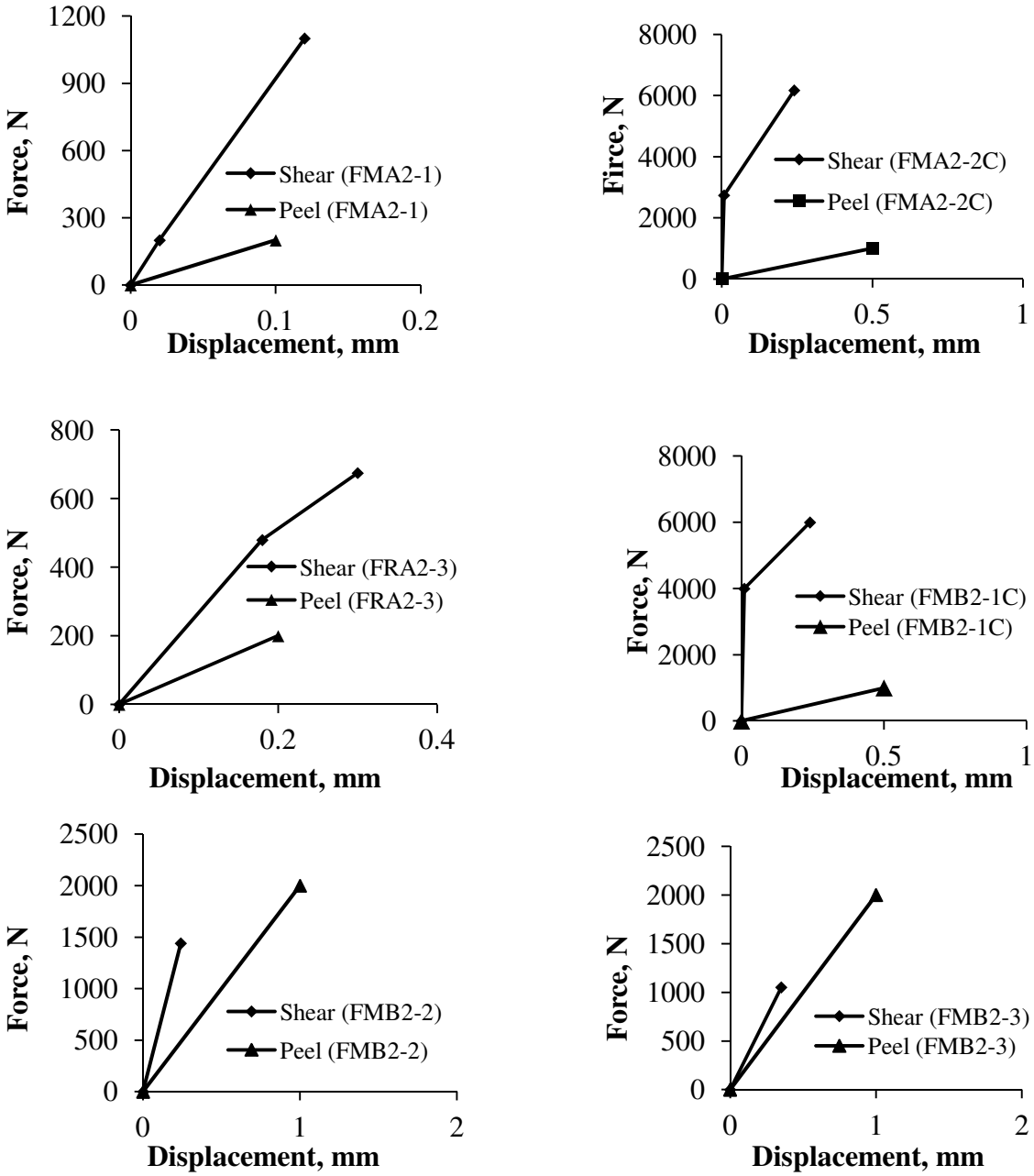

Fig. 5.23: Interfacial springs properties for slabs from manufacturer A.

Considering slabs with full concrete topping (FMA2-1, FRA2-3, FMB2-2, FMB2-3), the shear and peel behaviours were linear. The length of the concrete topping in those slabs helped distributing the shear stresses over a larger area. When the concrete topping length is reduced for slabs FMA2-2C and FMB2-1C, the shear stress intensifies causing the

nonlinear behaviour to become apparent. The maximum interfacial shear stiffness evaluated from the push-off tests FEA was found to be 102 (N/mm)/mm^2, while it reached 297 (N/mm)/mm^2. The interfacial peel stiffness did not seem to vary between the slabs and was found to be approximately 1.5 (N/mm)/mm^2.

5.3.2.5 Shear Stress Distribution

The shear stress distribution along the interface between the hollowcore slab and the concrete topping for slab FMA2-1 is shown in Fig. 5.24 and in Appendix 2 for the rest of the slabs. The yielding load is the load at which the composite slab stiffness changes from linear to nonlinear based on the load-deflection curve of the slab.

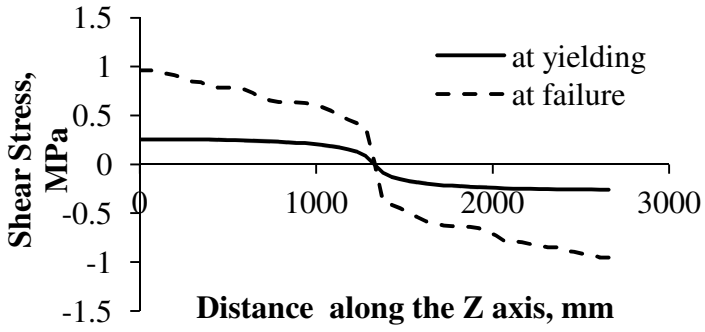

Fig. 5.24: Interfacial shear stress distribution slab FMA2-1.

Considering the full-scale test setup, where there is only one point load at mid-span, the maximum interfacial shear stress occurs at the end of the slab where the moment is equal to zero and the vertical shear is at maximum. The shear stress dissipates towards the mid-span section, where the moment is maximum and the vertical shear is equal to zero. The maximum interfacial shear stress sustained by each slab in the full-scale test is presented in Table 5.6.

Table 5.6: FEA maximum interfacial shear stress results

Slab Label	Shear Stress, MPa
FMA2-1	0.96
FMA2-2C	2.0
FRA2-3	0.33
FMB2-1C	3.2
FMB2-2	1.85
FMB2-3	0.75

With the exception of slabs FRA2-3 and FMB2-3, all tested slabs had sustained relatively higher than the 0.55 MPa and 0.7 MPa limits set by the ACI 318-08 (2008) and the CSA A23.3-04 (2004) design standards. The higher stiffness due to the increased thickness for slabs FRA2-3 and FMB2-3 had reduced the intensity of the interfacial shear stress for those slabs.

5.4 Conclusions

Modeling of the push-off and the full-scale tests using the finite element method was conducted in this chapter. The FEA showed comparable results with the experimental program conducted in Chapter 2. This demonstrates that the presented FEA approach and modeling procedures are adequate in capturing the behaviour of composite hollowcore with an acceptable accuracy. The FEA of the push-off tests was able to determine the nonlinear shear and peel stiffness coefficients of the interface between the hollowcore slab and the concrete topping. Those coefficients were then used as initial values in the FEA of the full-scale tests. The shear stresses were found to reduce the bond strength of

the interface layer causing the peel stiffness to significantly reduce. Bond strength evaluated using pull-off tests was found to be uncorrelated to the peel strength.

The use of the full concrete topping reduces the interfacial shear and peel stiffness causing them to behave linearly. When the concrete topping is reduced, the behaviour of the shear and peel changes to the nonlinear mode affected by the interfacial confinement provided by the applied load. This suggest that live loads tend to confine the interface layer in the area where they are applied causing a significant increase in the interfacial shear and peel stiffness. Considering the first stiffness branch of the FEA results, the shear stiffness of the tested composite hollowcore slabs ranged from 2.2 to 8.3 (N/mm)/mm^2 while the peel stiffness was found to be steady at 1.5 (N/mm)/mm^2.

5.5 References

ACI 318, 2008. Building code requirements for structural concrete (ACI 318-08) and commentary. Michigan, United States: American Concrete Institute.

Adawi A, Youssef MA, Meshaly M., 2014. “Analytical modeling of the interface between lightly roughened hollowcore slabs and cast-in-place concrete topping”. ASCE J Struct Eng.

Aiham Adawi, Maged A. Youssef and Mohamed E. Meshaly, 2015. “Experimental investigation of the composite action between hollowcore slabs with machine-cast finish and concrete topping”. Engineering Structures, 91, pp. 1-15

ANSYS® Academic Research, Release 15.0, 2013, ANSYS, Inc.

ASTM A416/A416 M-02, 2002. Standard Specifications for Steel Strand, Uncoated Seven-Wire for Prestressed Concrete. Pennsylvania, United States: ASTM International.

Balázs, GL, 1992. “Transfer control of prestressing strands.” PCI journal, 37(6), 60–71.

Bentz, E.C., 2000. “Sectional Analysis of Reinforced Concrete”, PhD Thesis, Department of Civil Engineering, University of Toronto.

Cheng, S. and Wang, X., 2010. “Impact of Interaction between Adjacent Webs on the Shear Strength of Prestressed Concrete Hollow-Core Units”, PCI Journal, Vol. 55, No. 3, pp. 46-63.

Collins, M.P. and Mitchell, D., 1991. “Prestressed Concrete Structures”, Prentice-Hall, 760 pp.

CSA A23.3, 2004, Design of concrete structures (A23.3-04). Mississauga, ON, Canada: Canadian Standard Association (CSA).

F.D. Queiroz, P.C.G.S Vellasco and D.A. Nethercot, 2007. “Finite element modeling of composite beams with full and partial shear connection”. Journal of Constructional Steel Research, 63 (2007), pp. 505-521.

M. Reza Salari, Enrico Spacone, P. Benson and Dan M. Frangopol, 1998. “Nonlinear Analysis of Composite Beams with deformable Shear Connectors”, Journal of Structural Engineering (ASCE), October 1998, pp. 1148-1158.

Porasz, A, 1989. “An Investigation of the Stress-Strain Characteristics of High Strength Concrete in Shear”, M.A.Sc. Thesis, University of Toronto.

Sandor Popovics, 1973. “A Numerical Approach to the Complete Stress-Strain Curve of Concrete”. Cement and Concrete Research, Vol. 3, pp. 583-599.

Taizo Nishiyama, Hosin (David) Lee and M. Asghar Bhatti, 2005. “Investigation of Bonding Condition in Concrete Overlay by Laboratory Testing, Finite Element Modeling, and Field Evaluation”. Journal of the Transportation Research Board, No. 1933, Transportation Research Board of the National Academies, Washington, D.D., 2005, pp. 15-23.

Willam, K.J. and Warnke, E.P., 1974. “Constitutive Model for Triaxial Behaviour of Concrete,” Seminar on Concrete Structures Subjected to Triaxial Stresses, International Association of Bridge and Structural Engineering Conference, Bergamo, Italy, p.174.

CHAPTER SIX

6 Summary and Conclusions

The ability of composite hollowcore slabs to resist flexural and vertical shear is governed by the strength of the interface layer between the slab and the concrete topping. North American design standards specify a surface roughness to assume interfacial shear stress thresholds. This thesis presented a comprehensive study of the interfacial shear and peel stresses for composite hollowcore slabs with machine-cast or lightly-roughened surface finishes, which do not qualify for composite action according to CSA A23.3-04 (2004) and ACI 318-08 (2008). It provides a substantial proof that such slabs can perform adequately up to ultimate design loads without the need for additional roughening or surface treatment. The following sections summarize the work conducted in each chapter and the conclusions withdrawn from them. While the research is fairly comprehensive yet additional work is required in order to steer a change in the related design standard provisions. The future work section highlights some areas that will help reach this goal.

6.1 Experimental Program

Chapter 2 examined the shear and peel behaviors of the interface between hollowcore slabs with machine-cast and lightly–roughened surfaces and the topping concrete through pull-off, push-off, and full-scale tests. The work conducted in this chapter is distinguished from previous work by adapting a comprehensive experimental program, which gave broader understanding of the performance of composite hollowcore slabs. Precast manufactures can follow the tests explained in this chapter to evaluate the adequacy of their products.

The surface roughness provided by the machine-cast finish was found to be much lower than the intentional roughness required by North American design standards. High variability of surface roughness was observed for different shipments from the same manufacturer. Pull-off tests results indicated that if the surface roughness of hollowcore

slabs with machine-cast finish exceeds 0.3 mm, their bond strength to the concrete topping is expected to satisfy the 0.9 MPa limit in A23.2 (2009). This surface roughness threshold can be used by imposing quality control measure by precast manufacturers of the tested slabs.

Push-off test results indicated that if the surface roughness of hollowcore slabs is acceptable and the slab is free from contamination, the shear strength of the interface layer between the slab and the concrete topping can be higher than the minimum acceptable shear stresses specified in North American design standards. The shear strength was found to vary significantly between manufacturers.

Full-scale three point bending tests have shown that hollowcore slabs with machine-cast finish and acceptable roughness can provide adequate composite strengths up to ultimate condition. Thus, the horizontal shear strength required by CSA A23.3-04 (2004) and ACI 318-08 (2008) can be met without the need for surface roughening. Two of the slabs had a gap in their concrete topping to limit the effective area of the topping. The topping of the two slabs experienced slip and peel deformations that did not affect the overall behavior. This can be regarded to the confining action provided by the load that acts on the topping. This suggests that the live loads increase the shear strength provided by the interface layer.

6.2 Analytical Modeling

In Chapter 3, an analytical model that simulates the interface between the hollowcore slab and the concrete topping during the push-off tests using continuous springs was presented. The springs depicted the interfacial shear and peel behaviors. The actual shear stresses were evaluated using the analytical model and found to be higher than the average measured values for all of the tested slabs. The actual values were found to be much higher than the specified code limits. The shear and peel stiffness, (k_s) and (k_p), of the interface between hollowcore slabs and concrete topping were estimated using the presented analytical model and were found to range from 6.8 to 31 (N/mm)/mm^2 and 2.0

to 6.3 (N/mm)/mm^2, respectively. The reported (k_s) and (k_p) values are unique for the tested slabs. The presented method can be repeated to evaluate these stiffnesses for slabs from different manufacturers. Structural engineers can then use (k_s) and (k_p) values to evaluate the actual shear stresses developed at the interface between hollowcore slabs and their concrete topping and judge on the appropriateness of using the composite action.

Two analytical methods, simplified and modified, were developed in Chapter 4 to evaluate the interfacial shear stress distribution along the interface between the concrete topping and the hollowcore slab during the full-scale tests. The simplified method ignores the moment and shear resistances of the concrete topping while they are considered in the modified method. Additionally, the simplified method assumes zero interfacial shear stress under the point load whereas the modified method retains continuity of shear stresses at that location. The analytical solutions are applicable up to the yielding load level where the composite slab is behaving in the linear elastic zone. The interfacial shear stress levels obtained from the analytical solutions were generally in good agreement with the traditional methods existing in the North American codes. Considering the slabs with reduced concrete topping, the analytical solutions revealed higher interfacial shear stresses than the limits mentioned in CSA A23.3-04 (2004), 0.7 MPa, and ACI 318-08 (2008), 0.55 MPa. However, those slabs exhibited reliable composite action up to the predicted failure loads. The interfacial shear stiffness (k_s) did not significantly affect the interfacial shear stresses for cases of full topping. When the concrete topping was reduced, the higher (k_s) value (19 (N/mm)/mm^2) produced more reliable results. Peel stresses were not a concern considering the linear analysis presented in this chapter.

In comparison with linear finite element analysis, it can be concluded that the modified method is the most adequate technique in evaluating the interfacial shear and peel stresses in composite hollowcore slabs. This method can be conveniently used by designers regardless of the concrete topping length where the shear and peel stiffness coefficients can be estimated using the analytical modeling explained in Chapter 3.

6.3 Finite Element Analysis

Modeling of the push-off and the full-scale tests using the finite element method was conducted in Chapter 5. The FEA showed comparable results with the experimental program conducted in Chapter 2. This demonstrates that the presented FEA approach and modeling procedures are adequate in capturing the behavior of composite hollowcore with an acceptable accuracy. The FEA of the push-off tests was able to determine the nonlinear shear and peel stiffness coefficients of the interface between the hollowcore slab and the concrete topping. Those coefficients were then used as initial values in the FEA of the full-scale tests. The shear stresses were found to reduce the bond strength of the interface layer causing the peel stiffness to significantly reduce. Bond strength evaluated using pull-off tests was found to be uncorrelated to the peel strength.

The use of the full concrete topping was found to reduce the interfacial shear and peel stiffness causing them to behave linearly. When the concrete topping is reduced, the behavior of the shear and peel changes to the nonlinear mode and was affected by the interfacial confinement provided by the applied load. This behavior suggests that live loads tend to confine the interface layer in the area where they are applied causing a significant increase in the interfacial shear and peel stiffness. Considering the first stiffness branch of the FEA results for the full-scale tests, the shear stiffness of the tested composite hollowcore slabs ranged from 2.2 to 8.3 (N/mm)/mm^2 while the peel stiffness was found to be steady at 1.5 (N/mm)/mm^2.

6.4 Future Recommended Work

In view of the results obtained and the conclusions withdrawn from the work performed in this thesis, the author believes that a large window for future work remains open. The following suggested areas of work are proposed:

1- Extending the presented experimental program to include more hollowcore slab manufacturers from all over North America. Additionally, study the effect of surface contamination and concrete curing techniques on the interface strength.

2- Investigate experimentally and analytically the effect of differential shrinkage and its residual stresses on the strength of the interface and delamination of the concrete topping.

3- Examine effect of creep on the interface strength due to long-term sustained loading.

4- Explore the use of advanced finite element analysis using contact elements in lieu of the nonlinear springs used in this study to better understand the combined effect of shear and peel interfacial stresses.

5- Investigate the behaviour of dynamic loading, such as floor vibration, on the composite action of hollowcore slabs.

6.5 References

ACI 318, 2008. Building code requirements for structural concrete (ACI 318-08) and commentary. Michigan, United States: American Concrete Institute.

CSA A23.3, 2004, Design of concrete structures (A23.3-04). Mississauga, ON, Canada: Canadian Standard Association (CSA).

APPENDIX ONE

A1.1 Strain Compatibility Procedure

The flexural capacities of the hollowcore slabs presented in Table 2.7 of Chapter 2 were estimated using the strain compatibility method as illustrated in Fig. A1.25.

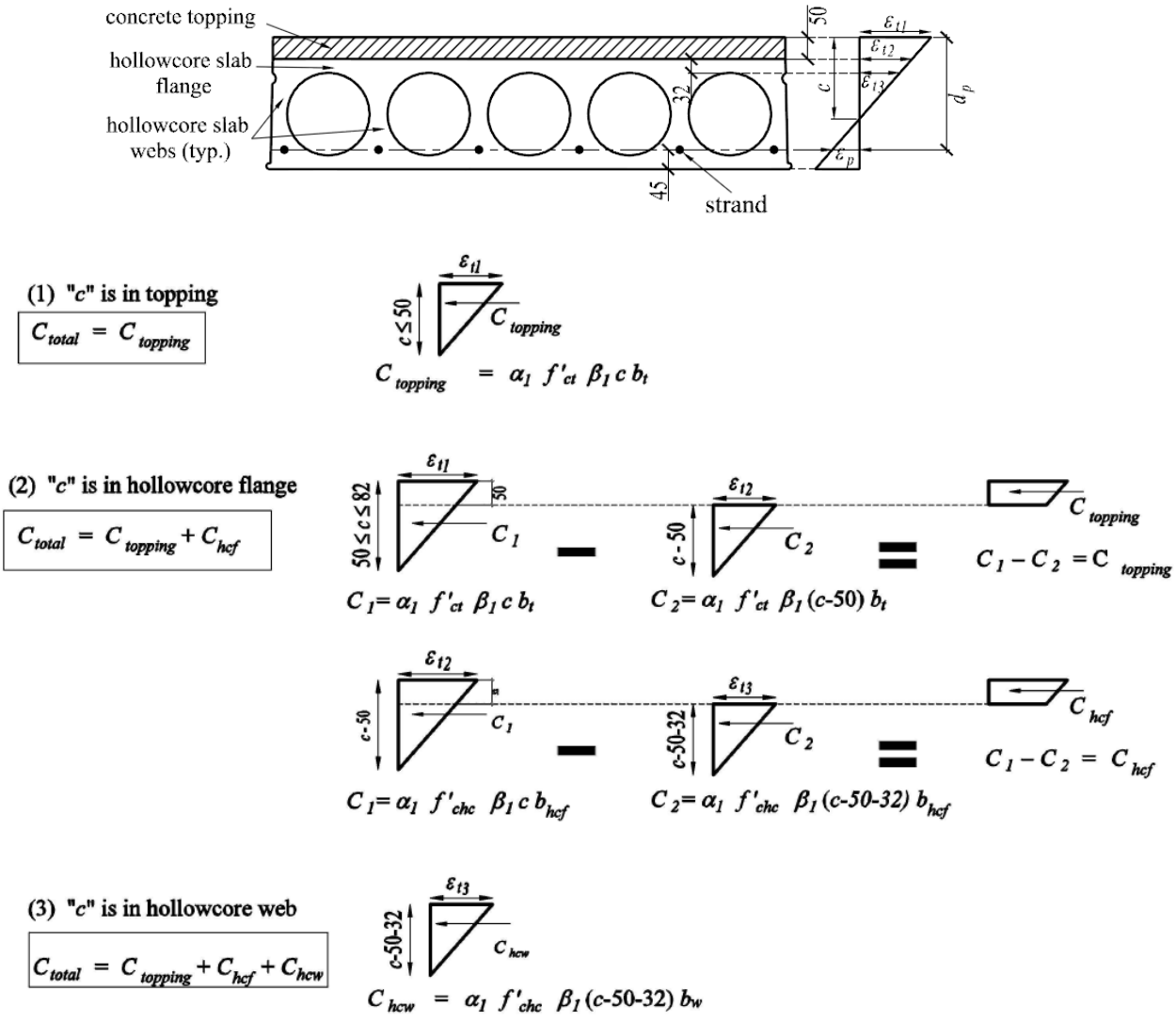

Fig. A1.25: Strain compatibility procedure.

In this method, the total compressive force (C_{total}) acting on the cross section is calculated using an iterated concrete strain profile by changing the value of the top strain (ε_{t1}) and checking for equilibrium.

Because of the difference in the concrete compressive strength between the hollowcore slab and the topping concrete, the values of the compressive stress block parameters (α_1 and β_1) cannot be determined using CSA A23.3-04 equations. Superposition was used such that the compression forces acting on the hollowcore slab and the concrete topping were evaluated separately using the corresponding concrete compressive strength.

A1.2 Contribution of Concrete Tensile Strength to Flexural

Shaded areas in Fig. A1.26 are used to calculate the tensile forces contributing to the flexural capacity. The areas are determined by iterations such that their centroids coincide with the centroids of the prestressing strands and their least dimension does not exceed 15 times the strand diameter.

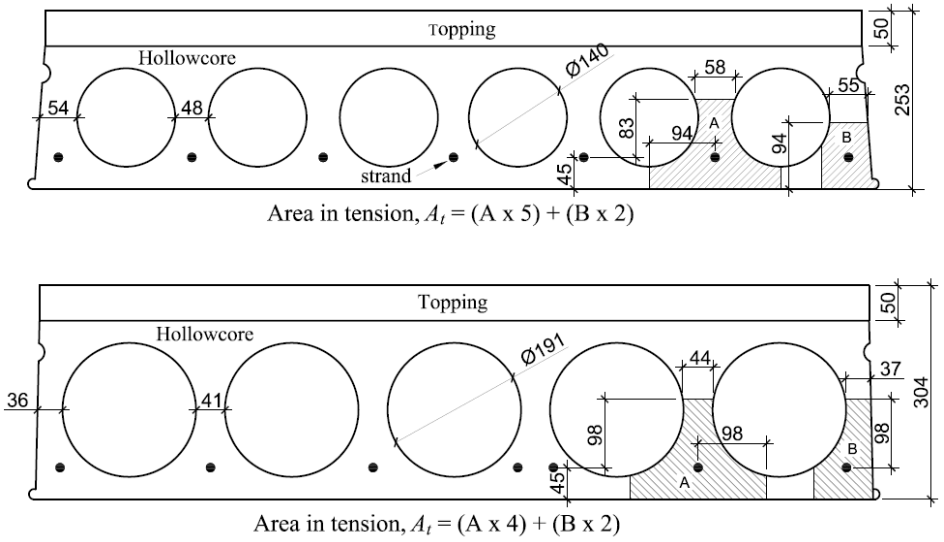

Fig. A1.26: Concrete tensile areas contributing to the flexural resistance.

A1.3 Effective Web Width for Shear Capacity

CSA A23.3-04 (2004) specifies an allowance for tapered and irregular cross sections when calculating the concrete area contributing to the vertical shear capacity. To determine this area, a trajectory line is constructed at 20^o from the vertical axis of the cross section that is tangent to the hollowcore slab void. Those lines are then extended to a distance that is equal to (d_v) measured from the strands level. The allowable area is calculated by evaluating the area of the region encompassed by those lines as shown in Fig. A1.27.

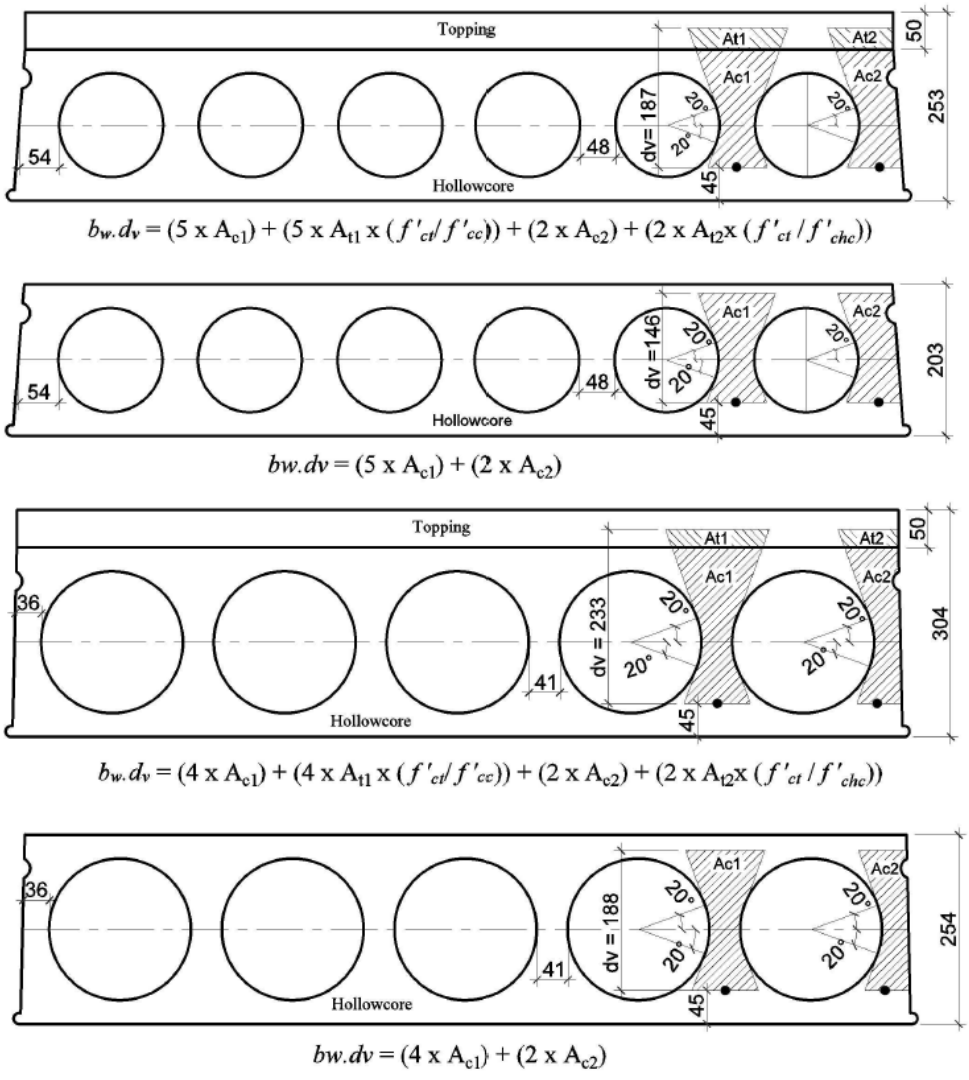

Fig. A1.27: Concrete tensile areas contributing to the flexural resistance.

A1.4 Tensile Strength Test for a Typical Prestressing Strand

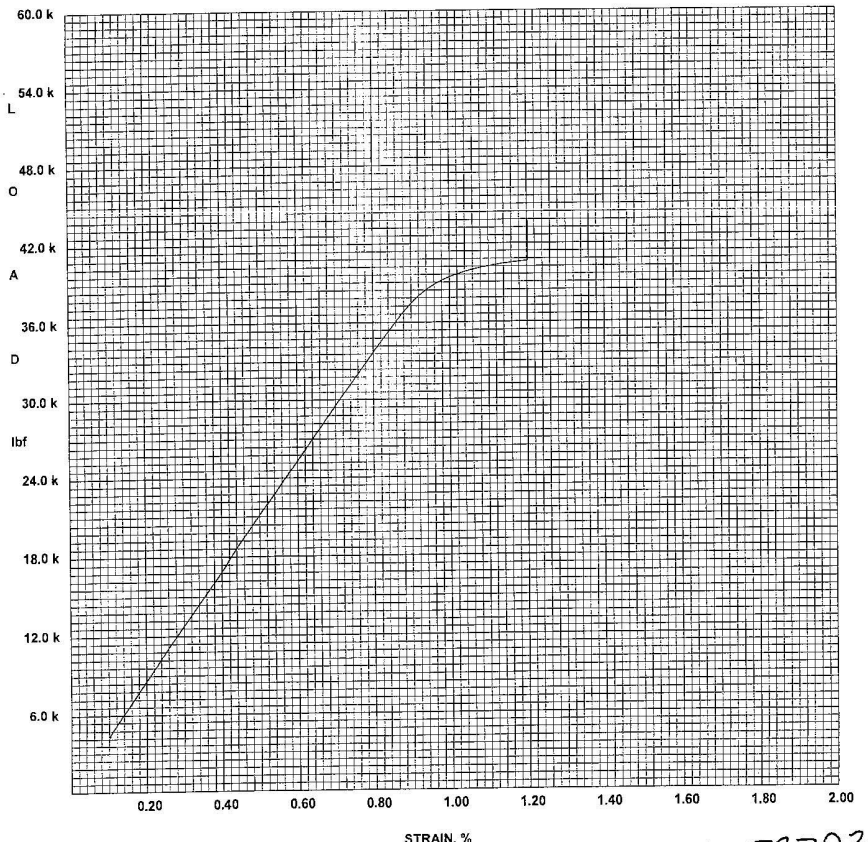

Insteel Wire Products
Prestressed Concrete Strand

1/2" 270 7W LOW RELAXATION

Test Number:	20034690
Tested By:	CDS
Ultimate Breaking Strength, lbf:	43663
Ultimate Breaking Strength, kN:	194
Load @ 1% Extension, lbf:	39391
Load @ 1% Extension, kN:	175
Ultimate Elongation, %:	5.9
Rep. Area, in²:	0.153
Rep. Area, mm²:	98.7
Actual Area, in²:	0.1530
Actual Area, mm²:	98.7194
Avg Modulus of Elasticity, Mpsi:	29.0
Avg Modulus of Elasticity, MPa:	199947.6
Reference:	

APPENDIX TWO

A2.1 FEA Final Iteration Results for the Push-off Tests

The final load-slip and load-peel relationships using the final iterations resulted from the finite element analysis of the push-tests are compared with the test results in Fig. A2.28.

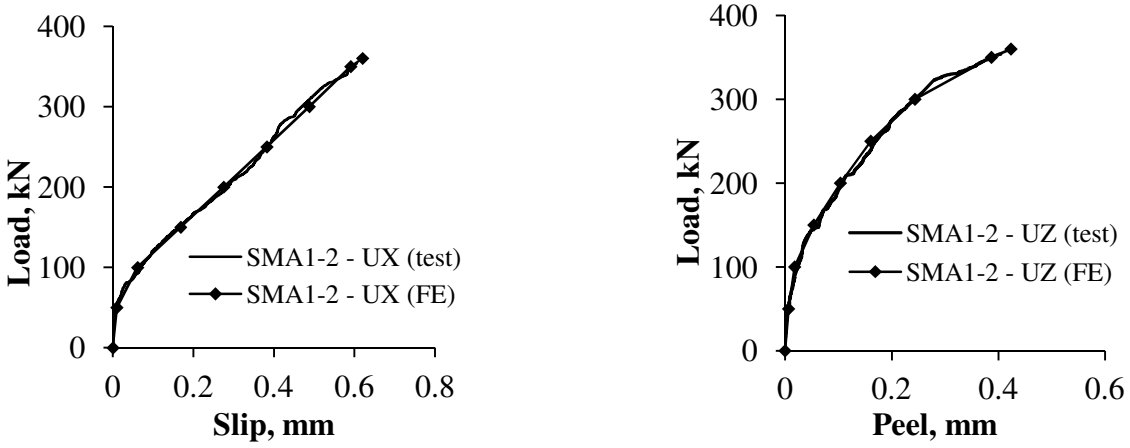

(a) Slab SMA1-2

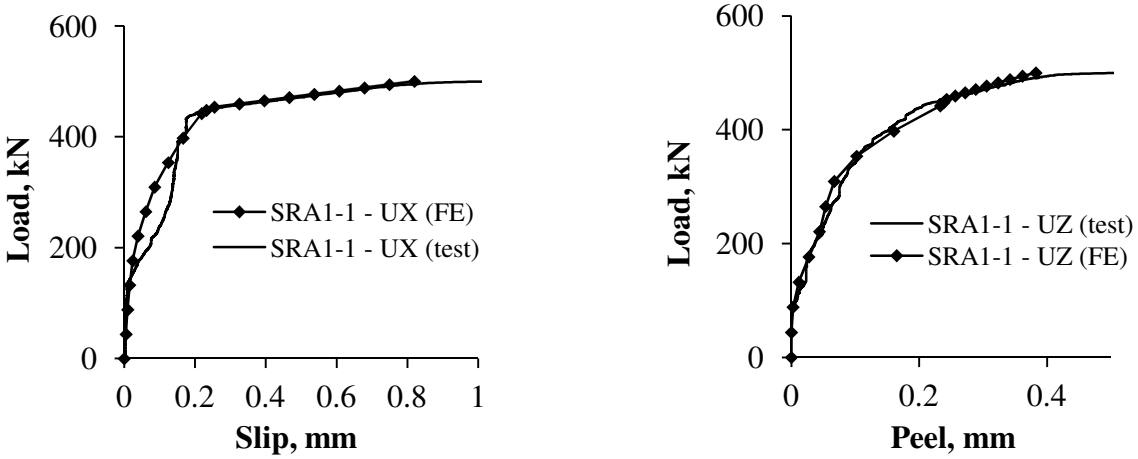

(b) Slab SRA1-1

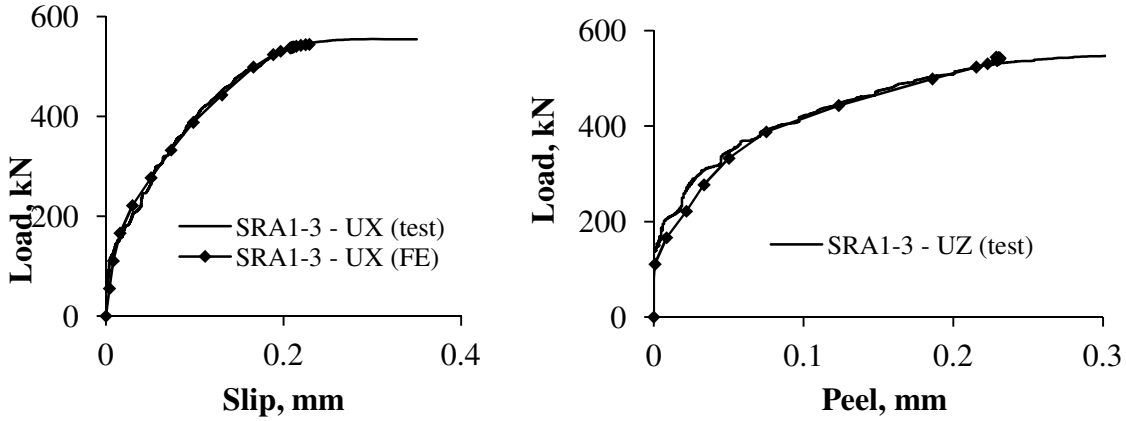

(c) Slab SRA1-3

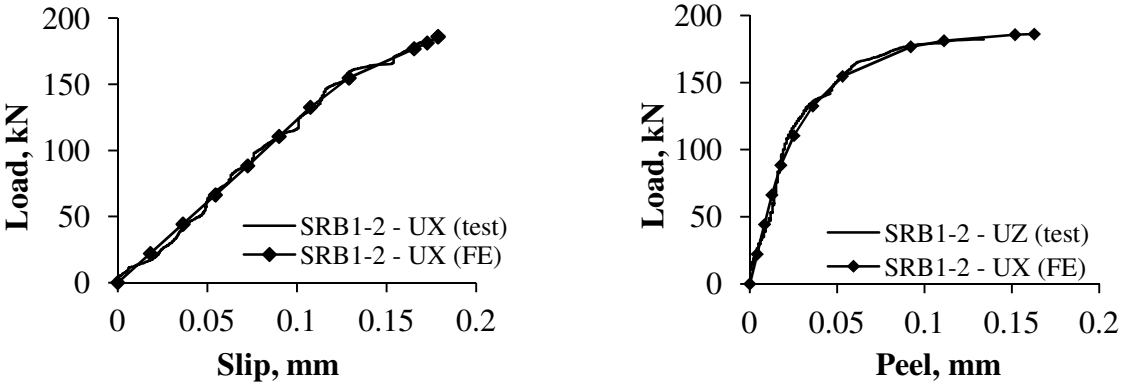

(d) Slab SRB1-2

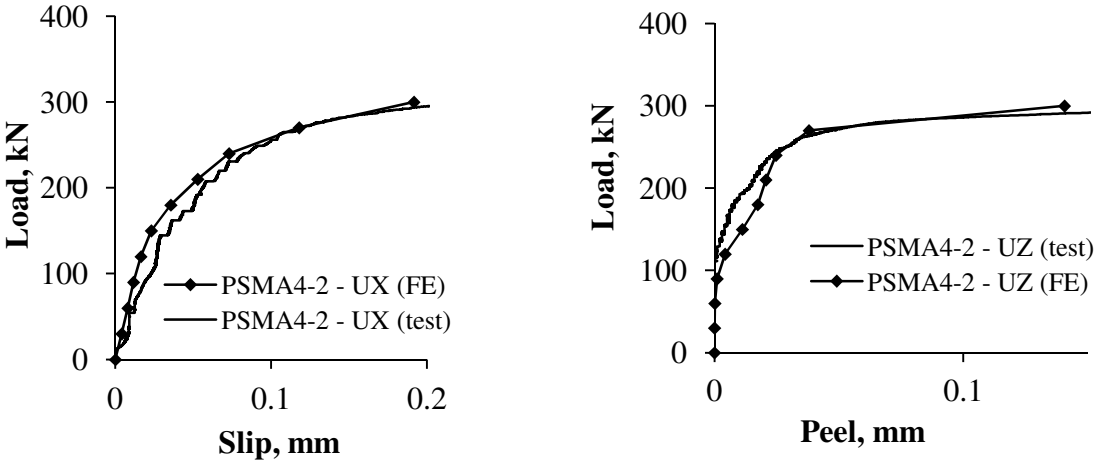

(e) Slab PSMA4-2

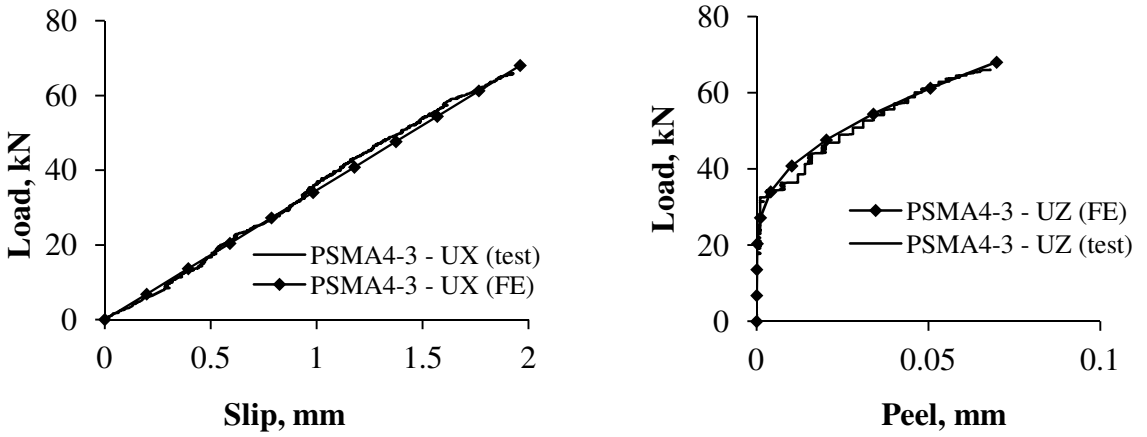

(f) Slab PSMA4-3

Fig. A2.28: FEA results for the push-off tests.

The final force-displacement curves for the shear and peel springs for each tested slab are shown in Fig. A2.29.

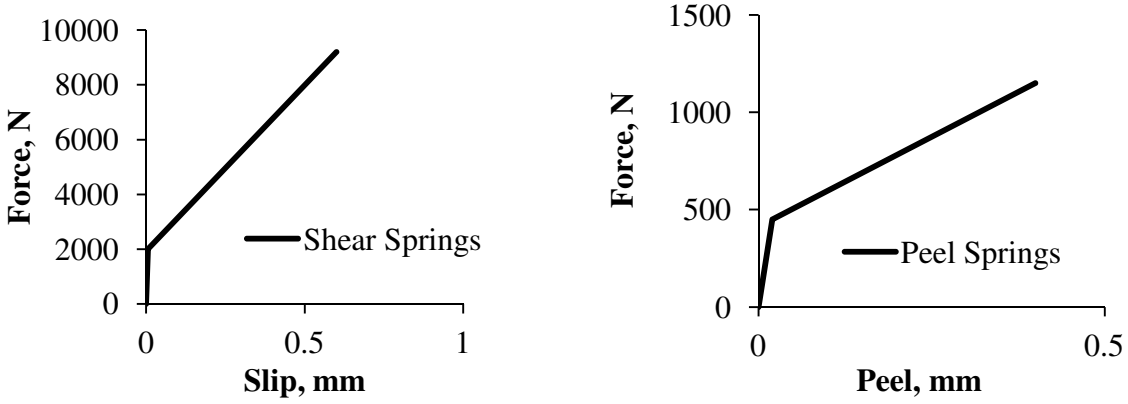

(a) Slab SMA2-1

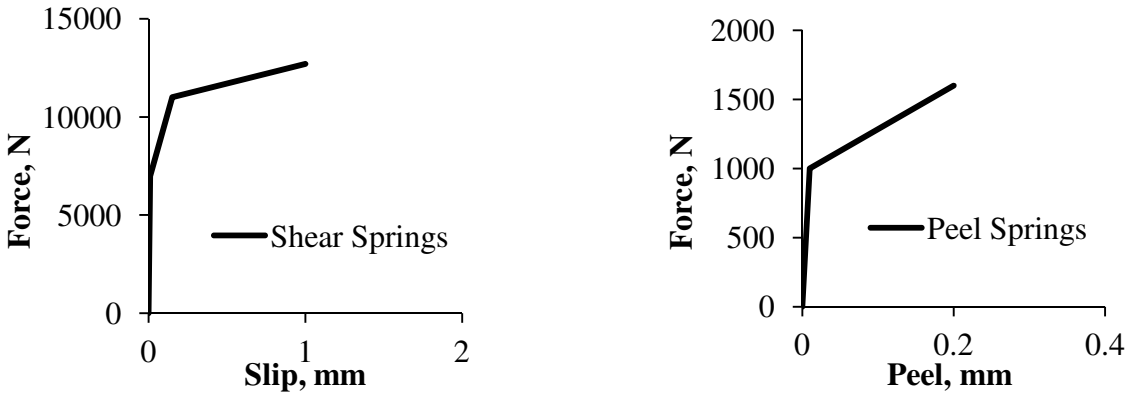

(b) Slab SRA1-1

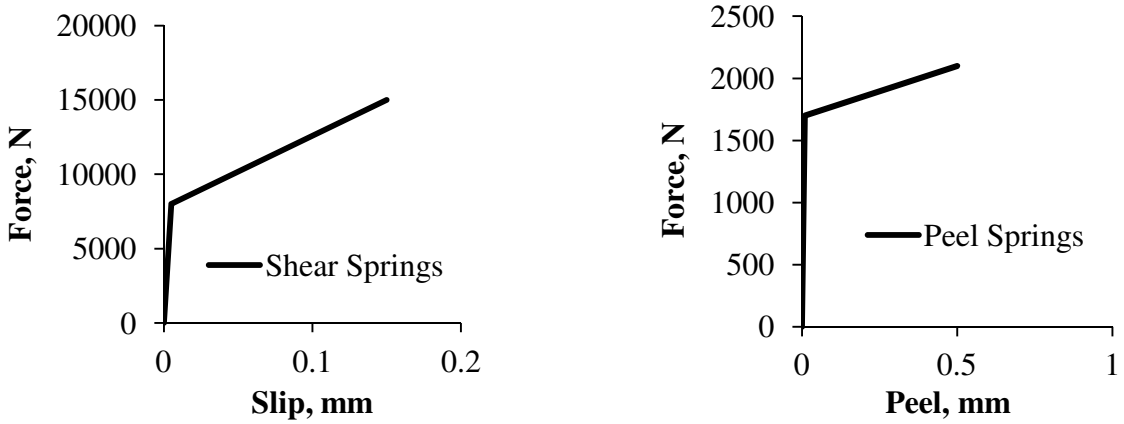

(c) Slab SRA1-3

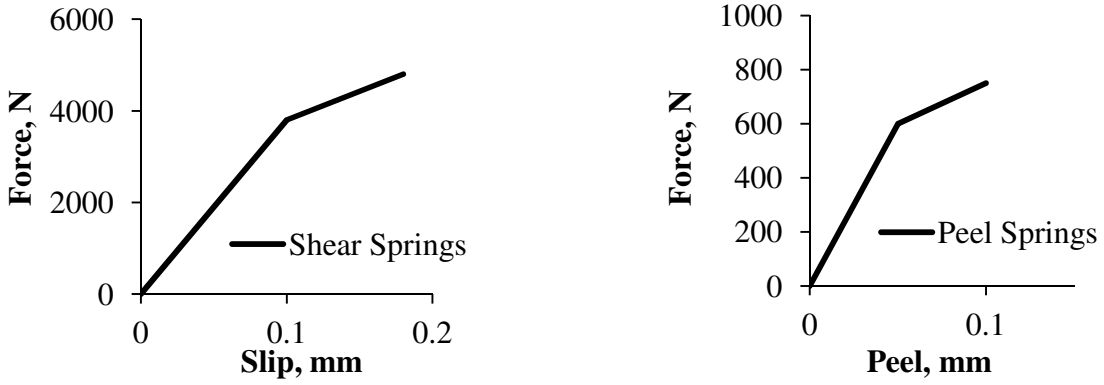

(d) Slab SRB1-2

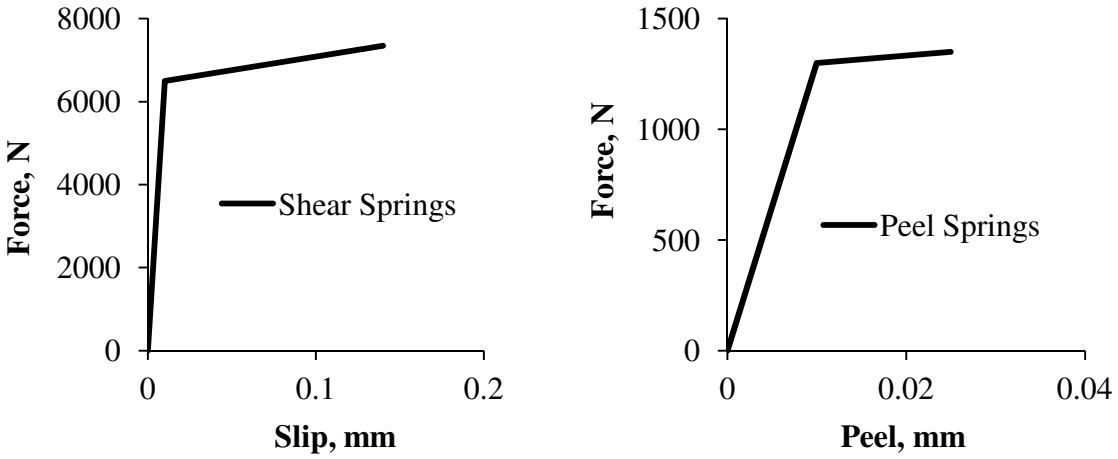

(e) Slab PSM4-2

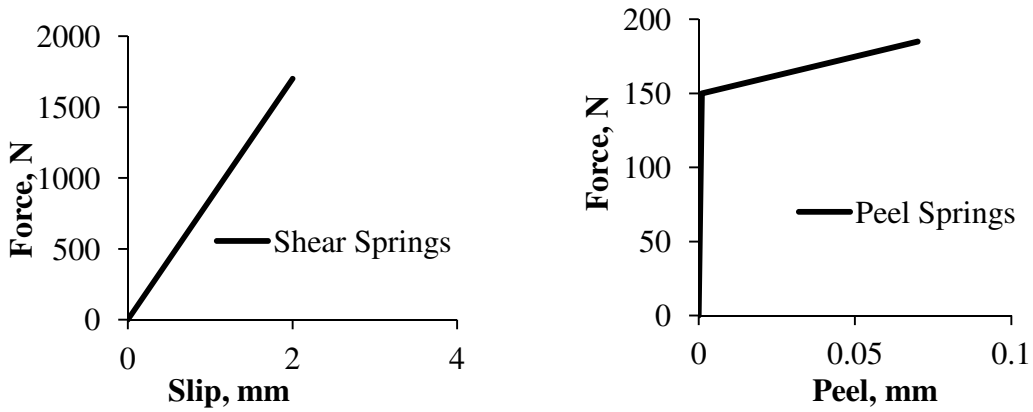

(f) Slab PSM4-3

Fig. A2.29: FEA results for the push-off tests.

Fig. A2.30 compares the test readings from strain gauges S1, S3 and S5 with the results obtained from the FEA.

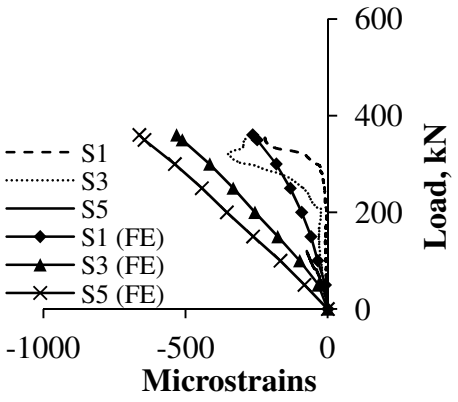

(a) SMA1-2

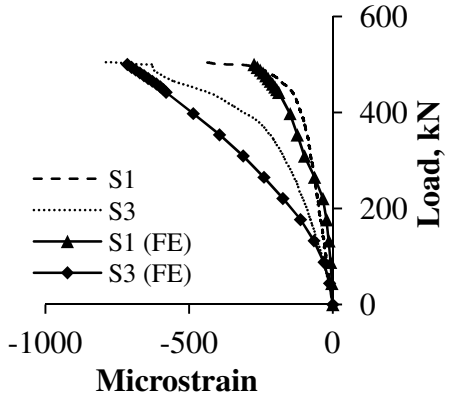

(b) SRA1-1

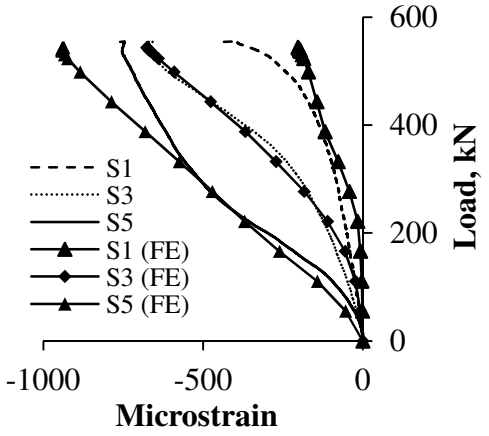

(c) SRA1-3

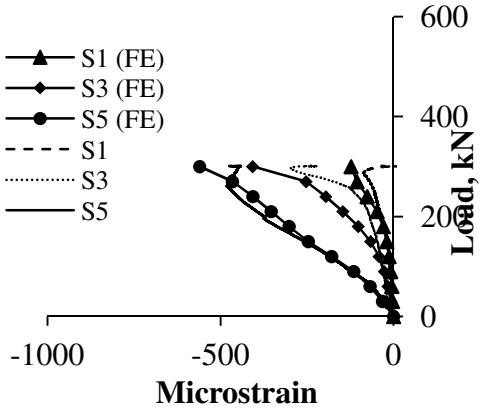

(d) PSMA4-2

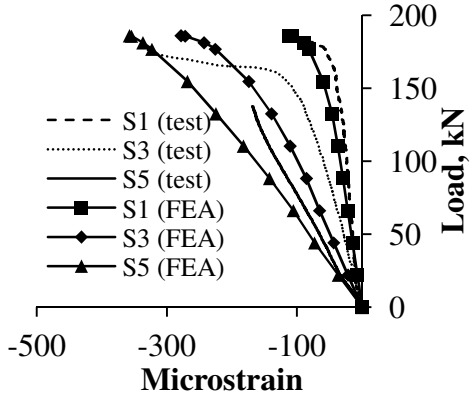

(e) SRB1-2

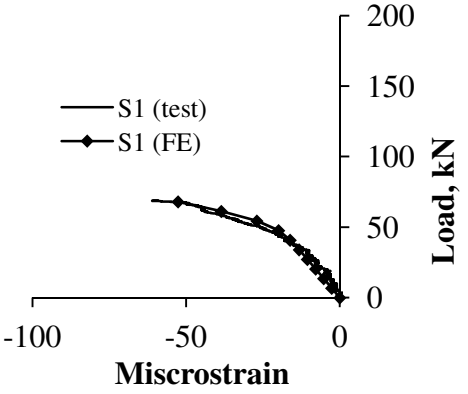

(f) PSMA4-3

Fig. A2.30: Strain results.

A2.2 Results of the Full-scale Tests FEA

The shear stress distribution along the interface between the hollowcore slab and the topping concrete are demonstrated in Fig. A2.31

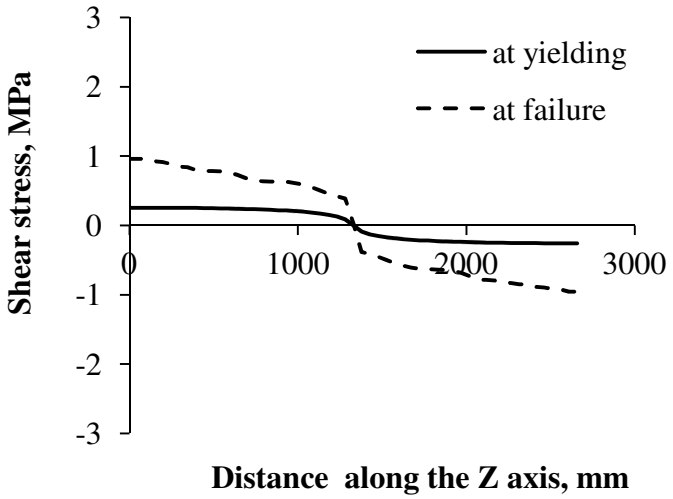

(a) Slab FMA2-1

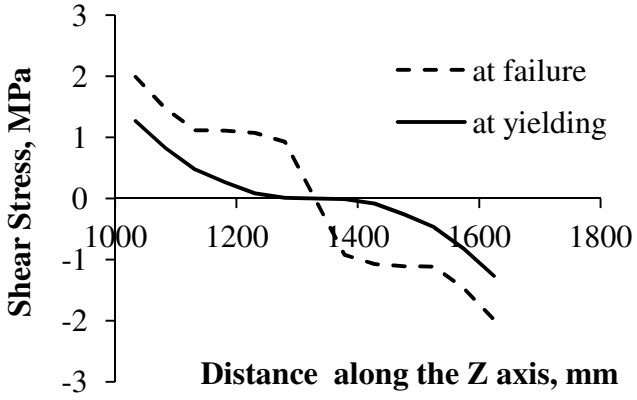

(a) Slab FMA2-2C

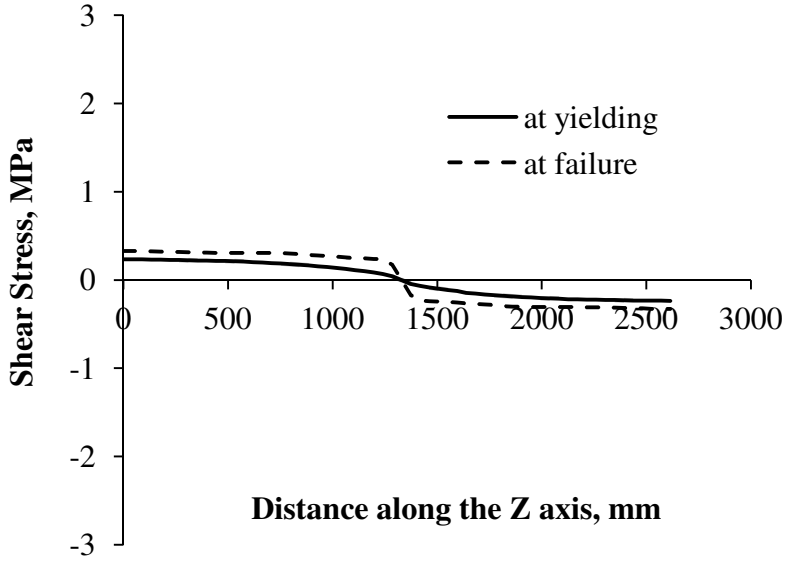

(a) Slab FRA2-3

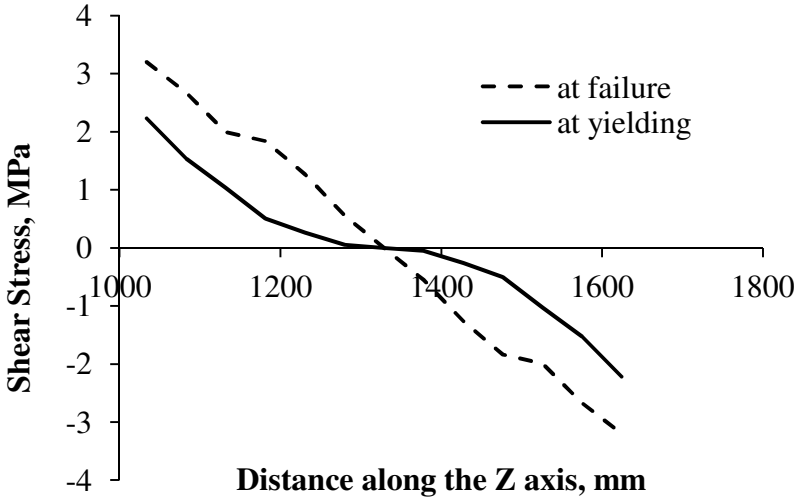

(a) Slab FMB2-1C

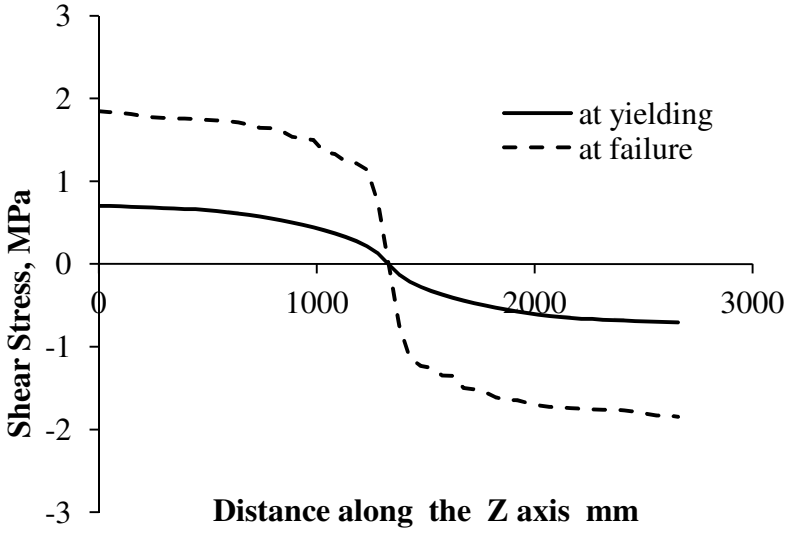

(a) Slab FMB2-2

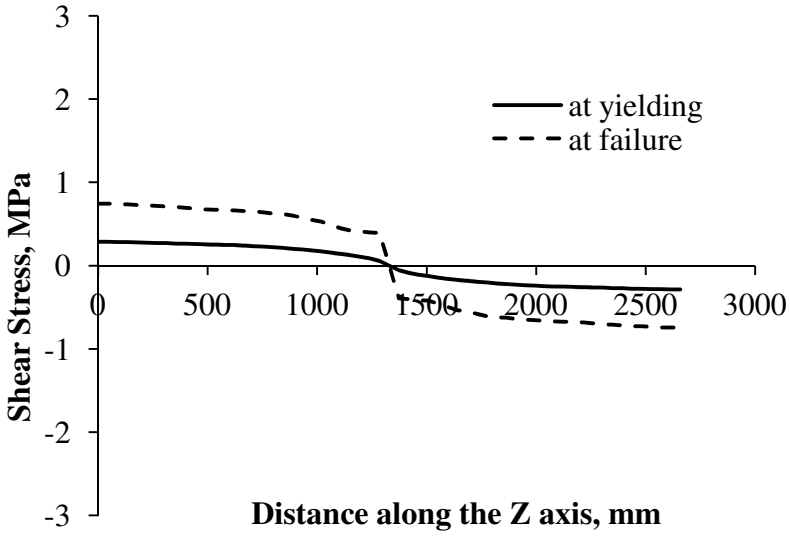

(a) Slab FMB2-3

Fig. A2.31: Shear stress distribution for the full-scale tests.

Curriculum Vitae

Name:	Aiham Adawi
Post-secondary Education and Degrees:	Jordan University Amman**,** Jordan 1994-1999 B.Sc. Western University London, Ontario, Canada 2005-2008 M.Eng.
Honours and Awards:	Industrial Postgraduate Scholarship (NSERC-IPSII) 2008-2011 Peter A. Rosati Award for Outstanding Teaching in Civil and Environmental Engineering Department Western University, 2011 USC Teaching Honor Roll Western University, 2011 Student Scholarship from the Canadian Precast and Prestressed Concrete Institute (CPCI), 2012 Graduate Student Teaching Award Western University, 2012
Related Work Experience	Lecturer and Course Instructor Civil and Environmental Engineering Dept. Western University, 2011-2014 Structural Precast Concrete Designer Prestressed Systems Inc. (PSI), Windsor, ON. (Jan-July) 2008

Publications:

Aiham Adawi, Maged A. Youssef, Mohamed Meshaly, "Experimental investigation of the composite action between hollowcore slabs with machine-cast finish and concrete topping" *Engineering Structures*, 91 (2015), p.p. 1-15.

Aiham Adawi, Maged A. Youssef, Mohamed Meshaly, "Analytical Modeling of the Interface between Lightly Roughened Hollowcore Slabs and Cast-In-Place Concrete Topping" *Journal of Structural Engineering* (ASCE), April 2015, Volume 141, Issue 4, p.p. 1-9.

Maged Youssef and **Aiham Adawi**, "COMPOSITE BEHAVIOR OF HOLLOWCORE SLABS AND CAST-IN-SIU CONCRETE TOPPING" *Proceedings of PCI Convention and National Bridge Conference*, 21-24 Sept., 2013, p. 20.

Abdulrahman Mohammed, Moncef Nehdi, and **Aiham Adawi**, (2008). "Recycling Waste Latex Paint in Concrete with Added Value". ACI Material Journal, V. 105, No. 4, July-August 2008.